Journal of
Materials Chemistry C

ROYAL SOCIETY
OF CHEMISTRY

REVIEW

View Article Online
View Journal

Cite this: DOI: 10.1039/d1tc01494c

# Substrate-immobilized noble metal nanoplates: a review of their synthesis, assembly, and application

Robert D. Neal,†[a] Robert A. Hughes,†[a] Arin S. Preston,[a] Spencer D. Golze,[a] Trevor B. Demille[a] and Svetlana Neretina *[ab]

Received 1st April 2021,
Accepted 28th May 2021

DOI: 10.1039/d1tc01494c

rsc.li/materials-c

Noble metal nanoplates are a unique class of two-dimensional (2D) nanomaterials whose planar geometry serves as one of the most important nanoscale building blocks. Referred to by names such as nanoplates, nanodisks, nanoprisms, and nanotriangles, they offer a distinct and compelling set of physicochemical properties renowned for their plasmonic response and catalytic activity. When immobilized on substrates, these same structures are empowered with new capabilities triggered by synergistic interactions with their support and coupling phenomena activated when adjacent nanostructures are held in place with nanometer-scale spacings. In this review, we bring together an impressive literature dedicated to the synthesis, assembly, and application of substrate-immobilized noble metal nanoplates where we highlight the interplay between the nanostructures and their support as a means for deriving a distinct and diverse product. Methods for obtaining substrate-bound nanoplates rely on colloid-to-substrate transfers or syntheses occurring directly on the substrate-surface and span a wide range of techniques including chemisorption, solvent evaporation assembly, air–liquid interfacial assembly, substrate- and seed-mediated syntheses, electrochemical syntheses, vapor-phase depositions, DNA-assisted assembly, and capillary assembly. Collectively, these techniques realize nanoplate formations that are random, close-packed assemblies, periodic arrays, and three-dimensional superlattices. Nanoplate functionality is demonstrated in sensor applications with a broad range of analytes that include explosives, environmentally persistent pollutants, illicit drugs, and microRNA biomarkers for cancer and cardiovascular disease, with proof-of-concept demonstrations as active plasmonics, skin-mountable sensors, point-of-care diagnostics, and electrochemical reactors. Together, this work demonstrates substrate-immobilized nanoplates as a powerful platform for realizing photo- and chemically-active surfaces of technological relevance.

## 1. Introduction

Nanometric objects are often described as building blocks because they, like all building blocks, represent a basic unit from which grander structures can be fashioned. Construction requires a foundation upon which building blocks are precisely placed and immobilized and where the underlying properties of both the block and foundation both empower and place limitations on design. Nanoscale building blocks, like their bulk-scale counterparts, provide the greatest utility when they take on simple geometric forms (*e.g.*, spheres, rods, cubes, and plates) because their underlying symmetries allow for periodic arrangements. Nanoplates, in particular, present a conceptually appealing geometry when forming two-dimensional arrangements on planar substrates because they can act as a tile or, when placed on-edge, markedly increase the accessible surface area. Within this context, noble metal nanoplates present numerous opportunities stemming from the formation of photo- and chemically-active surfaces reliant on their extraordinary plasmonic and catalytic properties.[1–5]

Noble metal nanoplates represent a seemingly simple construct but where synthesis is complicated by the fact that the underlying symmetry of their crystal structure is contrary to the formation of a geometrically anisotropic structure with a two-dimensional planar geometry. The face centered cubic (fcc) crystal structure expressed by most noble metals is, instead, far more amenable to the formation of spherical or symmetrically faceted three-dimensional geometries because these architectures exhibit

---

[a] *College of Engineering, University of Notre Dame, Notre Dame, Indiana 46556, USA. E-mail: sneretina@nd.edu*
[b] *Department of Chemistry and Biochemistry, University of Notre Dame, Notre Dame, Indiana 46556, USA*

† Equal contribution.

much lower surface energies. Even though nanoplates are intrinsically unfavorable from this thermodynamic standpoint, their occurrence in colloids at low yield was reported almost seventy years ago by Turkevich and co-workers[6] In 2001, the Mirkin group reported the first high-yield colloidal nanoplate synthesis,[2] a landmark discovery that is now complimented by an impressive and expanding literature that details methods of synthesis, assembly, structure–property relationships, and applications.[1–5] Crucial to the formation of colloidal nanoplates are defects in the form of twins or stacking faults that disrupt the ABCABC... stacking order of an fcc metal along one of its $\langle 111 \rangle$ directions, and in doing so, provides a break in symmetry that, under suitable synthetic conditions, can activate a two-dimensional growth mode.

As colloids, noble metal nanoplates have distinguished themselves as a distinct and important class of nanomaterials due to a unique set of characteristics.[1–5] Even though all nanoplates have two large area parallel surfaces as the common architectural element, the underlying geometry remains amenable to controllable structural variations at levels that eclipse all other classes of nanomaterials (*e.g.*, nanosphere, nanocube, nanorod, nanostar). Nanoplates can take on disk, triangular, hexagonal, and irregular shapes where further adjustments can be made to their width, aspect ratio, sharpness of corners, and faceting. Stemming from this degree of variability comes a diverse and tunable property set that includes (i) plasmonic resonances that can be tuned to values across the visible region of the electromagnetic spectrum and into the near-infrared, (ii) a wide variety of accessible plasmon modes arising from both in-plane (*i.e.*, dipolar, quadrupolar, hexadecapolar) and out-of-plane excitations, (iii) sharp corners and edges that support large plasmonic electric field enhancements, and (iv) a facet-dependent catalytic activity. Additionally, their two large-area atomically-flat facets are attractive from the standpoint of carrying out surface modifications that functionalize these surfaces so as to express an application-specific chemical activity.

Although noble metal nanoplates find applications as colloids, their placement on substrates in a manner that renders them immobile creates an entirely new set of possibilities in terms of both accessible properties and functionalities. These opportunities are spurred on by a related literature focused on defining substrate-based plasmonic structures with nanoplate geometries using lithographic techniques.[7–10] This body of work exemplifies the need for integrating nanoplates with wafer-based platforms so as to realize on-chip devices that capitalize on (i) the collective response of identically shaped and oriented nanostructures, (ii) coupling phenomena between adjacent structures, (iii) nanostructure-substrate interactions, and (iv) the intense electromagnetic fields confined within nanogaps formed between two resonantly excited plasmonic structures. With nanoplates and substrates both having a planar character, there is also an inherent synergy in symmetries that lends itself to device processing. Nevertheless, these lithographic techniques remain challenged by (i) cost, scalability, and throughput issues, (ii) nanoplate structures that are polycrystalline, (iii) the need for metal adhesion layers that can diminish the plasmonic response,[11] and (iv) a resolution limit that is insufficient to define sharp corners and sub-5 nm nanogaps.[12] These deficiencies have, hence, left an opening for an alternate approach reliant on substrate-immobilized single-crystal nanoplates where advantage is gained by exceeding certain lithographic capabilities or by replacing cost-prohibitive and technically demanding techniques with benchtop processes.

Herein, we review the literature as it pertains to the synthesis and application of substrate-immobilized noble metal nanoplates. The scope of the review is restricted to nanoplates having a single-crystal character, and as such, the vast literature dedicated to lithographically-defined polycrystalline structures is excluded from the discussion. Nanosheets, which are large-area two-dimensional materials that are only several monolayers thick,[1] are also not discussed. Additionally, we confine the discussion to nanoplates supported by large-area planar substrates but where exceptions are made when deemed appropriate. The nanoplate synthesis and assembly portion of the review is organized according to the various techniques by which substrate surfaces are populated with single-crystal nanoplates. It is followed by a section that explores the use of these substrate-immobilized structures in applications related to sensing and catalysis. Throughout the review, emphasis is placed on describing the role that the substrate plays in the synthesis, assembly, and functionality of nanoplates. We believe that it is this interplay that gives substrate-immobilized nanoplates a distinct and important character that is deserving of a dedicated review. It is hoped that its contents will generate interest, inspire new ideas, and motivate research responsive to the challenges that lie ahead.

## 2. Nanoplate synthesis and assembly

Methods for forming substrate-based nanoplates fall into two general categories that distinguish themselves by whether the nanoplates are (i) formed as a colloid and then assembled on the substrate surface or (ii) synthesized directly on the substrate surface. An important difference between these two methods is that direct synthesis allows for an intimate connection between the substrate and nanoplate whereas assembled colloids are separated from the substrate by their stabilizing ligands and/or the binding agents that are used to anchor colloidal structures to the substrate surface. Table 1 provides a summary of all the synthesis and assembly methods used to populate substrates with noble metal nanoplates. It should be noted that when describing methods reliant on the assembly of colloidal nanoplates that little emphasis is placed on describing the colloid growth since these methods have been reviewed extensively.[1–5]

### 2.1 Colloid-to-substrate transfers

The most straightforward method for obtaining substrate-based nanoplates is through a colloidal synthesis followed by its subsequent transfer to the substrate surface. By separating out the procedure into a two-step process in which nanoscale building blocks are first created and then attached, this approach takes advantage of well-established colloidal protocols

Table 1 Summary of the literature as it relates to the synthesis and assembly of substrate-immobilized noble metal nanoplates

| Method | Sub-category | Metal | Orientation | Shape | Substrate |
|---|---|---|---|---|---|
| Colloid-to-substrate transfers | Chemisorption to a functionalized substrate | Ag | Horizontal | Triangle | Ag film on glass[13] |
| | | | | | Au film on glass[13] |
| | | | | | Filter paper[14] |
| | | | | | Glass[13,15] |
| | | | | | Si[16] |
| | | Au | Horizontal | Triangle | Glass[17,18] |
| | | | | | Glass/3M tape[19] |
| | | | | | ITO/glass[20] |
| | | AuAg | Horizontal | Triangle | ITO/glass[21] |
| | Solvent evaporation assembly | Ag | Horizontal | Floriated | Quartz[22] |
| | | | | Irregular | PET[23] |
| | | | | Triangle | Ag film on glass[24] |
| | | | | | Glass[13] |
| | | Au | Horizontal | Hexagon | GCE[25] |
| | | | | Hexagon/triangle | Si[26] |
| | | | | Triangle | Si[27–31] |
| | | AuAg | Horizontal | Irregular | PET[23] |
| | Air–liquid interfacial assembly | Au | Horizontal | Triangle | Glass[32] |
| | | | | | Si[33,34] |
| | Dimer assembly | Au | Horizontal | Hexagon–sphere | Si[35,36] |
| | | | | Hexagon–sphere | ITO/glass[37] |
| | | | | Disk–disk | ITO/glass[38] |
| | | | | Disk–rod | Si[39] |
| Liquid–substrate interface | Substrate-mediated growth | Ag | Vertical | Irregular | GaAs[40–44] |
| | | AuAg | Vertical | Irregular | GaAs[45] |
| | | Pd | Vertical | Irregular | GaAs[41] |
| | Seed-mediated growth | Ag | Horizontal | Irregular | Glass[46] |
| | | | | | Si[47] |
| | | | Random | Triangle | Glass[48] |
| | | | Vertical | Irregular | Glass[49–51] |
| | | Au | Horizontal | Hexagon | ITO/glass[52] |
| | | | | | Sapphire[53,54] |
| | | | | Hexagon/triangle | ITO/glass[55] |
| | | | | | Quartz[56] |
| | | | | Irregular | Si[57] |
| Electrochemical | | Ag | Random | Irregular | Graphene[58] |
| | | | Vertical | Hexagon | Au film on Si[59] |
| | | | | Irregular | Au film on Si[60] |
| | | | | | Boron-doped Si[61] |
| | | | | | ITO/glass[62–66] |
| | | | | | Nickel foam-graphene[67] |
| | | Au | Vertical | Pentagon | Au film on Si[68] |
| | | Pd | Vertical | Irregular | Au film on glass[69,70] |
| | | Pt | Vertical | Irregular | Au film on glass[71] |
| | | Rh | Vertical | Irregular | ITO/glass[72] |
| Vapor-phase assembly | Assembly on bare substrate | Ag | Vertical | Pentagram | Sapphire[73] |
| | | | | Triangle | Sapphire[73] |
| | | Au | Horizontal | Hexagon/triangle | Graphene oxide[74] |
| | | | Random | Irregular | FTO/glass[75] |
| | | | | | Sapphire/Al[76] |
| | | | Vertical | Hexagon | Sapphire[77] |
| | | | | Parallelogram | Sapphire[77] |
| | | | | Rhombic | Sapphire[78] |
| | | | | Triangle | Sapphire[77] |
| | | AuPd | Vertical | Hexagon | Sapphire[78] |
| | | Pd | Vertical | Trapezoid | Sapphire[78] |
| | Assembly using nucleation sites | AuAg | Horizontal | Triangle | Sapphire[79] |
| | | AuCu | Horizontal | Triangle | Sapphire[80] |
| Directed-assembly | Seed-mediated growth | Au | Horizontal | Hexagon | Sapphire[53,54] |
| | | | | Spiral | Sapphire[81] |
| | DNA-assisted assembly | Au | Horizontal | Triangle/disk | Au film on Si[82] |
| | Capillary assembly | Au | Horizontal | Triangle | PDMS[83] |

having fine control over nanostructure size, shape, and composition. The high aspect ratios afforded by the nanoplate geometry also facilitate transfer processes in which there is a strong impetus for a nanostructure to settle on the substrate with its large-area surface lying flat. The various colloid-to-substrate transfer methods are divided into three general categories based on the attachment step. It is noted that most studies have focused on the triangular nanoplate geometry where more recent work has benefitted greatly from colloids with significantly higher size- and shape-purity due to greater refinement of the synthetic procedures and a nanoplate purification step reliant on depletion flocculation.[84] The section ends with a description of work demonstrating how the colloidal attachment technique is being advanced to realize dimer structures where at least one of the components is a nanoplate. Studies where nanoplates or nanoplate assemblies are formed solely on TEM grids are excluded from the entire discussion.

**2.1.1 Assembly through chemisorption to a functionalized substrate.** In this method, colloidal nanostructures are exposed to a chemically modified substrate surface designed to facilitate the chemisorption of nanoplates. Immobilization occurs as individual structures dispersed within the colloid randomly come into contact with the substrate surface. As such, the resulting nanoplate-coated surface does not attain any degree of ordering and the resulting areal density is strongly dependent on the (i) concentration of nanoplates within the colloid, (ii) substrate incubation time, and (iii) effectiveness of the substrate surface linker. The attachment step can be carried out by merely dipping the functionalized substrate into the colloid for the required time followed by its removal (Fig. 1a).[15,17,19–21] A rinsing procedure then removes any loosely bound structures and undesirable chemicals contained within the colloid. Various agents have been used to anchor nanoplates to the substrate surface including APTES (γ-aminopropyltriethoxysilane),[19–21] 3-APTMS (3-aminopropertrimethysiliane),[13] and MPTES ((3-mercaptopropyl)triethoxysilane)[17] where the key characteristic is that the linker molecule has an affinity to both the substrate and nanoplate.

In one of the earliest demonstrations, Zhang *et al.*[15] elegantly demonstrated the viability of this technique as it relates to Ag nanoplates. Their results, which are summarized in Fig. 1b–e, demonstrate how a well-developed colloidal chemistry can be transposed onto a substrate surface. The SEM image of the surface-immobilized structures (Fig. 1b) shows a population of nanoplates with a fairly uniform size distribution as well as a smaller quantity of unwanted roundish structures that were formed in the synthesis. Through systematic adjustments to the colloidal chemistry, the nanoplate size was systematically varied and then applied to the glass surface. Fig. 1c shows the normalized extinction spectra for the size progression where the primary localized surface plasmon resonance (LSPR) is varied over a range extending from 503 to 713 nm. The result differs from that of the colloid in that the LSPR is red-shifted and broadened due to the asymmetric dielectric environment imposed by the substrate and nanoplate coupling phenomena brought on by the close proximity attachment of nanoplates.[85,86] Fig. 1d and e shows an image of a glass slide after it has been decorated with nanoplates as well as for each of the colloids and its corresponding surface. Collectively, these results demonstrate that the methodology forwarded gives rise to photoactive surfaces with a high degree of tunability.

The chemisorption of nanoplates to substrate surfaces offers significant advantage in that it is a rapid, straightforward, and scalable method that can be carried out at room temperature

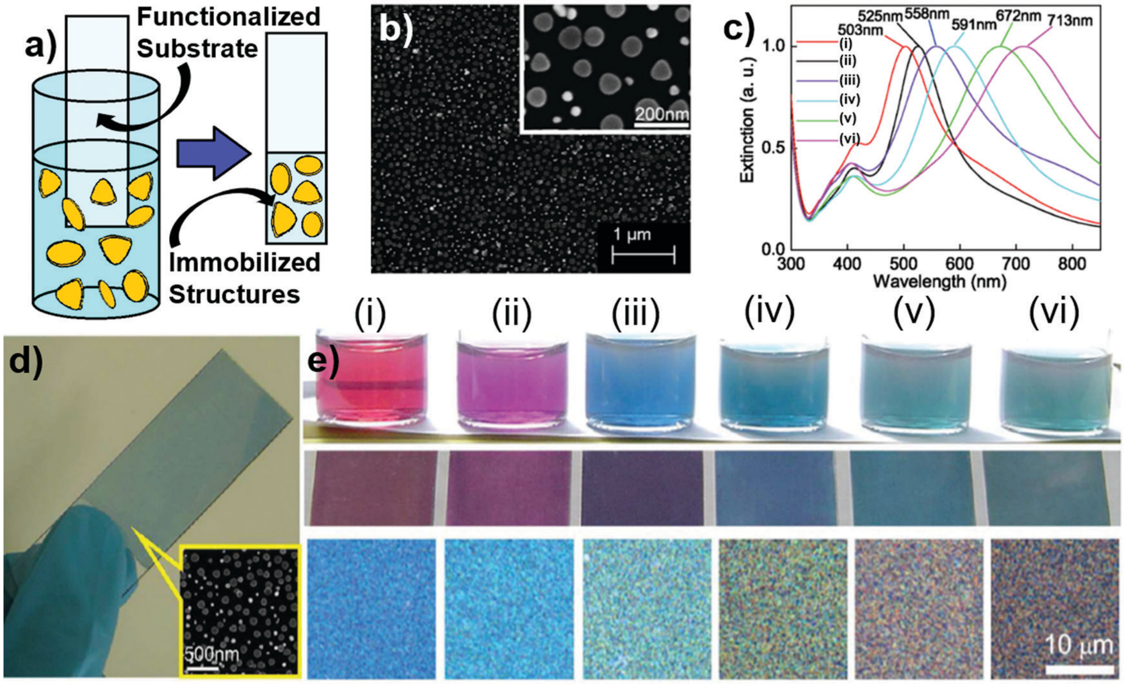

Fig. 1 (a) Schematic of the method used to anchor colloidal nanoplates to a substrate surface through chemisorption. (b) SEM image of Ag nanoplates as well as a smaller number of roundish nanoparticles that have been chemisorbed onto a Si substrate. (c) Normalized extinction spectra of nanoplate-decorated glass surfaces for structures of varying diameters. Optical images of (d) a nanoplate-coated glass slide and (e) the various nanoplate colloids (diluted compared to those used in the assembly process) and the resulting glass surface.Fig. 1b–e adapted with permission from ref. 15. Copyright 2011 American Chemical Society.

using aqueous solutions and which is amenable to a wide variety of substrate materials. Major deficiencies include an assembly process that does not facilitate the organized arrangement of nanoplates into the close-packed configurations that favor plasmonic hot spot formation and a nanostructure–substrate interface that is compromised by linker molecules. Moreover, the quality of the so-formed surface is highly dependent on the shape- and size-purity of the colloid. It should, however, be noted that several groups have attained a shape purity significantly higher than the colloid using a post-assembly technique in which tape is applied to the surface and then removed,[17–19] a procedure that selectively removes more loosely bound nanostructures having roundish or polyhedron geometries.

Also worthy of mention are two related strategies in which colloidal nanoplates are attached to surfaces without the use of a surface linker. The first sees colloidal Ag nanoplates chemisorb to graphene sheets placed within the suspension.[16] In the absence of a linker, the arrangement allows for enhanced coupling between the two materials. The nanoplate-decorated graphene sheets were then spin-coated onto Si substrates and dried. The second relies on the attachment of colloidal Ag nanoplates to the surface of filter paper.[14] In this case, the filter paper facilitates nanostructure adsorption with a texture that allows for the high surface loading of triangular nanoplates, a combination that substantially improves plasmonic hot spot formation.

**2.1.2 Solvent evaporation assembly.** When a drop containing nanostructures is applied to the surface of a substrate, the evaporation of the liquid component will inevitably leave the nanostructures resting on the substrate surface. The simplicity of the method is, however, in stark contrast to the complexity of the underlying physics governing the evaporation process[87,88] and the motions of the nanostructures within the vanishing droplet.[89] When the concentration of nanostructures within the droplet is sufficiently low, the evaporation process leaves isolated structures or small clusters on the surface. At the opposite extreme, where the nanostructure concentration is high, an evaporating drop will cause nanostructures to pile up at the receding contact line where the substrate and liquid meet. With nanostructures continuing to collect in this so-called accumulation zone, the receding contact line eventually becomes pinned, at which point it continues to evaporate, leaving a disorganized three-dimensional aggregate of nanostructures on the surface (*i.e.*, the 'coffee ring' effect[90]). Between these two extremes, however, lies a parameter space that if carefully manipulated can give rise to organized assemblies of close-packed nanostructures.[87,91] Although such techniques have been widely applied, their application to nanoplates presents unique challenges and opportunities.

Solvent evaporation assembly has been routinely used to obtain supported nanoplates by merely drop-casting colloids onto planar surfaces[13,22,24–29] (Fig. 2a) or TEM grids.[92] Although the resulting assemblies often exhibit some degree of order, it has proved quite challenging to produce close-packed monolayers even over limited areas. Unlike spherical nanostructures, which readily assemble into close-packed formations, the organization of triangular nanoplates into such arrangements places additional constraints on the assembly process since it must provide for the in-plane rotational degrees of freedom needed to accommodate a three-fold symmetric object. The lack of shape- and size-control inherent to many triangular nanoplate syntheses further aggravates any semblance of long-range order. Nevertheless, significant progress has been made in this regard, and in doing so, has realized assemblies that are highly valued for the plasmonic hot spots that occur where the tips of the nanotriangles meet.

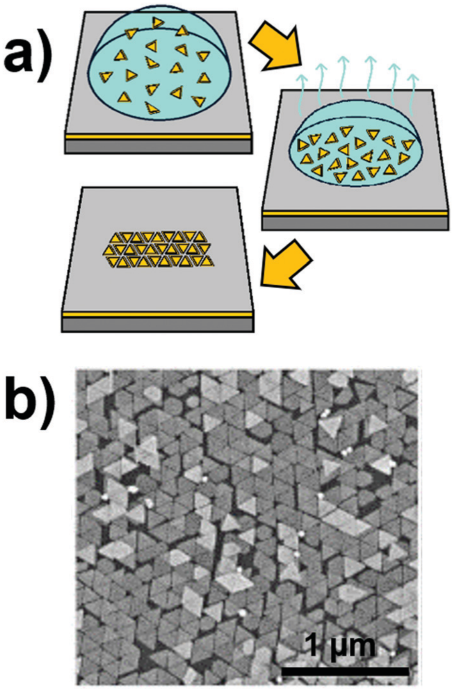

Fig. 2 (a) Schematic showing triangular nanoplate assembly induced by an evaporating droplet and (b) an SEM image of the close-packed array formed. Fig. 2b reproduced with permission from ref. 30. Copyright 2010 WILEY-VCH.

The environment within an evaporating drop is characterized by internal flow patterns arising from differential evaporation rates across its surface. Such flows drive nanostructure motions within the drop as its contact line recedes. Nanoplates within the drop inevitably interact with each other, and as such, the coulombic forces between structures decide whether the assembly proceeds in an organized or haphazard fashion. With these interactions being largely decided by the manner in which the nanoplates are capped with surface agents, the choice of agent becomes paramount. CTAB (cetyltrimethyl ammonium bromide), a capping agent used in numerous nanoplate syntheses, has proven unsuitable for the assembly of close-packed nanotriangle monolayers due to the indiscriminate attachment of nanoplates to one another, a characteristic that leads to highly disordered three-dimensional aggregates.[30] In response, assembly processes have invoked a ligand-exchange procedure in which CTAB is displaced with a capping agent that is more amenable to an orderly assembly process. Walker *et al.*[30] were the first to demonstrate such a procedure for triangular Au nanoplates. Prior to the evaporation-driven assembly process, a procedure was applied in which CTAB was displaced by TMA

(*N*,*N*,*N*-trimethyl(11-mercaptoundecyl)ammonium chloride). Fig. 2b shows an SEM image of the assembled monolayer. It reveals an arrayed pattern where local order is observed but where the close-packing of structures is interrupted on intermediate length scales. In a recent demonstration, Liyanage *et al.*[93] not only demonstrated the assembly of suitably capped Au nanotriangles but also showed that the surface functionalization of the Si substrate could act as a programmable synthetic lever able to controllably induce the assembly of nanoplate bilayers and trilayers. Kim *et al.*,[27] using triangular Au nanoplates with beveled edges, showed that subtle differences in the nanoplate geometry can have a decided impact on the assembly process. Ye *et al.*[28] showed that the assembly is strongly influenced by the nanoplate density within the droplet, with high densities giving rise to face-to-face configurations instead of close-packed arrangements. Collectively, the literature shows that capping agents, the shape and size uniformity of the colloid, substrate surface preparation, nanoplate density, and the evaporation rate all play key roles in finding the correct balance needed to guide the assembly process along a path yielding organized surfaces of nanoplates.

Although solvent evaporation assembly has proven successful in generating densely packed monolayers and bilayers of nanoplates, it is less than satisfactory from a number of standpoints. The technique struggles to produce large areas of arrayed structures where a surface coverage of even 0.055 mm$^2$ represents a significant benchmark.[30] Moreover, the arrayed areas are typically fragmented, showing patches of empty substrate adjacent to arrayed areas. Additionally, exerting parametric control over the assembly process is challenging because an evaporating droplet represents a rapidly evolving system. The degree to which the nanostructures adhere to the substrate is also in question since there is an inherent contradiction in having well-bonded structures and an assembly process requiring nanoplate mobility.

Noteworthy is that Fu *et al.*[31] devised a technique for forming multilayer assemblies of triangular Au nanoplates that is closely related to the solvent evaporation method. The assemblies were formed through the placement of a colloid onto a 30° tilted Si substrate maintained in a high humidity environment at elevated temperatures (*i.e.*, 60 °C). A significant aspect of their process is that the self-assembly into close-packed arrangements occurred for CTAB-capped nanoplates, hence eliminating the need for a ligand-exchange process. Also of note is the study carried out by Sun *et al.*[23] in which Ag nanoplates with a high degree of shape and size dispersity were drop-cast onto a flexible polyethylene glycol terephthalate (PET) substrate followed by a 65 °C heat treatment for 12 h under vacuum. The resulting assemblies were of high density and multilayered.

#### 2.1.3 Air–liquid interfacial assembly.

Interfacial assembly is emerging as a powerful tool for the formation of colloidal nanostructures into close-packed monolayers.[94–96] The approach takes advantage of the fact that nanostructure confinement at an interface is thermodynamically favored to an extent that surface-adsorbed nanostructures are trapped in what is, in essence, a two-dimensional coordinate system. With a liquid interface simultaneously providing surface mobility to the trapped structures, it creates an ideal environment for their assembly into ordered configurations. Once this occurs, the entire assembly can be transferred to the surface of a substrate. Such self-assembly processes typically proceed by applying drops of a colloid dispersed in an organic solvent to the surface of pure water, followed by the evaporation of the solvent. As the solvent evaporates, nanoparticles accumulate at the air–liquid interface forming nanoparticle islands that grow in size and then merge to form large-area monolayer thick assemblies. This approach has been widely used to assemble both organic and inorganic nanomaterials. Achievements as well as a detailed understanding of the mechanisms guiding air–liquid interfacial assembly have been recently reviewed by Liu *et al.*[96] With nanostructure shape being an important mechanistic aspect to any interfacial assembly process, the application of this technique to triangular nanoplates is one that has garnered significant interest.

The air–liquid interfacial assembly process requires that the nanostructures be dispersed in an organic solvent prior to its application to the water surface. This alone poses challenges for the assembly of triangular Au nanoplates because the most synthetically robust growth modes utilize aqueous solutions with CTAB as the capping agent. CTAB is particularly troublesome because standard procedures for collecting and redispersing nanostructures into organic solvents lead to their irreversible aggregation. Scarabelli *et al.*[32] circumvented this issue using a multistep multiday CTAB-to-PVP ligand-exchange process followed by nanoplate redispersal into an ethanol–hexane mixture. When the mixture is suitably applied to the water surface, its immiscibility and low surface energy cause it to evenly spread out. In time, evaporation processes lead to the formation of a monolayer thick assembly over square-centimeter areas. Their work demonstrated that nanotriangles with edge lengths varying from 50 to 150 nm could be assembled in this manner. Lee *et al.*[33] later demonstrated that the mere addition of PVP to the aqueous nanoplate solution 15 min prior to centrifugation was sufficient to allow for triangular nanoplate redispersal into an ethanol–hexane mixture. In doing so, they too were able to assemble triangular nanoplates over square-centimeter areas. The extraction process used to transfer the two-dimensional assembly to the substrate surface was the Langmuir–Schaeffer method[95] in which a substrate is brought into contact with the assembled layer and then removed. Fig. 3a and b shows a schematic of the removal process and an SEM image of the Au nanotriangle array after being transferred to a Si substrate. The array shows densely packed structures exhibiting short-range order.

With large-area capabilities, scalability, ease of fabrication, efficient use of nanomaterials, amenability to a wide range of substrate materials, and cost effectiveness, the air–liquid interfacial assembly technique has, in many ways, surpassed the other colloid-to-substrate transfer methods in terms of competencies and appeal. Nevertheless, further refinement to both the technique and the associated colloidal syntheses will be required if it is to emerge as a robust platform for forming close-packed arrays of triangular nanoplates. Arrays formed to

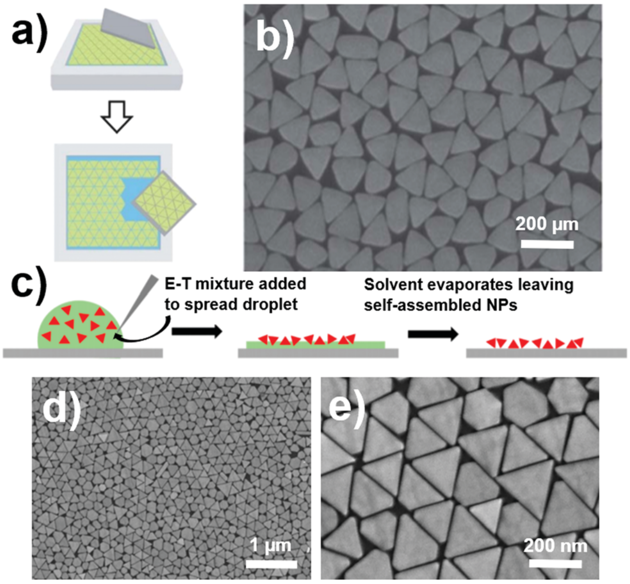

Fig. 3 (a) Schematic of the Langmuir–Schaeffer method used to transfer triangular Au nanoplates to a Si substrate and (b) an SEM image of the resulting surface. (c) Schematic of a straightforward method for forming substrate-based nanotriangle arrays in which an ethanol–toluene mixture is added to a drop of an aqueous colloid followed by evaporation. SEM images of Au nanotriangle assemblies derived from this simple method at (d) low- and (e) high-magnification. (a and b) Reproduced with permission from ref. 33 and (c–e) adapted with permission from ref. 34. Copyright 2013 Royal Society of Chemistry. Copyright 2017 American Chemical Society.

date are challenged in terms of sustaining a regular periodicity, showing nanostructure misalignments, vacancies, misshapen and oddly sized structures, and fragmented areas. Additionally, the technique is currently limited to just close-packed arrangements and it has also not yet demonstrated a multilayer assembly capability for triangular nanoplates.

Interestingly, Liebig *et al.*[34] devised a simple method for obtaining close-packed arrays of Au nanotriangles that is closely related to the air–liquid interface assembly technique. Their process, which is shown schematically in Fig. 3c, sees a drop of the aqueous colloid placed on the substrate surface, after which it is injected with an ethanol–toluene mixture. The injection leads to solvent spreading that, when followed by evaporation, causes the assembly of triangular nanoplates on both quartz and Si substrates. For this method, the nanotriangle colloid synthesis utilizes a phospholipid–AOT mixture (*i.e.*, PL90G and adioctyl sodium sulfosuccinate) instead of CTAB to promote Au nanotriangle growth.[97] Moreover, they showed that an appropriately chosen ethanol–toluene ratio was a critical factor if nanotriangle stacking is to be avoided. Both low- and high-magnification SEM images of the arrays produced are shown in Fig. 3d and e. Using this method, the authors estimated that they assembled as many as three billion triangular nanoplates over a 1 cm$^2$ area.

### 2.1.4 Assembly of dimers.

Once nanoplates are immobilized on the substrate surface as standalone structures, their surfaces can be functionalized such that an encounter with a colloidal nanostructure will lead to its attachment. In this manner, substrate-bound dimers separated by linker molecules can be formed. In a series of impressive demonstrations, Wang and co-workers assembled both homodimers and heterodimers from Au nanostructures where at least one of the two structures is a nanoplate.[35–39] They then analyzed the optical response of the substrate-bound dimers at the single-particle level. Their findings reveal a remarkable set of plasmonic responses activated by coupling phenomena between the dimer structures as well as the underlying substrate. This section describes the methods by which these dimer structures are formed.

Fig. 4a shows the stepwise scheme used to assemble substrate-based dimers as applied to the formation of nanodisk–nanorod

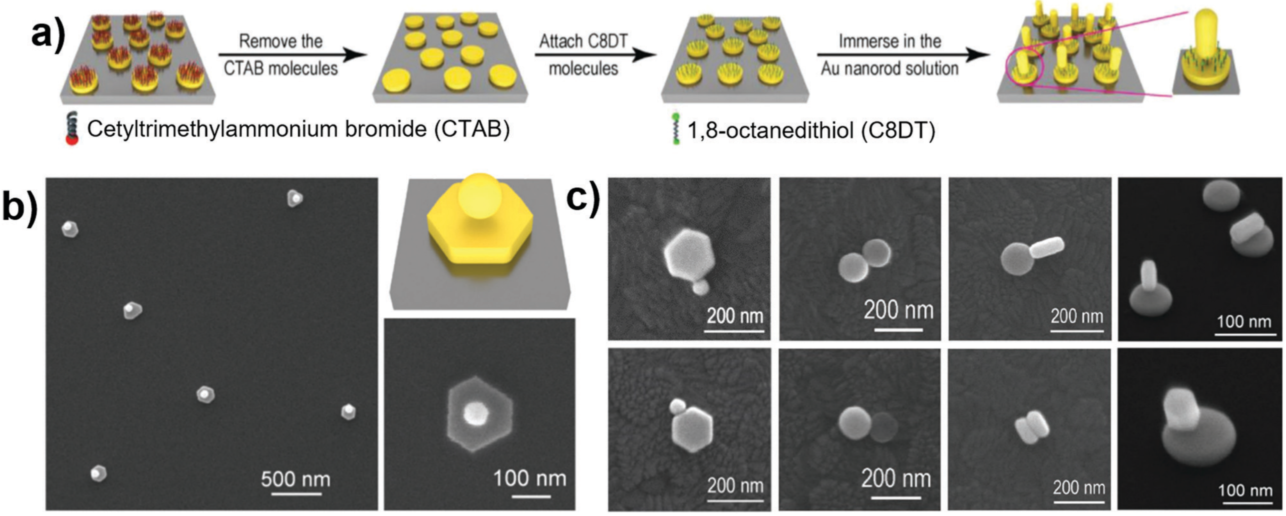

Fig. 4 (a) Schematic of the assembly process used to yield nanodisk–nanorod heterodimers. (b) Low- and high-magnification SEM image of nanoplate–nanosphere Au heterodimers and an associated schematic. (c) SEM images of dimer structures formed from various nanoscale building blocks. (a and b) Adapted with permission from ref. 39 and 35, respectively. (c) Adapted with permission from ref. 37, 38 and 39. Copyright 2021 WILEY-VCH. Copyright 2020 Royal Society of Chemistry. Copyright 2017 Royal Society of Chemistry. Copyright 2018 WILEY-VCH. Copyright 2021 WILEY-VCH.

heterodimers.[39] CTAB-capped nanodisks are first formed in a colloidal synthesis that sees faceted nanoplates synthesized and then anisotropically etched to yield a circular geometry.[98] The structures are then drop-cast onto a freshly cleaned substrate and dried under an $N_2$ gas flow. The CTAB is then removed from the nanodisks with ethanol. Once cleaned, the nanodisks are functionalized in an overnight procedure that leads to the formation of a 1,8-octanedithiol self-assembled layer on the Au surface. By having two thiol groups located at the opposite ends of an alkyl chain, the 1,8-octanedithiol molecule allows for a covalent Au–S bond with the nanodisk while presenting an equivalent bonding site at its opposite end. When placed in a water/acetonitrile mixture containing a Au nanorod colloid, encounters will occur in which rods are captured at these bonding sites so as to realize a dimer configuration. It is important to note that the two Au structures are not in contact but are instead separated by dithiol linkers that maintain a 1–2 nm nanogap.

Fig. 4b shows both low- and high-magnification SEM images of nanoplate–nanosphere heterodimers in which the sphere is affixed to the top surface of the nanoplate. This specific dimer assembly process gave rise to the highest reported yields ($\approx 90\%$).[35] With the ability to introduce various building blocks into the assembly process and a variety of distinct attachment points, there exist numerous dimer configurations including those shown in Fig. 4c. The nanodisk-nanorod configuration is particularly interesting in that there exists a strong preference for the nanorod to have its long axis pointing away from the surface of the disk. The authors attributed this preferential orientation to the lower number density of CTAB molecules present on the high curvature ends of the nanorod as it allows for the more effective penetration of the dithiol linkers.[39]

The dimer structures realizable through this assembly process have demonstrated extraordinary polarization-dependent optical properties attributable to plasmonic responses brought about by (i) light confinement within the nanogap, (ii) symmetry-breaking configurations, and (iii) interactions with high index of refraction substrates such as Si. Various configurations have resulted in prominent Fano resonances,[37] the strengthening of substrate-induced Fano resonances,[35] and directional scattering.[39] Although these dimer structures now have a proven ability to manipulate light, such functionalities have only been observed in single-particle optical measurements. There, hence, remains the somewhat daunting challenge of fabricating identical dimer structures at high density and high yield where suitably applied controls see every dimer orient identically on the substrate surface.

## 2.2 Syntheses at the liquid–substrate interface

With colloidal syntheses exerting exacting controls over nanostructure growth modes, a related approach sees these same chemistries performed directly on substrate surfaces immersed in liquid media. The general approach is conceptually appealing in that there exists an entire library of colloidal synthetic protocols that can, in principle, be practiced at the liquid–substrate interface. Moreover, the substrate itself adds a new set of potential synthetic levers to nanostructure syntheses that are derived from its optical, electronic, chemical, and morphological properties. Although such approaches have been applied to the growth of a wide variety of substrate-based nanostructures,[99] their application to nanoplates has proved more challenging. One of the main hurdles has been seeding nanoplate growth in high yield, a requirement that is far more important than it is in colloidal growth modes since nanostructure shape purification processes such as centrifugation and depletion flocculation are impractical for nanostructures that are rigidly attached to the substrate surface. Presented in this section are two approaches for realizing nanoplate growth at the liquid–substrate interface where the key difference is the method by which the two-dimensional growth mode is seeded.

**2.2.1 Substrate-mediated growth.** In a synthesis that is remarkable in its simplicity, Sun and co-workers demonstrated Ag nanoplate growth on n-type GaAs substrates.[40–43] The room temperature synthesis merely entails the removal of the native oxide layer from the GaAs substrate followed by the placement of a drop of aqueous $AgNO_3$ on its surface. In a matter of minutes, Ag nanoplates with a growth trajectory that is out of the surface emerge where the synthesis can, at any point, be terminated by rinsing away the reactant. SEM images of the structures produced show highly faceted nanoplates at densities of $1 \times 10^9$ cm$^{-2}$ (Fig. 5a and b). TEM characterization reveals large-area [111]-oriented planar surfaces (Fig. 5a, inset). The selected area electron diffraction (SAED) pattern also exhibits the $\frac{1}{3}\langle 422\rangle$ reflections that are nominally forbidden for an fcc metal but which arise due to stacking fault defects along the [111]-axis.[100] Their presence is important in that these symmetry-breaking defects are considered mechanistically crucial to the emergence of a two-dimensional growth mode.[101,102] TEM analysis also reveals that nanoplate growth is accompanied by the formation of an oxide on the substrate surface that is only penetrated by the portion of Ag nanoplate formed in the earliest stages of growth (*i.e.*, the seed). Additionally, syntheses carried out show that (i) variations to the $AgNO_3$ concentration impact the nanoplate thickness with larger values leading to thicker plates, (ii) nanoplate orientation is unaffected by changes to the crystallographic orientation of the substrate, (iii) the growth mode allows for nanoplate growth on n-type Si substrates but with a somewhat diminished nanoplate quality, and (iv) the same growth mode is amenable to the formation of Pd nanoplates but not of Au.

Although the nanoplate growth proceeds by simply placing aqueous $AgNO_3$ on the substrate surface, it is incorrect to surmise that this synthesis requires only a single reactant because it is the oxidation of GaAs that drives the reaction. With the understanding that the substrate is synthetically active, Sun *et al.*[42,43] proposed a detailed mechanistic framework, the essence of which is described here. An important aspect of their model is that the nucleation of Ag seeds on the substrate surface is a distinct and separate process from a slower two-dimensional growth that gives rise to nanoplate formation. The early-stage growth, which is reliant on the reduction of $Ag^+$ ions by electrons trapped in surface states or defects near the conduction band ($E_c$) of n-type GaAs, is rapid but becomes unsustainable as the supply of these electrons is

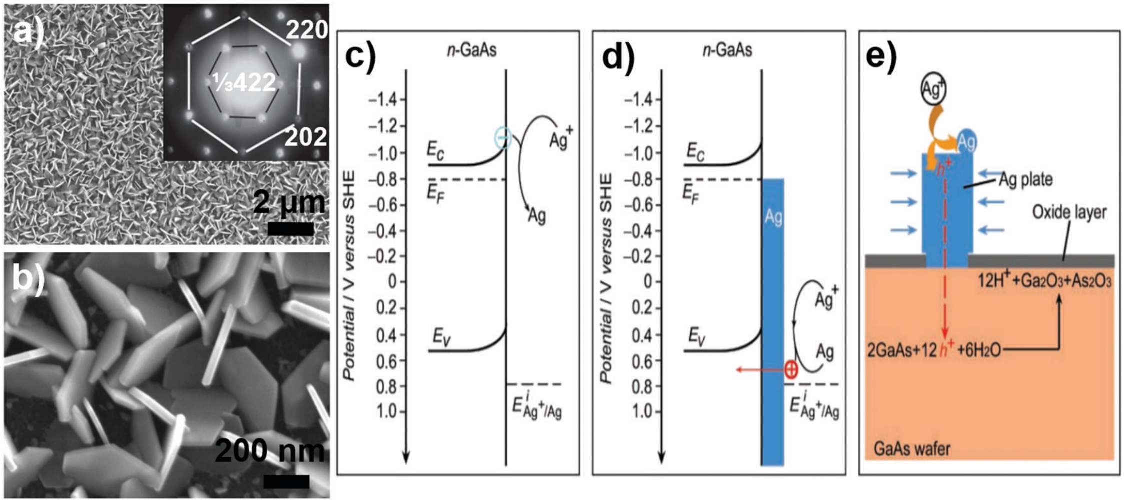

Fig. 5 SEM images at (a) low- and (b) high-magnification of Ag nanoplates formed by a GaAs substrate-mediated growth. The inset to (a) is a SAED pattern for a single nanoplate taken along the [111] zone axis. Energy level diagrams showing the $Ag^+$ reduction processes leading to (c) seed and (d) nanoplate growth. (e) Schematic showing the chemical processes responsible for Ag nanoplate growth on n-type GaAs. (a), (b) and (c)–(e) were adapted with permission from ref. 43 and 42, respectively. Copyright 2010 American Chemical Society. Copyright 2010 WILEY-VCH.

exhausted. Fig. 5c schematically shows this reduction process from the standpoint of the energy band diagram of GaAs as altered by the band bending that occurs when it comes in contact with aqueous $AgNO_3$. Each of the Ag nanocrystals formed in this process then act as seeds with the potential to initiate nanoplate growth and where the nucleation of additional seeds becomes less probable as the oxide builds up on the substrate surface. The initially high rate of reaction is also beneficial in that it is likely to promote the stacking fault defects that favor the two-dimensional growth mode. The late stage nanoplate growth, as shown in Fig. 5d, is reliant on the reduction of $Ag^+$ at the seed surface that is enabled by the injection of holes ($h^+$) that then diffuse through the growing nanoplate and eventually enter the valence band ($E_V$) of GaAs *via* the seed–substrate connection point. These holes then facilitate a reaction that sees the surface of GaAs oxidized. Fig. 5e schematically displays the overall reaction given by:

$$12AgNO_3 + 2GaAs + 6H_2O \rightarrow 12Ag + Ga_2O_3 + As_2O_3 + 12HNO_3$$

The substrate-mediated synthesis devised by Sun and co-workers is advantageous in terms of ease of synthesis, a product that is free of capping agents, and where a direct electrical connection exists between the nanoplates and substrate. It is disadvantageous in that (i) nanoplate shape, size, and orientational control is lacking, (ii) the synthesis has only been demonstrated over limited areas using small drops of reactants (*i.e.*, 10's of μL), (iii) it has only been successfully applied to Ag and Pd, and (iv) the choice of substrate is limited by the growth mechanism. It is, however, noteworthy that steps have been taken to mitigate some of these shortcomings by galvanically replacing Ag nanoplates with $Au^{3+}$ to obtain alloyed structures that are chemically more stable[45] and through the demonstration of a light-mediated growth step that is able to induce Ag nanoplate growth on a p-type GaAs substrate.[42] Also of note is the recent work of Zhao *et al.*[44] that demonstrated site-selective Ag nanoplate growth on GaAs at substrate positions that underwent deformation due to a nanotip indentation process.

### 2.2.2 Seed-mediated growth.

In one of the earliest attempts at nanostructure growth at the liquid–substrate interface, Geddes and co-workers[48] carried out a triangular nanoplate synthesis using the procedure schematically shown in Fig. 6a. The overall strategy used was one where a colloid of Ag seeds was prepared and then attached to a glass slide functionalized with 3-(aminopropyl) triethoxysilane (APS) to promote seed adhesion, after which the substrate was rinsed and submersed in a growth solution promoting nanoplate growth. Although this work provided a proof-of-principle demonstration of the seed-mediated growth method as it pertains to nanoplates, the synthesis was unsatisfactory in that it yielded nanoplates with irregular shapes in low yield. Since this demonstration, a number of studies have appeared in the literature that have advanced variations to the same overall approach,[46,47,49–53,55–57] three of which are highlighted in this section.

In the first example, Zamborini and co-workers[103] carried out a Au nanoplate synthesis that yielded a surface populated by both nanoplates and near-spherical Au nanoparticles (Fig. 6b). An interesting aspect of this work is that they showed that the vast majority of three-dimensional nanostructures could be selectively removed from the substrate in a post-synthesis procedure where the sample was exposed to either sonication or the attachment of an adhesive tape that is then peeled off. Using this shape-purification method, it was possible to obtain nanoplate yields as high as 95%, albeit at a rather low areal density (Fig. 6c). In the second example, Muench *et al.*[49] formed Ag seeds on substrates and exposed them to a 70 °C growth solution containing potassium sodium tartrate, iron(III) nitrate, $AgNO_3$, $HNO_3$, and $NH_3$. The reaction yielded an interconnected network of nanoplates with a growth trajectory that is directed away from the substrate surface (Fig. 6d). Key to this

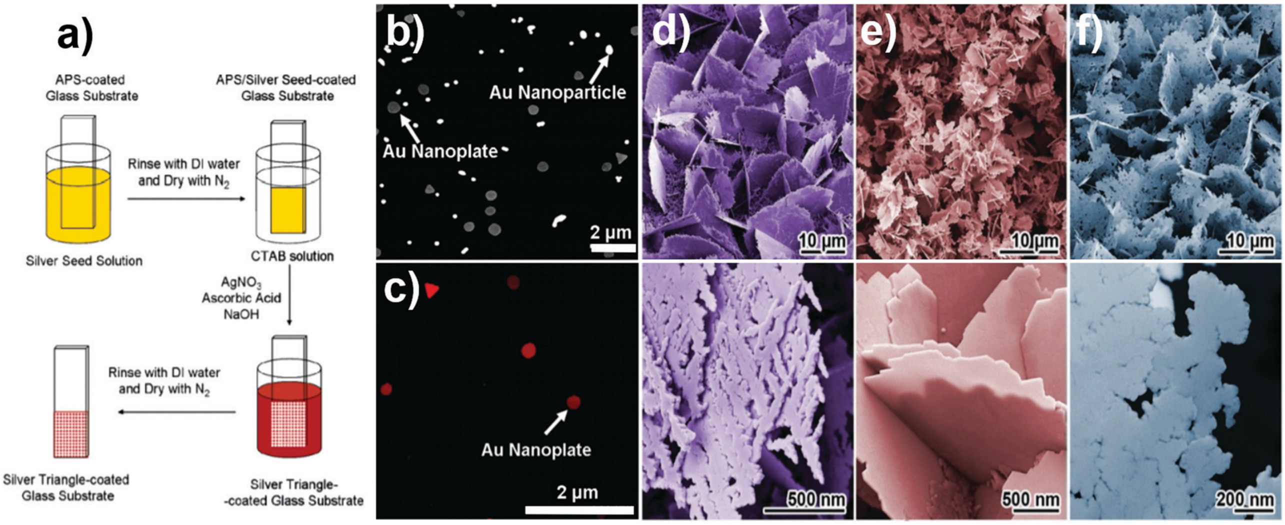

Fig. 6 (a) Schematic showing a seed-mediated method for Ag nanoplate growth on an APS-functionalized substrate. (b) SEM image of a sample synthesized using the seed-mediated approach showing near equal numbers of nanoplates and nanoparticles and (c) an AFM image of a surface formed using the same synthesis followed by a sonication procedure that selectively removes unwanted structures. (d) SEM images of an interconnected nanoplate network taken at low- and high-magnification and the altered morphologies obtained when reaction kinetics are (e) enhanced and (f) diminished. (a–f) Reproduced with permission from ref. 48, 103, and 49, respectively. Copyright 2005 American Chemical Society. Copyright 2010 American Chemical Society. Copyright 2018 WILEY-VCH.

success was the formation of an Fe(III) tartrate complex that acted as a shape-directing agent able to promote a two-dimensional growth mode. Enhanced reaction kinetics, obtained through an increase in pH, gave rise to nanoplates with an altered geometry (Fig. 6e) and allowed for a self-seeding modality. Reduced reaction kinetics, caused by the addition of CTAB, also altered the reaction product (Fig. 6f). The significance of this work is heightened by the fact that the synthesis was amenable to a wide variety of substrates including those that are metallic, insulating, flexible, and curved. In the third example, Xu *et al.*[104] induced Ag nanoplate formation on glass substrates using a light-mediated liquid-state reaction. By focusing 800 nm femtosecond laser pulses onto a substrate surface submerged in a growth solution containing $AgNO_3$, trisodium citrate, and aqueous ammonia, they were able to self-seed nanoplate formation at just the illuminated site. This capability allowed them to raster the laser beam in a set pattern to obtain arrays of well-defined micrometer-scale areas from which nanoplates emerged while leaving the remainder of the substrate bare. It should also be noted that the substrate-based seed-mediated method has also been used to generate periodic arrays of Au nanoplates using seeds defined using lithographic methods in combination with directed assembly,[53,54] a subject that is discussed separately in Section 2.5.1.

## 2.3 Electrochemical syntheses

Electrochemical methods for generating substrate-based nanostructures[105–109] are fundamentally different from other solution-based methods in that ions are reduced onto the surface of a substrate not by a reducing agent but by electrons derived from an external power supply. With the substrate having to play the dual role of nanostructure support and electrode, it is imperative that it be conducting. Nanostructure shape-control is most readily achieved if an insulating sacrificial template is first formed on a substrate surface having nanopores that extend over its entire thickness (*e.g.*, anodic aluminum oxide,[110] porous silica,[111] polymeric micelles[105]). Electrodeposition onto just the exposed electrode leads to nanostructure formation whose shape mimics that of the pore, after which the template is removed. Alternatively, shape-control can be achieved by adjusting the liquid-state chemical environment of the electrolyte so as to selectively promote the growth of particular geometries. The method utilizes many of the same shape-controlling agents as employed in colloidal syntheses,[112] but where their effectiveness can be altered by the applied potential. With a lack of suitable templates, nanoplate syntheses through electrochemical means have relied exclusively on the latter methodology.

**2.3.1 Electrochemical cell methods.** When compared to other methods for forming substrate-bound nanoplates, electrochemical syntheses are truly unique in that they allow for the application of a distinct set of synthetic levers. These levers are complimented by an equally distinct set of reaction monitoring techniques from which an understanding of the deposition can be derived. As a consequence, these nanoplate syntheses share commonalities but where the diverse nature of the technique leads to a reaction product that is often decided by the nuances of a particular approach. Fig. 7a shows a schematic of the basic configuration for a three-electrode electrochemical cell in which a working electrode, counter electrode, and reference electrode are immersed into an electrolyte containing ions of the target material and synthesis-specific additives. Nanoplate deposition takes place on the working electrode, and as a result, it defines the area over which deposition occurs and where its makeup is crucial in determining the reaction product. Most syntheses have

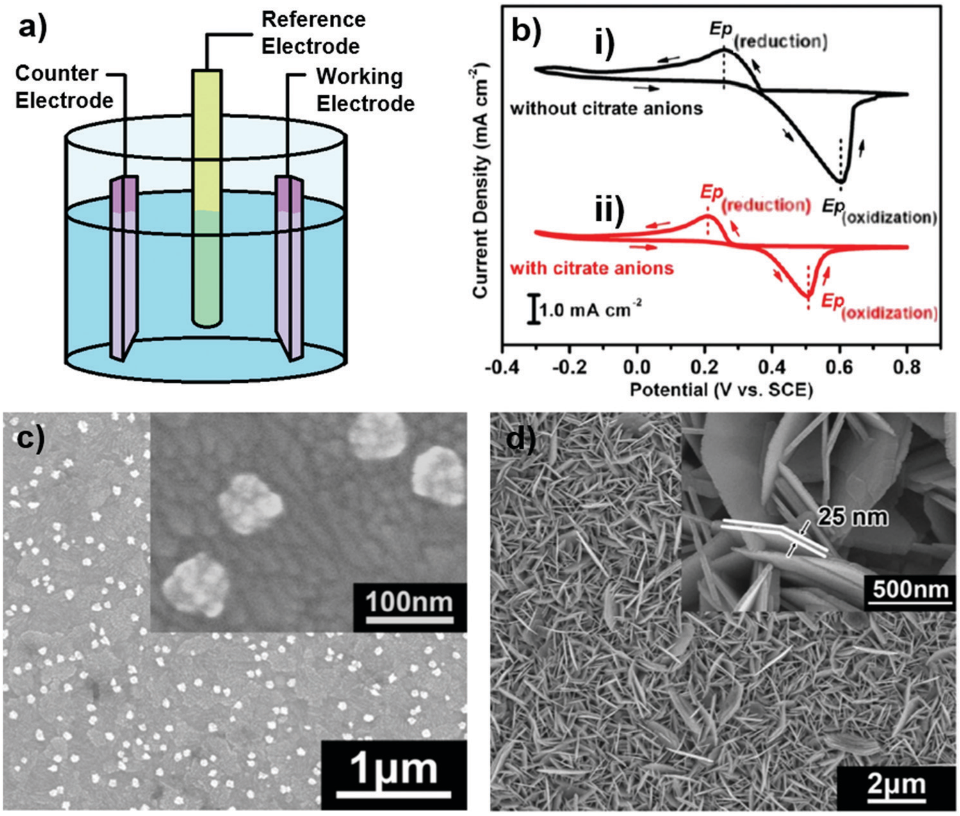

Fig. 7 (a) Schematic of an electrochemical cell. (b) Cyclic voltammogram traces carried out on an ITO substrate in an electrolyte of $AgNO_3$ and $KNO_3$ in the (i) absence and (ii) presence of aqueous sodium citrate. SEM images of (c) Ag seeds on ITO and (d) the Ag nanoplates derived from them. (b–d) Reproduced with permission from ref. 65. Copyright 2015 American Chemical Society.

employed insulating substrates onto which a continuous conducting film of either indium tin oxide (ITO)[62–66,72] or Au is applied.[59,60,68–71] ITO electrodes typically require that their surface be decorated with seeds able to promote nanoplate growth modes. Au electrodes can be advantageous in that they can self-seed metal nanoplates but a Cr underlayer is often required to ensure adhesion. Heavily boron-doped Si,[61] graphene,[58] and nickel foam-graphene[67] have also been successfully used as the working electrode. Pt is typically employed as the counter electrode but where nanoplate syntheses have also utilized graphite,[64] Ag,[113] and boron-doped Si.[61] Calomel[65,70,72] and Ag/AgCl[68,71] have been used as reference electrodes but where many nanoplate syntheses have opted to forego their use in lieu of a two-electrode modality. Nanoplates are typically formed at room temperature under ambient conditions. Although most studies have used standard electrochemical cell configurations for nanoplate syntheses, nonstandard techniques that have been employed include the (i) use of a working electrode that is slowly retracted from the electrolyte so as to obtain a time-dependent progression in the morphological evolution of the nanostructures from a single synthesis[62] and (ii) sonication of the entire cell as the growth proceeds.[67]

Once a suitable potential is applied to the electrochemical cell, positive ions within the electrolyte are reduced to a neutral species that readily deposits onto the working electrode. The local chemical environment around the electrode is strongly influenced by changes to the applied potential which in turn affects the deposition rate and the adsorption–desorption characteristics of any capping agents onto the emerging nanostructures. Nanoplate syntheses have been successfully carried out in potentiostatic[61,62,65,68,72] (*i.e.*, constant potential), galvanostatic[60,62,64] (*i.e.*, constant current), and potentiokinetic modes[69,70,113] (*i.e.*, the applied potential is cycled). The potentiokinetic mode provides more synthetic levers because the reduction and oxidation potentials, frequency, duty cycle, and total number of cycles all become adjustable parameters. Such capabilities also lend themselves to the use of cyclic voltammetry as a technique for monitoring deposition/dissolution cycles, information that can be used to target an appropriate deposition potential[65] and which provides key insights into the role that capping agents play in the reduction process.[65,70] In an elegant example, Wu *et al.*[65] used cyclic voltammetry to target the deposition potentials for both Ag seeds and nanoplates onto ITO surfaces. Fig. 7b shows the cyclic voltammogram traces obtained with and without the inclusion of citrate (*i.e.*, the capping agent) in the electrolyte. For both cases, well-defined oxidation and reduction peaks are apparent but where the peak potential ($E_p$) in both the reduction and oxidation peaks are shifted to lower potentials. The shift provides a clear indication that citrate anions inhibit the reduction of $Ag^+$ ions. In view of these results, potentiostatic conditions were chosen in which the applied potentials for seed and nanoplate depositions were set to $-0.4$ and 0.25 V, respectively, where the discrepancy in values allowed for the rapid formation of seeds while allowing for the mild overpotential that favors the formation of Ag nanoplates. Fig. 7c and d shows SEM images of the seeds and nanoplates formed. The use of cyclic voltammetry in defining nanoplate deposition conditions is a capability that is unique to electrochemical syntheses and which has been used to define the narrow deposition potential windows in which nanoplates grow.[65,72]

**2.3.2 Seeding electrochemically grown nanoplates.** Metal nanoplate electrochemical syntheses are heavily reliant on processing steps that ready the surface of the working electrode for nucleation events that effectively seed two-dimensional growth modes. In general, three seeding methods are used where, in all cases, the density of nanoplates is largely determined by the processing conditions. The first method forms seeds as a colloid of metal nanoparticles and then applies them to the substrate. Spin-coating provides the most straightforward method for applying seeds to an ITO-coated surface[62,63] but where poor uniformity in seed coverage can translate into nonuniformities in the nanoplate density. Far superior results in terms of uniformity can be achieved by functionalizing ITO with an APTMS (3-aminopropyltrimethoxysilane) layer that promotes seed attachment when submersed in a colloid.[64] This method also allows for the systematic variation of the seed density by varying the exposure time. The second method grows seeds electrochemically using conditions that provide a larger driving force than those used to promote nanoplate formation.[58,65,72] This seed nucleation step is driven by a short duration pulse (*i.e.*, 10's of milliseconds) at high-negative overpotential where multiple pulses can be used to increase the seed density. The seeds shown in Fig. 7c, which are about 70 nm in diameter and display numerous lobes, were produced by this method. The technique is advantageous in that it leads to high uniformity over large areas and can be carried out in the electrochemical cell immediately prior to the nanoplate synthesis. The third method nucleates nanoplates off a deposited Au film.[60,61,68–70] Although this method is sometimes referred to as seed-free, it is recognized that the defect structures known to promote nanoplate growth are also present in deposited Au films.[114]

**2.3.3 Electrochemical synthesis of nanoplates.** Nanoplates formed by electrochemical deposition collectively represent a diverse set of syntheses. The vast majority of the literature has, however, focused on the synthesis of noble metal nanostructures having an fcc crystal structure. As such, the diversity of synthetic protocols remain connected by recurring characteristics in terms of the parametric controls applied and the reaction products formed. In this section, emphasis is placed on these commonalities but where key differences are highlighted. Within this realm, the electrochemical synthesis of nanoplates has been carried out for Au,[68] Ag,[58–67] Pt,[71] Rh,[72] and Pd.[69,70]

For a standard metal nanoplate synthesis, the electrochemical growth solution is less complicated than that typically used in colloidal syntheses, often consisting of just a metal precursor and a shape-directing agent. Aqueous $KAu(CN)_2$,[68] $AgNO_3$,[60] $H_2PtCl_6$,[71] $RhCl_3$,[72] and $K_2PdCl_4$[69] have all been successfully used to source metal ions. Shape-directing agents are chosen that preferentially bind to the (111) facet of the particular metal being targeted. When supplied in excess, such agents quickly cap any newly formed (111) facets while providing unfettered access to others. In doing so, it allows the (111) facet to emerge as the dominant surface on the nanostructure. The choice of an effective shape-directing agent is, hence, metal-dependent and is mechanistically influenced by the binding affinities of particular agents to various facets. Shape-directing agents used in electrochemical syntheses include sodium citrate ($C_6H_5Na_3O_7$) for Ag[65] and Rh,[72] CTAB for Pd,[69,70] PVP (polyvinylpyrrolidone) for Ag,[60,62] and $H_3BO_3$ (boric acid) for Ag.[61] In this regard, the use of $KAu(CN)_2$ as the precursor in the synthesis of Au nanoplates stands out as unique in that no specific shape-directing agent was added.[68]

Although the various components needed for the electrochemical synthesis of metal nanoplates have been independently described, it should be recognized that all of these aspects are highly intertwined. A successful synthesis, hence, requires the convergence of a unique set of substrate, seed, applied voltage, metal precursor, and shape-directing agents, that when suitably combined launches a sequence of nucleation and growth events from which nanoplates emerge. To treat the capping agent concentration as an independent variable, for example, does not account for the fact that its need is dependent on the (i) size of the substrate, (ii) number of structures seeded and the size to which they are allowed to grow, (iii) degree to which the applied voltage alters its adsorption to particular metal facets, and (iv) the extent to which the metal precursor concentration raises or lowers the (111) facet protection required. Instead, nanoplate syntheses should be understood as interplay between numerous factors where small changes can upset the balance, resulting in either a gradual or sudden collapse of the growth mode. Notwithstanding, the literature generally points toward nanoplate growth parameters that favor the slow advancement of nanoplate growth fronts and where, for a set potential, the capping-agent-to-precursor concentration ratio represents an especially important interdependency.[65]

Nanoplates grown *via* electrochemical synthesis are distinct in that the growth trajectory is, more often than not, out of the substrate surface such that the edge of the nanoplate is pointing upward. As the nanoplates grow both vertically and laterally, their growth fronts inevitably collide and then merge to form an interconnected network. Fig. 8a shows a top view image of Au nanoplates expressing this configuration. The nanoplates are highly faceted and, while many of them grow vertically, others are slanted off the normal. When the same nanoplates are viewed in cross section (Fig. 8b), growth is also observed to have occurred near the substrate surface. If a nanoplate is viewed in isolation,[62] then its overall geometry is trapezoidal instead of hexagonal due to an apparent truncation by the substrate surface. Such breaks in symmetry are commonly observed when nanostructures are formed on planar surfaces because the substrate surface acts as a highly directional steric barrier to an otherwise symmetric growth mode.[99,115] Nanoplates produced in this manner can vary widely in size, ranging from hundreds of

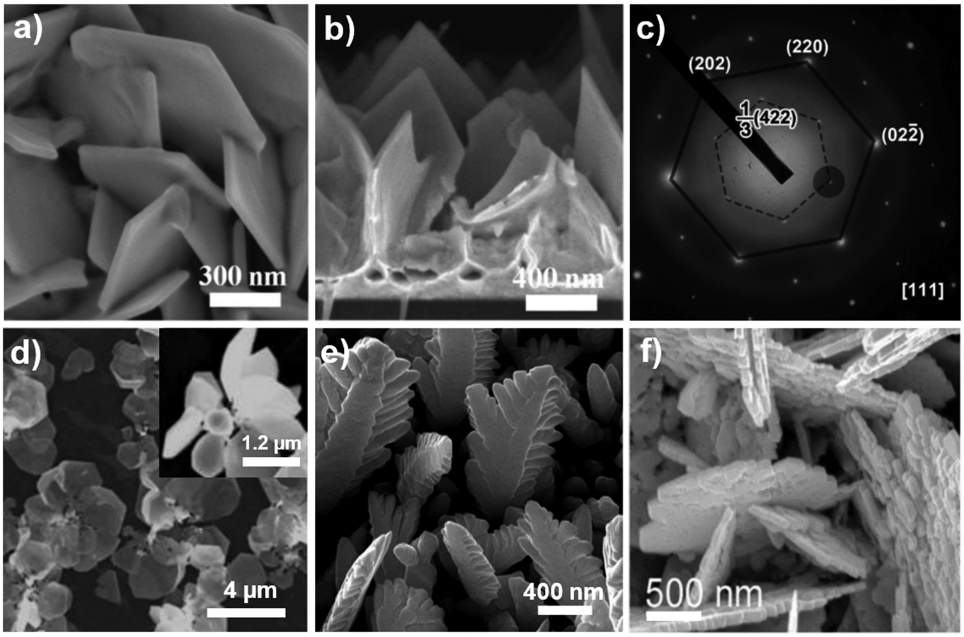

Fig. 8 SEM images of electrochemically grown Au nanoplates from a (a) top and (b) side view perspective. (c) TEM diffraction pattern derived from a Ag nanoplate exhibiting the forbidden $\frac{1}{3}\langle 422\rangle$ reflection associated with stacking faults. SEM images of (d) Ag and (e) Pd nanoplate formations with complex morphologies. (f) Roughened Ag nanoplates formed by simultaneously occurring electroplating and electrocorrosion processes. (a–e) Adapted with permission from ref. 68, 65, 58 and 70, respectively. (f) Adapted from ref. 61 with permission. Copyright 2011 American Chemical Society. Copyright 2015 American Chemical Society. Copyright 2013 Elsevier Ltd. Copyright 2009 American Chemical Society. Copyright 2014 Royal Society of Chemistry.

nanometers to 10 µm, with thicknesses typically in the 20 to 70 nm range. Nanoplate densities can be as high as $10^9$ cm$^{-2}$.[64] Although the degree of nanoplate anchoring to the substrate surface is synthesis-dependent, robustness to sonication has been widely reported.[62,65,69] When electrochemically grown, nanoplates offer both a high surface-area-to-volume ratio and durability, and as such, provide an intriguing platform for applications.

Despite their truncated shape and unusual growth trajectory, electrochemically grown nanoplates are, from a crystallographic perspective, quite similar to those grown by other methods. Fig. 8c shows a SAED pattern for a Ag nanoplate that has been removed from the substrate surface and laid down horizontally on a TEM grid. As anticipated, the diffraction pattern reveals the {220} reflections consistent with its planar surfaces expressing (111) facets. As is often the case, the diffraction pattern reveals the $\frac{1}{3}\langle 422\rangle$ forbidden reflections[100] associated with the stacking fault defects that provide the two-dimensional symmetry-breaking structure needed for planar growth.[101,102] The fact that they exist in electrochemically grown nanoplates[60,62,113] strongly suggests that the underlying growth mechanism shares many similarities with other synthesis methods. The sides of nanoplates vary considerably among the various metals and synthetic protocols, with rough, roundish, and highly faceted edges all having been observed.

Even though electrochemically grown nanoplate surfaces often express a morphology similar to that shown in Fig. 8a and b, it is by no means the only reaction product obtainable. In fact, the parametric windows from which such nanoplates emerge can be quite narrow. Outside of these windows, irregularly shaped structures are most commonly formed but where fascinating complex geometries such as those shown in Fig. 8d and e can also be realized. Yang *et al.*[61] devised a single-step synthetic scheme in which they intentionally roughened the Ag nanoplate surface in an effort to further increase its surface area. Using an electrolyte consisting of $AgNO_3$ and $H_3BO_3$ they were able to create an interplay between electroplating and corrosion processes that resulted in the roughened nanoplate surfaces shown in Fig. 8f. $H_3BO_3$ was decisively demonstrated as the shape-control agent while a local decrease in pH due to the formation of $HNO_3$ (nitric acid) near the working electrode was postulated as the cause of the corrosion. In a related strategy, they transformed both the Ag nanoplate morphology and composition by exposing them to aqueous $HPtCl_4$,[61] a process that led to the galvanic replacement[116] of Ag with Pt.

#### 2.3.4 Electrochemical growth mechanisms.

Even though the synthetic aspects of electrochemically grown metal nanoplates have been explored in detail, only a single study[65] has delved into the mechanistic constructs leading to their unique character. Although seeds lined with planar defects are a requirement for the synthesis of colloidal nanoplates, there is no direct evidence for their existence in any of electrochemical studies performed. Indirect evidence, however, does point toward their existence since such defects have been observed in electrochemically grown nanoplates (Fig. 8c). A significant percentage of the seeds derived from colloidal syntheses that are then deposited onto the working electrode almost certainly have such defects. Those formed through electrochemical means, such as the ones shown in Fig. 7c, are also likely to be riddled with defects due to the fast growth rate. Moreover, their lobed morphology and comparatively large size point toward a polycrystalline character, and as such, it is not surprising that each seed nucleates multiple nanoplates. Likewise, nanoplates derived from polycrystalline Au films are highly granular and contain a high density of stacking faults.[114] Additionally, it cannot be ruled out that electrochemical syntheses trigger the formation of planar defects or that the seeds restructure on the electrode prior to the nanoplate nucleation event. In any event, the need for a symmetry-breaking structure is apparent as (111) capping agents alone tend to favor octahedral geometries.[112] Furthermore, the existence of such symmetry-breaking defects, by themselves, cannot account for the near-vertical orientation of the nanoplates as this would require that the seeds have favorable crystallographic orientations relative to the underlying substrate (*e.g.*, [211], [110]).

Insights into the mechanisms by which electrochemical syntheses give rise to vertical growth trajectories are most readily obtained by monitoring the time-dependent growth sequence. Fig. 9a–c shows one such example where electrochemically deposited seeds were grown on an ITO substrate followed by nanoplate depositions lasting 300, 900, and 3600 s. It reveals that the early stages of growth are far less directional than those that emerge in the latter stages. With this understanding Wu *et al.*[65] forwarded the growth mode that is schematically shown in Fig. 9d. Its underlying premise is that vertical growth, while having little mechanistic advantage in the early stages of synthesis, becomes increasingly preferred as growth continues due to a $Ag^+$ concentration gradient that develops in the growth solution directly adjacent to the substrate. They argued that, by applying a relatively low potential to the working electrode, the driving force that brings $Ag^+$ ions would be sufficiently small so as to allow fast growing nanoplates to use up reactants before they reached the underlying structures. Moreover, nanoplates growing at oblique angles would have their growth fronts obstructed and then extinguished upon any encounter with a fast-growing vertical nanoplate. The benefit derived from such a gradient is supported by the work of Wang *et al.*[66] who demonstrated the mere placement of a semiporous AAO membrane just above the working electrode was a decisive factor in the emergence of a nanoplate growth mode where they too postulated that a favorable concentration gradient was responsible. Although it is difficult to affirm this growth mode for all electrochemical syntheses yielding vertical nanoplates, it is nevertheless conceptually appealing to invoke a mechanism by which other growth trajectories are neutralized.

### 2.4 Vapor-phase syntheses

The vapor-phase synthesis of substrate-based nanoplates with a single-crystal character is quite challenging for fcc metals. Such syntheses require that metal atoms arrive to a heated substrate if they are to have sufficient mobility to form organized configurations, yet the high temperatures needed tend to drive the structure toward morphologies that have low surface energies. Nanostructure morphologies, hence, tend toward the equilibrium

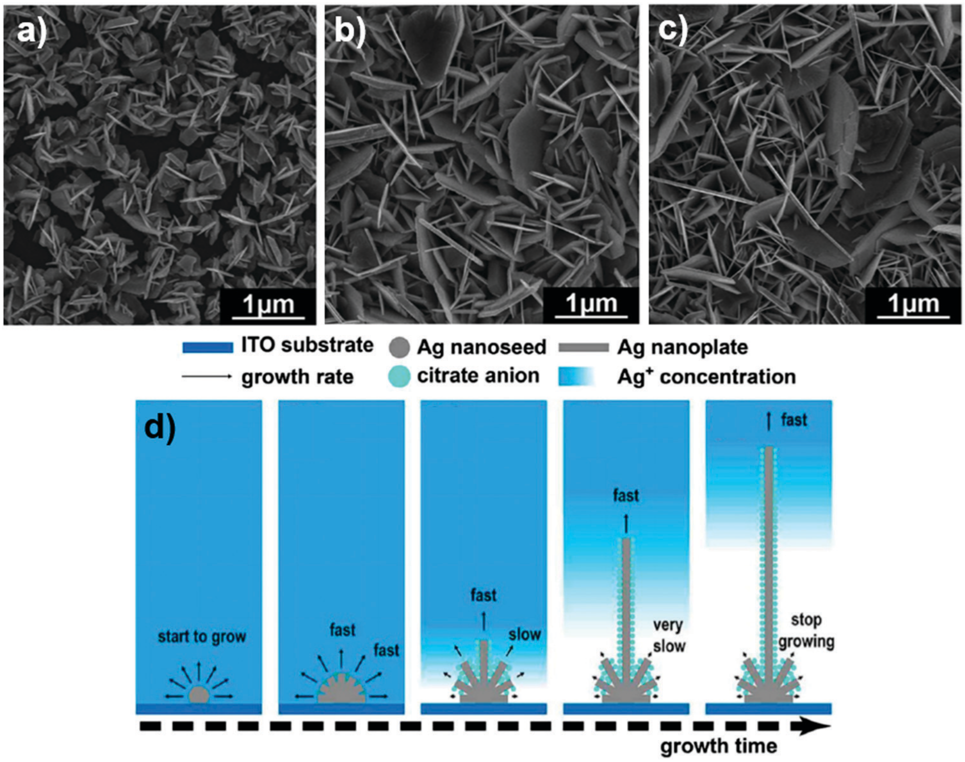

Fig. 9 SEM images showing the progression in Ag nanoplate growth for synthesis times of (a) 300, (b) 900, and (c) 3600 s. (d) Schematic illustrating the proposed mechanism by which vertical nanoplates emerge in the electrochemical synthesis of Ag. Reproduced with permission from ref. 65. Copyright 2015 American Chemical Society.

Wulff shape which is a truncated octahedron with eight hexagonal {111} facets and six square {100} facets.[117] With the nanoplate geometry representing an intrinsically high surface energy morphology, there exists an inherent contradiction that is difficult to resolve. Moreover, the high temperatures involved make the use of traditional capping agents impractical. As such, nanoplate formation in the vapor phase must rely on factors that alter adatom kinetics to drive the nanostructure geometry toward a nonequilibrium shape in an environment strongly favoring thermodynamic tendencies. Presented in this section are two vapor phase methods yielding nanoplate geometries where both operate in a kinetic regime where temperatures are sufficiently high that both metal adatom deposition and desorption events are possible. The key difference between the two approaches is that one has metal vapor arriving to an initially bare substrate[73,77,78] while the other has vapor arriving to a surface populated with near-hemispherical Au nanostructures that act as heterogeneous nucleation sites.[79]

**2.4.1 Vapor-phase assembly on bare substrates.** Fig. 10a shows a schematic of a straightforward synthesis scheme that has been used by Yoo and co-workers for generating nanoplates of Au,[77,78] Ag,[73] Pd,[78] and AuPd[78] having a growth trajectory that is away from the substrate surface. Their method sees inert gas flowed over a heated crucible containing bulk pieces of a metal from which a vapor is derived that is carried downstream to a planar substrate maintained at a somewhat lower temperature. The temperatures used must be sufficiently high that the metal has a significant vapor pressure but not so high that spontaneous nucleation events on the substrate surface become improbable. Standard conditions for Au and Pd see the crucible heated to 1200 °C in an Ar carrier gas ($P$ = 1–10 Torr, flow = 100 sccm) while maintaining the substrate at 1000 °C.[78] The processing temperature used for Ag is considerably lower (≈ 820 °C) due to its comparatively higher vapor pressure.[73] For all cases, the nanoplate synthesis terminates by rapidly cooling the sample so as to ''lock-in'' the nonequilibrium geometry.

For the case of Ag, this rather simple methodology gave rise to the pentagonal nanoplates shown in Fig. 10b. These structures are remarkable in that they achieved edge lengths between 30 and 80 μm and thicknesses ranging from 180 to 230 nm in a synthesis lasting only a few hours. The nanoplates, which grow in a direction normal to the substrate surface, also align parallel to one another due to the heteroepitaxial relationship they each share with the R-plane sapphire substrate. TEM measurements performed on a nanoplate resting on a holey carbon grid (Fig. 10c) reveals crisp faceting with a crystalline character showing a [111] zone axis. TEM measurements also reveal two parallel twin planes along the zone axis but where it is noted that nanoplates formed on other substrates showed no such features. Similar vapor phase syntheses carried out using other metals show that the nanoplate shape has a strong elemental dependency as Au, Pd, and AuPd nanoplates formed on A-plane sapphire realized rhombic, trapezoidal, and hexagonal morphologies, respectively.[78] Moreover, the work revealed that the substrate material and crystallographic orientation plays a deciding role in determining the nanoplate growth trajectory.[78] Also of significance is that the nanostructure shape was largely dependent on the position of the substrate within the tube furnace, with nanobelts, nanowires, and nanopyramids forming as the substrate is placed progressively closer to the vapor source.[77] Another key feature of nanoplates produced in this manner is that they exhibit pristine surfaces because they have never been exposed to capping or stabilizing agents. Fig. 10d and e shows SEM and AFM characterization of triangular Au

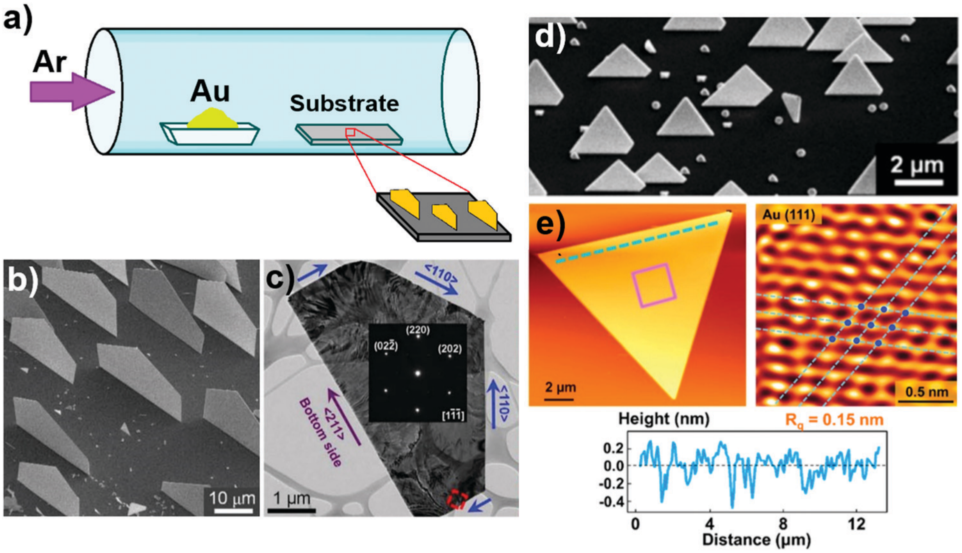

Fig. 10 (a) Schematic of the vapor-phase assembly process used to form nanoplates of Au, Ag, Pd, and AuPd. (b) Tilted view SEM image of pentagonal Ag nanoplates with a growth trajectory that is normal to the substrate surface. (c) TEM image and SAED pattern for a single nanoplate resting on a TEM grid. (d) Tilted view SEM image of triangular Au nanoplates. (e) AFM images and contour plot of a single nanoplate exhibiting an atomically smooth (111) plane. (b–e) Reproduced with permission from ref. 73 and 77, respectively. Copyright 2019 Royal Society of Chemistry. Copyright 2017 American Chemical Society.

nanoplates produced in the vapor phase. It reveals a well-ordered atomically flat (111) surface topography over a length of 13 μm.

The vapor-phase transport method for generating nanoplates with a growth trajectory that is away from the substrate surface is one that is mechanistically fascinating. In its early stages, metal adatoms arrive to a bare substrate surface but where their subsequent desorption severely hinders the formation of metal clusters. The high temperature environment created is, hence, far removed from standard physical vapor deposition processes that are used to deposit continuous metal films where temperatures are chosen to minimize adatom desorption in favor of a hit-and-stick modality. Nevertheless, conditions can be established in which clusters form as a low probability event, after which they can act as seeds capable of promoting continued growth. It is at this seed nucleation stage where the heteroepitaxial relationship between the metal and substrate is established, a process that, to a large extent, decides how the growing nanostructure will evolve because it establishes the directions able to support (111) planar growth. As the structure grows, the vapor transport mechanisms evolve in that it becomes increasingly likely that adatoms arrive to the structure through direct impingement rather than by their diffusion along the substrate surface. Once they arrive, the low coordination that a lone adatom has to the (111) planar surface (*i.e.*, 3) allows for its fast diffusion to the nanoplate edge where it is more strongly coordinated. Under such circumstances, it is not surprising that the metal deposition flux and deposition temperature become highly intertwined parameters, capable of determining the extent to which lateral and vertical growth occur. It is, therefore, these interdependencies that decide whether nanowires, nanobelts, or nanoplates emerge. Interestingly, Yoo *et al.*[78] attributed the strong shape-dependency observed for Au, Pd, and AuPd nanoplates formed on A-plane sapphire to the lattice mismatch with the substrate whereby larger values hindered lateral nanoplate growth at the interface.

With numerous advantages that include ease of synthesis, shape-control, pristine surfaces, and a large-area nanoplate capability, this vapor phase assembly route has obvious appeal. Nevertheless, it is disadvantageous in that it requires high processing temperatures, lacks nanoplate position and size controls, and where the gradients in nanostructure shape can occur if large-area substrates are used. It is, however, noteworthy that three studies have been forwarded that aimed to produce nanoplates in the vapor phase at lower temperature using metal precursors that are more amenable to low temperature vapor transport.[74–76] Each of these studies realized nanoplate growth and, hence, represent a significant stride forward but where the overall capabilities demonstrated do not yet rival high temperature syntheses.

**2.4.2 Vapor-phase assembly using nucleation sites.** Fig. 11a shows a schematic of the two-step vapor-phase assembly process used to form triangular AuAg nanoplates in which roundish Au nanostructures are first formed using solid-state dewetting[118] and then reheated with a Ag foil in close proximity. The dewetting step takes advantage of the fact that room-temperature-deposited films when formed on a low surface energy oxide substrate represent a metastable configuration that, when heated, reorganize into nanostructures with a significantly lower surface-to-volume ratio so as to reduce the overall surface energy of the metal-substrate system.[119] When ultrathin Au films (*i.e.*, 17 nm) undergo this procedure on a [0001]-oriented sapphire substrate, there is a strong tendency for the resulting nanostructures to orient with their [111] axis normal to the substrate surface due to the heteroepitaxial relationship formed at the metal-oxide interface.[120] When these so-formed Au nanostructures are placed near a Ag foil (*i.e.*, 0.5 mm) and heated to sufficiently high temperatures (*i.e.*, 775 °C), atoms sublimate from the foil and land on the substrate surface, at which point they travel along the surface until they either arrive at a Au nanostructure or desorb from the surface. Many of the Ag atoms interacting with the Au structure are integrated into it to form an alloy and it is the kinetics of this entire process that lead to a shape transformation giving rise to the nanoplate geometry.

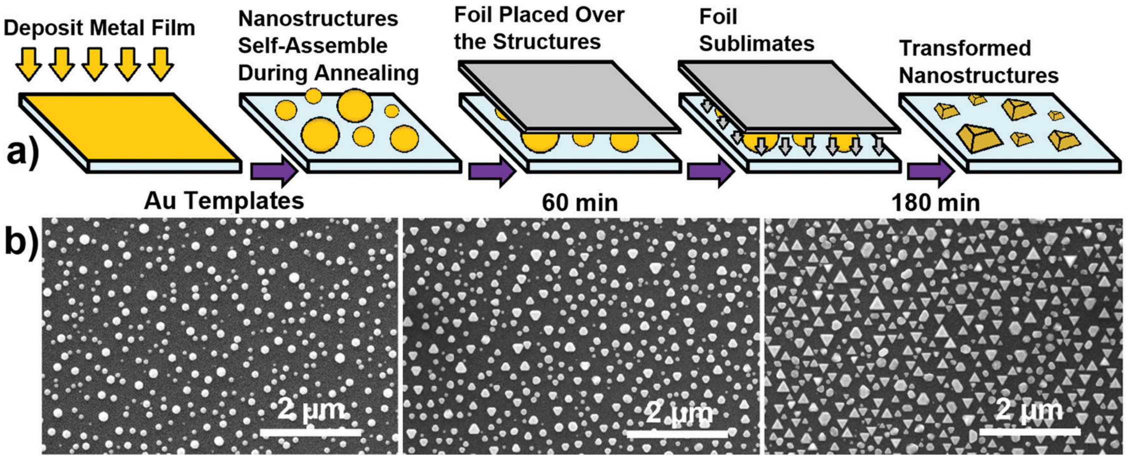

Fig. 11 (a) Schematic showing the procedure by which near-hemispherical Au nanostructures are transformed into triangular AuAg nanoplates through their exposure to a Ag vapor derived from an adjacent foil. (b) SEM images showing the time-progression in nanostructure morphology during the transformation process. (b) Reproduced with permission from ref. 79. Copyright 2015 Royal Society of Chemistry.

Fig. 11b presents SEM images showing the time-progression in nanostructure morphology as dewetted Au nanostructures are exposed to the Ag foil. Before exposure the structures appear roundish but where a close inspection reveals weak faceting. After 1 h, many of the structures have undergone a significant shape-change, often appearing triangular but with rounded corners. When exposed to the Ag foil for 3 h, a large percentage of the structures take on a triangular nanoplate configuration with sharp corners. The structures are epitaxially aligned where triangles point in an upward and downward direction in equal numbers. The existence of two equally probable in-plane orientations is a common occurrence for [111]-oriented fcc metals because structures with an ABCABC... stacking order have no advantage in terms of epitaxy over structures that have the reverse ACBACBA... stacking order. This difference, however, leads to a 180° in-plane rotation of all crystallographic axes.[79] Accompanying the shape change is a composition that morphs from pure Au to a well-mixed alloy with nearly equal amounts of Au and Ag. It should be noted that the same growth pathway was also amenable to the formation of AuCu structures using a Cu foil.[80] Although it has proved successful for these two cases, the route is limited in that (i) it has not proved viable for pure metals and (ii) the allowable nanoplate size is limited by the fact that longer processing times lead to thicker structures rather than higher aspect ratios.

The mechanisms by which roundish Au structures are transformed into AuAg nanoplates are quite involved[79] but where an appreciation is gained through the understanding of five essential mechanistic aspects. The first stems from the heteroepitaxial relationship between Au and the sapphire substrate because it causes the formation of [111]-oriented structures, an orientation that is maintained throughout the morphological and compositional transformation. The second mechanistic requirement is that the transformation occurs at a temperature that is high enough to sublimate Ag from the foil but not so high as to have a flux of Ag arriving to the surface that is able to spontaneously nucleate Ag islands that grow in the intervening spaces between the Au nanostructures. The third is the kinetic disruptions to growth originating from Ag atoms preferentially arriving to an evolving structure at its perimeter, a process that preferentially favors the growth of those facets in contact with the substrate surface. The fourth, and perhaps the most significant, involves the kinetic processes that favor the facet-to-facet diffusion of atoms travelling from a (111) to a (100) facet over those travelling in the opposite direction. This difference, which is ascribed to an Ehrlich–Schwoebel barrier based on molecular dynamics (MD) simulations,[121] provides the mechanism by which atoms preferentially collect on and grow the (100) surface. This seemingly subtle difference eventually sees (100) facets extinguished in favor of those that are (111), a process quite analogous to colloidal growths that give rise to (111)-faceted octahedrons by favoring the growth on other facets through the use of a (111) capping agent. The fifth mechanistic requirement, which accounts for the Au–Ag alloying, arises from the miscibility of Au and Ag and the intermixing in the solid-state brought on by vacancy diffusion. Of specific note is that this growth mode does not mechanistically require stacking fault defects to proceed.

### 2.5 Syntheses utilizing directed-assembly

With colloidal syntheses exerting precise chemical controls over nanostructure architecture and lithographic processes allowing for the definition of features with exacting controls over positioning, there has been a strong impetus for forming hybrid strategies in which lithographically-defined features regulate the placement of colloidal nanostructures as well as their orientation relative to the substrate surface. Successful strategies for achieving this outcome have led to the formation of organized surfaces of complex nanostructures that are otherwise unrealizable.[122] The application of these methods to nanoplates has proven particularly challenging. Three approaches have, however, led to the formation of periodic arrays of nanoplates by directing the assembly of (i) sputter-deposited material into organized patterns of nanostructures that then act as seeds in a solution-based synthesis,[53,54,81] (ii) DNA-functionalized nanostructures into nanopores defined in a (poly)methyl methacrylate (PMMA) layer using electron beam lithography (EBL),[82] and (iii) colloidal nanoplates into topographical features patterned into the substrate surface using capillary forces.[83] This section details these approaches where specific challenges related to the directed-assembly of nanoplates are highlighted.

**2.5.1 Seed-mediated nanoplate growth at the liquid–substrate interface.** This approach to forming nanoplate arrays follows a synthetic strategy whose basic premise is to form seeds on the substrate surface at lithographically-determined locations and then, using the exacting chemical controls accessible through colloidal syntheses, transform them into the desired nanostructure architecture.[99,123] Key to its success has been the ability to define seeds that have a single-crystal character whose orientation relative to the underlying surface is set by a substrate-imposed heteroepitaxial relationship. When such seeds are subjected to liquid-state seed-mediated syntheses, they, like their colloidal counterparts, promote facet growth based on their underlying crystallographic symmetries but, in addition, exert control over the orientation that the nanostructure has with respect to the substrate surface.[115,124] With seed-mediated nanoplate syntheses requiring that seeds not only have a single-crystal character but also symmetry-breaking defects that promote two-dimensional growth, the fabrication of suitable seeds became the overriding hurdle in forming nanoplate arrays. Fig. 12a presents a schematic that outlines the three-stage processing route that has overcome this hurdle.[53] It combines nanoimprint lithography, a vapor-phase directed-assembly process, referred to as dynamic templating, and a light-driven liquid-state Au nanoplate growth mode, the details of which are described in this section.

The seed requirements for the synthesis of aligned nanoplate arrays are far more stringent than those used to promote the growth of colloidal nanoplates. The fundamental difference is that colloidal seeds require stacking fault defects along any

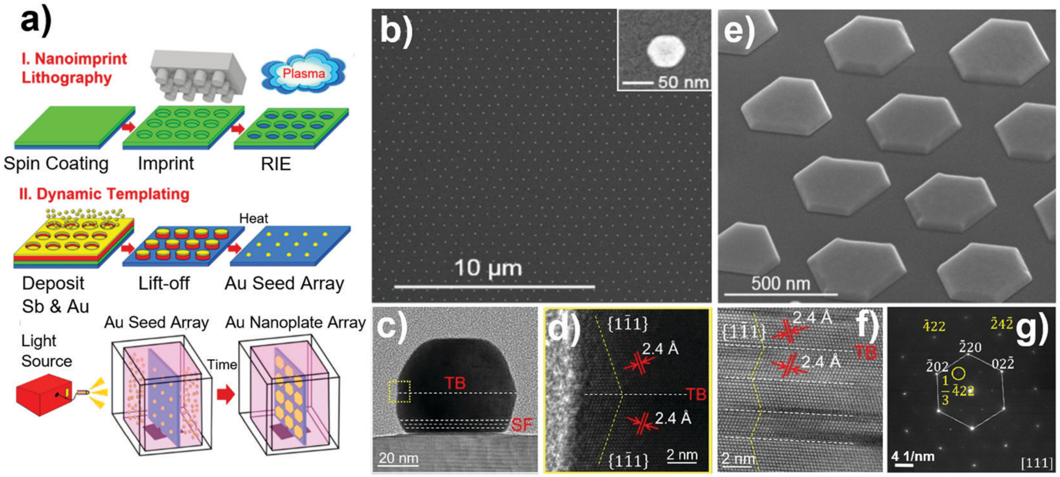

Fig. 12 (a) Schematic of the three-stage procedure used to form periodic arrays of Au nanoplates. (b) SEM image of a Au seed array where the inset shows an expanded view of a single structure. (c) TEM image of a Au seed and (d) a HRTEM image of a twin boundary defect for the area denoted by the yellow box. (e) Tilted view SEM image of a Au nanoplate array. Evidence for stacking fault defects in the nanoplates as indicated by a (f) HRTEM cross-sectional image and (g) SAED pattern taken along the [111] zone axis showing forbidden $\frac{1}{3}\{422\}$ reflections. Reproduced with permission from ref. 53. Copyright 2019 American Chemical Society.

one of the equivalent ⟨111⟩-directions as they tumble in the nanoplate growth solution whereas substrate-based seeds must be rigidly held in place with their [111]-axis perpendicular to the substrate surface where stacking fault defects occur along just this axis. If this requirement is not met, then nanoplate growth trajectories will be randomized in much the same manner as they are in electrochemical syntheses. Moreover, colloidal syntheses allow for the separation of unwanted reaction products derived from "flawed" seeds through centrifugation or depletion flocculation whereas the product of similarly flawed substrate-based seeds remain firmly attached to the substrate surface.

The first stage in seed fabrication sees nanoimprint lithography used in combination with reactive ion etching (RIE) to define an array of cylindrically shaped openings in a polymeric resist. In the second stage, layers of Sb and Au are sequentially deposited into the openings as well as on top of the patterned resist. This is followed by a standard lift-off process that leaves behind an array of 240 nm diameter Au-capped Sb disks. The disks are then subjected to a high-temperature vapor-phase directed-assembly process that sees the ultrathin Au layer (*i.e.*, 2.5 nm) at the top of each disk assemble into a single nanostructure as a sacrificial Sb layer sublimates from the surface. This so-called dynamic templating technique[119,125] shares many similarities with solid-state dewetting[118] but where the inclusion of an Sb layer greatly enhances the spatial extent over which Au can assemble into a single nanostructure. Fig. 12b shows an SEM image of the seed array formed. This technique for making seed arrays is advantageous in that it (i) is an inexpensive benchtop process that does not require cleanroom facilities, (ii) allows for large-area processing capabilities (*i.e.*, 1 $cm^2$) for arrays that express true long-range order, (iii) produces seeds with a high degree of size-uniformity, (iv) promotes crystallinity, heteroepitaxy, and seed adhesion due to the high processing temperatures used, and (v) results in seed surfaces that are pristine in that they have never been exposed to a capping or stabilizing agent.

The seeds when examined in cross-sectional TEM appear as weakly faceted [111]-oriented Au nanostructures with stacking faults (SF) and twin boundaries (TB) that run parallel to the substrate surface and extend from one side of the seed to the other (Fig. 12c and d). The fact that planar defects appear in these structures is not surprising since Au has a low stacking fault energy;[102] however, the strong tendency for defects to run parallel to the substrate when equivalent ⟨111⟩-directions exist shows that the substrate is playing a decisive role in their formation. With stacking faults tending to cluster near the seed surface, strains due to lattice mismatch were considered the likely origin of these stacking faults. It should, however, be noted that a smaller subset of these seeds have an internal defect structure that is not conducive to the nanoplate growth mode.

Golze *et al.*[53] showed that periodic arrays of Au nanoplates could be grown by immersing these seed arrays into a room-temperature aqueous solution of $HAuCl_4$, PVP, and methanol, followed by their illumination with a broadband light source for 4 h. Their growth mode was adapted from the colloidal work of Wei and co-workers,[126] a protocol that is noteworthy because it was the first plasmon-driven synthesis yielding Au nanoplates. Fig. 12e shows an SEM image of the nanoplates formed where the in-plane alignment of the hexagonal structures is a direct consequence of seed-substrate heteroepitaxy. HRTEM images indicate that these planar structures are lined with stacking fault defects that extend from one side of the nanoplate to the other (Fig. 12f), a result confirmed by the forbidden $\frac{1}{3}\langle 422\rangle$ reflections observed in SAED patterns taken along the [111] zone axis (Fig. 12g). Although this work represents a significant breakthrough in substrate-based nanoplate synthesis, its relevance is tempered by a nanoplate yield of only 80% that arises from seeds that lack the internal defect structure needed to promote two-dimensional growth. Improvements in this regard were, however, recently made by Demille *et al.*[54] who, using a different nanoplate growth in which Brij-700 served as both the capping and reducing agent, achieved a 95% yield of nanoplates by selectively removing unwanted three-dimensional structures through sonication. Another recent discovery of note is the modification of the substrate-based Au nanoplate synthesis so as to realize three-dimensional chiral nanostructures with spiral geometries.[81]

**2.5.2 DNA-Assisted assembly.** This approach to forming nanoplate arrays is part of a broad-based strategy in which colloidal suspensions of nanoparticles act as discrete building blocks that populate a surface that has been lithographically modified with target sites capable of capturing colloidal structures in a highly deterministic manner.[89,122,127] When applied to nonspherical nanostructures, such directed-assembly processes are further challenged by the objective of forming trapping sites that place controls on both nanostructure placement and orientation. Among the various techniques, DNA-mediated assembly has shown truly extraordinary capabilities in terms of the site-selective positioning of colloidal metal nanostructures on substrate surfaces where precise control is exerted over nanostructure orientation. The basic concept behind this approach is for DNA-functionalized colloidal nanostructures to become anchored to lithographically-defined areas on the substrate surface that have been functionalized with the complementary DNA strand. The technique, whose capabilities are rapidly evolving, has been applied to nearly all commonly synthesized nanostructure architectures[127–129] including nanoplates.[82]

The DNA-assisted assembly of nanoplate arrays was demonstrated by Lin *et al.*[82] for both Au nanotriangles and circular nanodisks. The design of topological traps for these structures begins with an understanding of the size and shape characteristics of the colloid as produced using well-established synthetic protocols.[130,131] The substrate, which is a Au-coated Si substrate with an intermediate Cr adhesion layer, was spin-coated with PMMA followed by top-down EBL processing that patterns an array of pores that selectively exposes the underlying Au film at precise locations. Each pore is designed to fit a single colloidal nanostructure but where the dimensions have sufficient slack to accommodate size variations within the colloid and to increase the trapping yield to an acceptable value. For nanotriangles the pore shape is also triangular to limit the in-plane rotational degree of freedom of the trapped structure. The exposed Au at the bottom of each pore is then functionalized with a single-stranded oligonucleotide that acts as the bonding site for a colloidal nanostructure that is functionalized with the complementary oligonucleotide. A top-down directed-assembly process then proceeds by submerging the substrate in a heated colloid for 1 to 2 h under constant agitation. The PMMA is dissolved in a post-assembly process that also sees the DNA bonds between the Au film and the trapped nanostructure condense due to a change in solvent polarity, and in doing so, causes a transfer of the nanostructures from the solution phase to the solid state.[127,132]

Fig. 13a and b shows an SEM image of the triangular pores formed in PMMA and the resulting Au nanotriangle array. The triangular nanoplates show a high degree of in-plane alignment but where some are noticeably tilted. Arrays produced in this manner also show defects in the form of vacancies and sites occupied by oddly shaped nanostructures that were contained within the colloid. Notwithstanding, the arrays produced represent a significant breakthrough in terms of advancing high-yield nanoplate arrays. In the same study, it was also demonstrated that DNA-assisted assembly could also be used to create stacks of dissimilarly shaped nanostructures. The assembly method used sequential processes in which an array of one structure is formed followed by its exposure to a second assembly process using a differently shaped nanostructure functionalized with the oligonucleotide that is complimentary to that of the first particle. A third nanostructure can then be attached by, once again, alternating the oligonucleotide used. Fig. 13c and d shows images of stacked nanotriangle–nanocube and nanotriangle–nanocube–nanosphere assemblies formed in periodic arrays, an achievement that is quite remarkable.

Although DNA-mediated assembly has only been demonstrated for substrate-based nanoplates in a single study, the overall versatility of the technique as applied to a broad range of nanostructures is considerable. Offering size, shape, composition, and positional control over arrayed nanostructures as well as various arrangements of stacked structures, the technique provides capabilities that are currently unrivaled for single-crystal nanostructures.[122,133] It is, however, technically demanding in that the lithographic demands are exacting and must be coordinated with the correspondingly stringent demands placed on the shape- and size-purity of the colloid. These needs also make the process cost-prohibitive and time-intensive. The requirement to form arrays on Au films also poses a limitation. It should, however, be recognized that the technique and its associated capabilities have seen rapid development and will likely continue to do so.

**2.5.3 Capillary assembly on textured substrates.** Capillary assembly also belongs to the group of assembly techniques that uses lithographically-defined surfaces to trap colloidal nanostructures at site-specific locations.[89,122] It takes advantage of the remarkable properties exhibited by a drop of a colloidal suspension as it lands and then evaporates from a surface. Under suitable conditions, convectively driven laminar flows due to differential evaporation rates across the surface of the drop drive the suspended nanoparticles to the contact line where the substrate, droplet, and air meet. Over time, a region of densely packed nanostructures, referred to as the accumulation zone, forms at the perimeter of the droplet that is then dragged over the substrate surface as continued evaporation causes the drop's contact line to recede. If, however, this accumulation zone is dragged over a substrate topography textured with an array of suitably designed trapping sites, then nanostructures become lodged within these sites. The force responsible for trapping is a downward acting component of the capillary force.[134] Although significant progress has been made in terms of engineering surfaces and processing routes able to capture and orient nanorods[135,136] and nanocubes,[83,137] only Zhou *et al.*[83] has successfully applied this approach to nanoplates. Their techniques and results are described in this section.

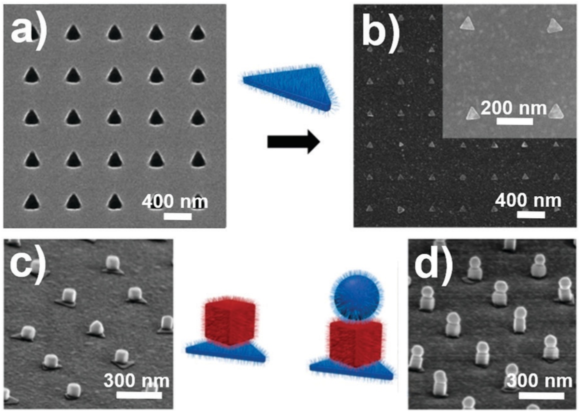

Fig. 13 SEM images of (a) triangular pores patterned into PMMA and (b) the periodic array of triangular Au nanoplates formed using DNA-assisted assembly. Arrays of stacked nanostructures formed through the sequential DNA assembly of (c) nanotriangles and nanocubes and (d) nanotriangles, nanocubes, and nanospheres. Adapted with permission from ref. 82. Copyright 2018 American Association for the Advancement of Science.

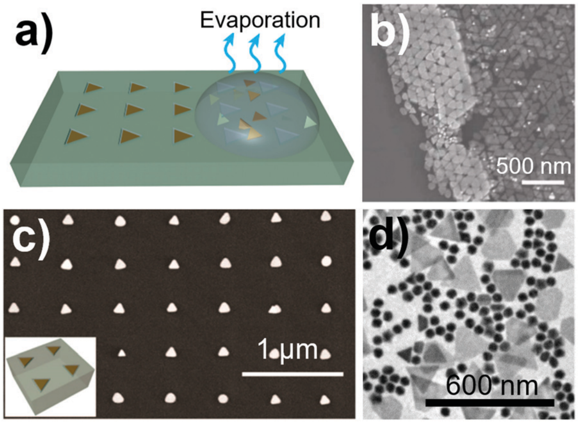

Fig. 14 (a) Schematic showing the directed-assembly of triangular Au nanoplates into lithographically-defined target sites using capillary assembly. SEM images of a (b) dried accumulation zone and (c) periodic array of triangular nanoplates. (d) TEM image of the product of the colloidal nanoplate synthesis that includes a large number of near-spherical nanostructures. Adapted with permission from ref. 83. Copyright 2014 American Chemical Society.

Similar to DNA-mediated assembly, the design of topological traps begins with an understanding of the colloid. Zhou *et al.*[83] used the seed-mediated protocol devised by Millstone *et al.*[138] that sees triangular Au nanoplates as well as a population of near-spherical structures form in an aqueous mixture of $HAuCl_4$, CTAB, ascorbic acid, and NaOH where a post-synthesis treatment can be used to shape-purify the product. With an understanding of the average nanoplate edge-length and thickness, triangular-shaped traps forming recessed regions on an otherwise planar surface are designed to be somewhat larger than the nanoplate so as to increase the trapping probability while still spatially confining the nanoplate to an extent that its orientation within the trap is assured. The trap depth must be sufficiently large to ensure that a trapped nanoplate remains pinned as the drop's contact line recedes while being thin enough to accommodate just a single structure. Periodic arrays of appropriately designed topological traps were fabricated using an EBL-defined Si surface with raised triangular features to which a PDMS (polydimethylsiloxane) layer was molded to and then peeled from. The resulting PDMS surface with triangular indents then served as the substrate for capillary assembly.

Prior to the assembly process, the triangular nanoplates are dispersed in aqueous CTAB. The process is then initiated by pipetting a drop of the colloid onto a topographically altered PDMS surface (Fig. 14a) that is heated to 40 °C and housed in a chamber maintaining a relative humidity of 40%, conditions that were chosen to optimize the evaporation rate of the droplet. Under these conditions nanoplates were trapped over an area of $0.3\ \text{mm}^2$ where the droplet's contact line moved at an average speed of $4\ \mu\text{m s}^{-1}$. It should be noted that, while this droplet method provides simplicity, more sophisticated techniques exist for obtaining much larger areas and where tighter controls are placed on the evaporation process.[89,122]

In the initial stages of the capillary assembly process, a population of nanoplates builds up to form an accumulation zone. Fig. 14b shows a zone that was dried out prior to SEM imaging. The high density of nanoplates realized ensures that there will be ample opportunity for a trapping site to capture a structure. The high density also restricts nanoplate mobility, making them more susceptible to trapping. Fig. 14c shows an SEM image of an array of trapped structures. It was determined that optimum trapping performance occurred for 7.5 nm thick nanoplates with an edge-length of 100 nm when the traps had an edge-length of 150 nm and a depth of 20 nm. Such traps were occupied with a single nanoplate at an 80% yield with a standard deviation in the angular distribution of 6°. In the same study, it was shown that trapping efficiency was not markedly affected if the colloid shape-purity was compromised by the presence of near-spherical structures (Fig. 14d). In such a scenario, these unwanted structures are carried along in the accumulation zone but are never trapped in the recessed regions because the trap design does not facilitate their capture. Although this inability to trap near-spherical structures would eventually contaminate the accumulation zone to an extent that it would diminish trapping efficiency, it is nevertheless significant that the assembly process can tolerate some degree of shape polydispersity within the applied colloid. A key disadvantage of this process as it relates to nanoplates is that the depth of the trapping site is significantly larger than the nanoplate thickness, and as a result, the nanoplate does not protrude above the PDMS surface. This shortcoming negates the possibility of using a post-assembly contact transfer printing process[137] that allows arrayed structures to be transferred to a more technologically relevant substrate such as Si.

## 3. Applications

This section describes application-based research utilizing substrate-immobilized nanoplates. With the on-chip format lending itself to device applications, it is not surprising that much of this section is dedicated to sensor fabrication. The considerable breadth of sensor design is founded on modalities that take advantage of the unique plasmonic, catalytic, and morphological properties expressed by noble metal nanoplates. Their catalytic, photocatalytic, electrocatalytic, and electrophotocatalytic activity has also demonstrated utility in a wide range of reactions.

### 3.1 Surface enhanced Raman scattering (SERS)

The inelastic scattering of photons by a molecule gives rise to a Raman spectrum that is unique to it because of a distinct set of vibrational modes. With each molecule type having its own characteristic peaks in the spectral response, the Raman spectrum provides what is, in essence, a ''molecular fingerprint'' that can act as a highly specific, nondestructive, and label-free method for identifying molecular species. The weak Raman signals expressed by most molecules, however, lead to a lack of sensitivity that, to a large degree, negates its effectiveness as a sensing platform. The surface-enhanced Raman scattering (SERS)[139–141] technique overcomes this inherent weakness by using plasmonic nanostructures to amplify the Raman signal from molecules adsorbed onto their surface to an extent that peaks otherwise lost in the noise appear prominently in the spectrum. Once the selectivity of Raman scattering is combined with SERS enhancements, which can reach values as large as $10^{10}$, it allows for the rapid recognition of analytes at trace-level concentrations. As such, SERS sensing is being advanced as a powerful analytical tool where there is every indication that it will emerge as a pervasive technology.

The SERS enhancement resulting from a plasmonic nanoparticle is largely dependent on the intensity of the electromagnetic fields formed at its perimeter when illuminated. Nanostructures specifically designed to have sharp corners and edges give rise to regions of highly concentrated electromagnetic fields, referred to as ''hot spots'', whose presence disproportionately contributes to the SERS enhancement. These electromagnetic hot spots are further concentrated when the plasmonic nanostructures are in close enough proximity to one another to form gaps with nanometer-scale dimensions. With this understanding, it is not surprising that triangular nanoplates have been intensively investigated as candidate materials for SERS sensors as they exhibit sharp corners and readily assemble into close-packed configurations with a spatial organization that favors the formation of nanogaps near their sharp tips. A further advantage of the nanoplate geometry stems from the ability to tune the LSPR to a desired value by adjusting its edge length[2] since this allows for a resonant wavelength that is near that of the laser excitation used in SERS detection.

Given these significant advantages, it is not unexpected that discoveries in synthesis are often accompanied by an assessment of their SERS capabilities. As a result, nanoplates of various sizes, shapes, and compositions have undergone SERS testing where they can populate surfaces in sparse, dense, close-packed, or stacked arrangements. The majority of these studies have used readily accessible probe molecules whose primary function is to provide a model analyte whose SERS detection acts as a quantitative metric for the effectiveness of the structures produced. Such work is not discussed in this section. Instead, studies are showcased that use nanoplates to detect analytes whose relevance is nearer to real-world sensing applications in the detection of explosives, environmentally persistent pollutants, illicit drugs, and biological species. Table 2 provides a summary of these SERS studies as well as those carried out on probe molecules.

**3.1.1 Chemical detection using SERS.** The rapid, accurate, and straightforward detection of trace quantities of explosives as a means to mitigate security threats represents a challenge of paramount importance.[151,152] Liyanage *et al.*[19] have advanced a versatile SERS-based sensing platform aimed at addressing this challenge that offers high selectivity and reproducibility, a long shelf-life, and cost-effectiveness. Fig. 15a presents a schematic illustrating both the fabrication and utilization of their SERS nanosensor. The sensors are produced by assembling colloidal Au nanotriangles onto a rigid substrate at densities high enough to promote the formation of plasmonic hot spots. The nanostructures are then brought into contact with a flexible adhesive that upon removal transfers the structures while maintaining their original layout. The plasmonically-active tape is then used as a SERS substrate where analytes can be applied either by drop-casting liquids or bringing the adhesive surface and associated nanoplates into contact with the residue residing on a surface of interest. The surfaces then undergo SERS analysis that quantitatively assesses the chemical species detected.

The sensors produced were tested for the explosives TNT (2,4,6 trinitrotoluene), RDX (cyclotrimethylenetrinitramine), and PETN (pentaerythritol tetranitrate). Fig. 15b and c shows plots of the SERS intensity for the most prominent TNT and PETN peak as a function of the concentration applied. The results are of significance in that they allow for a quantifiable result with a limit of detection in the parts-per-quadrillion range, a result that the authors partially attribute to the strong binding affinity that nitrogen containing explosives have for Au. In a demonstration of the real-world applicability of this sensing platform, experiments were carried out in which explosives were applied to a person's thumb after which thumbprints were successively made on ten different glass slides. SERS sensors were then applied to and peeled from each of the thumbprints and analyzed for explosive residue. Fig. 15d shows the SERS spectra and a plot of a characteristic peak intensity *versus* slide number for experiments directed toward the detection of TNT and PETN. For both cases, explosives were detected in steadily decreasing amounts as the residue transferred from the person's thumb lessened. The demonstration is of significance in that it reveals that trace detection is possible through the direct sampling of surfaces without the need for wet swabbing as is typical for current detection methods. The use of Au nanoplates instead of Ag allowed for significant SERS signals while maintaining a sensor shelf-life of at least five months. Noteworthy is that Sun *et al.*[23] also demonstrated the SERS detection of TNT and RDX

Table 2 Summary of SERS measurements utilizing nanoplates

| Application | Compound sensed | Metal | Shape | Synthesis route | Spacing |
|---|---|---|---|---|---|
| Probe molecule | 2-Naphthalenethiol (2NT) | Au | Triangle | Air–liquid interfacial | Close-packed[33] |
| | 4-Mercaptobenzoic acid (4MBA) | Au | Triangle | Solvent evaporation | Close-packed[92] |
| | 4-Mercaptopyridine (4-MP) | Au | Triangle | Air–liquid interfacial | Close-packed[32] |
| | 4-Nitrothiophenol (4-NTP) | Au | Triangle | Air–liquid interfacial | Close-packed[34,142] |
| | Benzenethiol (BT) | Au | Triangle | Air–liquid interfacial | Close-packed[32] |
| | Crystal violet dye (CV) | Au | Triangle | Air–liquid interfacial | Close-packed[32] |
| | DMAB[a] | Au | Triangle | Air–liquid interfacial | Close-packed[34] |
| | FAD[b] | Ag | Irregular | Seed-mediated | Dense[104] |
| | Methylene blue (MB) | Au | Hexagon/triangle | Solvent evaporation | Sparse[26] |
| | MMC[c] | Ag | Triangle | Seed-mediated | Dense[46] |
| | 4-Aminothiophenol (4-ATP) | Ag | Irregular | Electrochemical | Dense[62,64] |
| | | | Irregular | Seed-mediated | Dense[47] |
| | | Au | Rod/triangle | Colloidal assembly | Dense[143] |
| | BDAC[d] | Au | Triangle | Solvent evaporation | Close-packed[92] |
| | | | | Air–liquid interfacial | Close-packed[142] |
| | Rhodamine 6G (R6G) | Ag | Irregular | Electrochemical | Dense[61,63,66] |
| | | Ag | Triangle | Solvent evaporation | Dense[24] |
| | | Au | Rod/triangle | Colloidal assembly | Dense[143] |
| | | | Triangle | Solvent evaporation | Close-packed[27,29] |
| Pollutants | Hg | Au | Rod/triangle | Colloidal assembly | Dense[143] |
| | PCBs[e] | Ag | Irregular | Electrochemical | Dense[63] |
| | Pyrene | Au | Hexagon/triangle | Solvent evaporation | Sparse[26] |
| | Methyl parathion (MP) | Ag | Triangle | Colloid chemisorption | Dense[16] |
| | | | Dendritic | Solvent evaporation | Sparse[22] |
| | Thiram | Ag | Triangle | Colloid chemisorption | Dense[16] |
| | | | | Seed-mediated | Dense[46] |
| Explosives | 2,4-Dinitrotoluene (2,4-DNT) | Au | Triangle | Air–liquid interfacial | Close-packed[32] |
| | Ag | Ag | Triangle | Colloid chemisorption | Dense[14] |
| | PETN[f] | Au | Triangle | Colloid chemisorption | Sparse[19] |
| | RDX | Ag | Irregular | Solvent evaporation | Close-packed[23] |
| | | Au | Triangle | Colloid chemisorption | Sparse[19] |
| | | Au/Ag | Irregular | Solvent evaporation | Close-packed[23] |
| | Trinitrotoluene (TNT) | Ag | Irregular | Solvent evaporation | Close-packed[23] |
| | | Au | Triangle | Colloid chemisorption | Sparse[19] |
| | | Au/Ag | Irregular | Solvent evaporation | Close-packed[23] |
| Illicit drugs | Despropionyl fentanyl | Au | Triangle | Colloid chemisorption | Dense[144] |
| | Heroin | Au | Triangle | Colloid chemisorption | Dense[144] |
| | JWH-018 | Au | Triangle | Colloid chemisorption | Dense[144] |
| | Cocaine | Au | Triangle | Colloid chemisorption | Dense[144] |
| | | | | Solvent evaporation | Close-packed[93] |
| | Fentanyl | Au | Triangle | Colloid chemisorption | Dense[144] |
| | | | | Solvent evaporation | Close-packed[93] |
| Biosensing | Avidin | Au | Triangle | Vapor phase | Standalone[77] |
| | cTnIs[g] | Au | Triangle | Vapor phase | Standalone[145] |
| | C-Reactive protein (CRP) | Au | Triangle | Vapor phase | Standalone[146] |
| | Cystine | Au | Triangle | Colloid chemisorption | Standalone[147] |
| | I223R/H275Y viruses | Au | Triangle | Vapor phase | Standalone[148] |
| | Jagged1 protein (JAG1) | Au | Triangle | Vapor phase | Standalone[149] |
| | Mahoney (PV1M) | Ag | Irregular | Electrochemical | Dense[61] |
| | MicroRNAs | Au | Triangle | Colloid chemisorption | Sparse[150] |
| | Poliovirus type 1 sabin (PV1S) | Ag | Irregular | Electrochemical | Dense[61] |
| | Protein A/G | Ag | Irregular | Electrochemical | Dense[61] |
| | Streptavidin | Au | Triangle | Colloid chemisorption | Close-packed[21] |
| | Biotin | Au | Triangle | Colloid chemisorption | Close-packed[21] |
| | | | | Vapor phase | Standalone[77] |
| | DNA | Ag | Irregular | Electrochemical | Dense[61] |
| | | Au | Triangle | Colloid chemisorption | Close-packed[20] |

[a] 4,4′-Dimercaptoazobenzene. [b] Flavin adenine dinucleotide. [c] 7-Mercapto-4-methylcoumarin. [d] Benzyldimethyl-hexadecylammonium chloride. [e] Polychlorinated biphenyls. [f] Pentaerythritol tetranitrate. [g] Cardiac troponin I proteins.

where they increased the sensor shelf-life by using AuAg alloys obtained through the partial galvanic replacement of Ag nanoplates with Au. Additionally, Scarabelli *et al.*[32] demonstrated the detection of 2,4-dinitrotoluene (2,4-DNT).

Another important example of chemical sensing is the rapid detection and identification of illicit drugs, a topic of vital importance to clinical and forensic toxicology that can have a decided impact on public health and safety.[153,154] With the need for tests that are able to sample surfaces, liquids, and biofluids in a wide variety of settings, current methods are challenged by long assay times, insufficient sensitivity, multistep procedures, and the inability to reanalyze samples due to the destructive nature of the detection technique used. With the potential to overcome many of these drawbacks, SERS

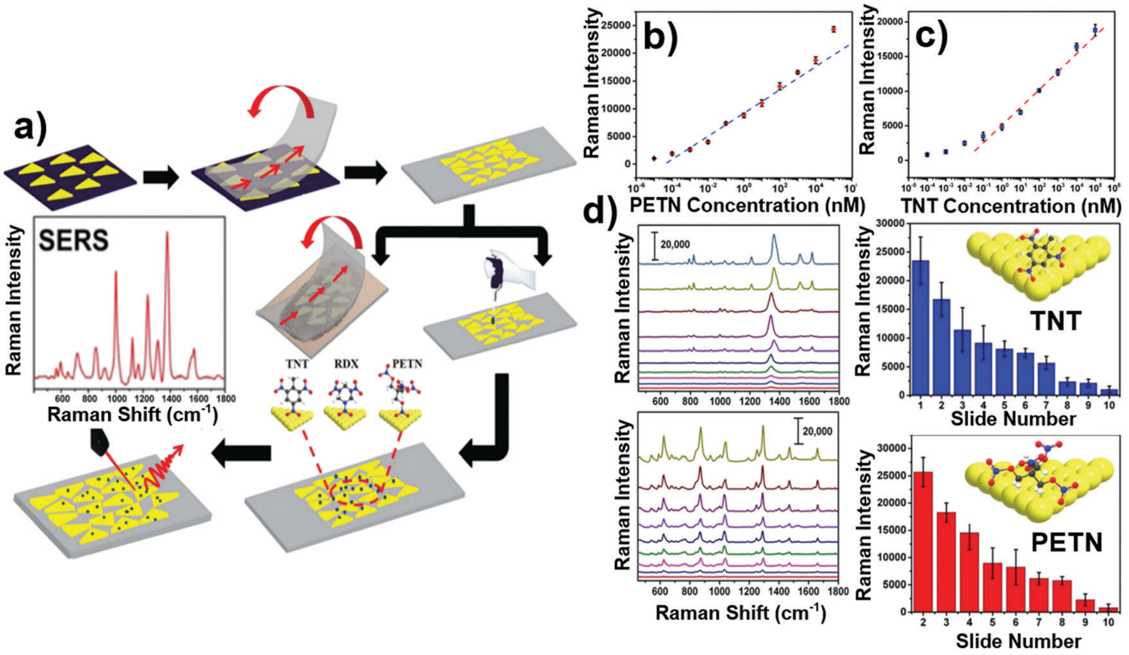

Fig. 15 (a) Schematic showing the procedure for preparing and using triangular Au nanoplates as the active component in an adhesive-based SERS sensor. The SERS intensity for the (b) 1380 cm$^{-1}$ TNT and (c) 1570 cm$^{-1}$ PETN peaks as a function of the applied concentration. (d) SERS spectra and plots of the SERS intensity (counts s$^{-1}$) for the 1380 cm$^{-1}$ TNT and 1570 cm$^{-1}$ PETN peaks obtained from thumbprints with explosive residues that were applied to ten glass slides where each successive print has less residue and a correspondingly smaller SERS signal. Adapted with permission from ref. 19. Copyright 2018 Royal Society of Chemistry.

provides an attractive alternative. In a recent study, Sardar and co-workers[93] advanced a highly sensitive SERS detection platform and demonstrated its use in the detection of fentanyl and cocaine in human plasma. Their SERS substrates were prepared by synthesizing Au nanotriangles followed by their assembly into close-packed formations using the solvent evaporation assembly technique (see Section 2.1.2). The targeted application, because it required nanostructure compatibility with bodily fluids, necessitated the use of Au and a ligand-exchange process that leaves the nanotriangles stabilized by polyethylene glycol thiolate (PEG60-S). In their study, they optimized the assembly process for maximum SERS enhancements by varying the contact angle of the evaporating drop through modifications to the Si substrate surface with APTES (γ-aminopropyltriethoxysilane), PHTMS (phenyl-methoxysilane), and OCTMS (n-octyl-trimethoxysilane). The results reveal that the surface modifications alter the contact angle of the applied droplet (Fig. 16a), and in doing so, fundamentally change the nature of the resulting nanotriangle assemblies. With APTES-modified surfaces resulting in a single-layer close-packed formation and surfaces modified with OCTMS giving rise to a three-dimensional superlattice, it was concluded that increases to the contact angle favor assemblies in which the nanostructures are stacked. The three different assembly types were assessed as SERS substrates for the detection of fentanyl. Fig. 16b shows a plot of the SERS intensity for the characteristic fentanyl peak at 1334 cm$^{-1}$ *versus* the applied concentration. The results not only reveal that the three-dimensional nanotriangle superlattices have a far superior performance but also show a level of detectability that is five times greater than those reported in the literature.[93] This level of performance was attributed to a high density of plasmonic hot spots arising from both neighboring and underlying nanostructures as well as the ability of the analyte to permeate the three-dimensional nanotriangle assembly. In a further demonstration of the superlattice assemblies as a practical SERS substrate, the authors carried out a study aimed at the detection of fentanyl and cocaine in human plasma obtained from emergency ward patients. Fig. 16c shows the SERS spectra obtained for six different patients where an examination of the characteristic peaks reveal fentanyl for four of them and cocaine for three. Is it notable that the SERS spectrum for one of the patients revealed that both drugs were present in their plasma. Additional tests performed on samples from drug-free patients presented no evidence for either drug. It should also be noted that all of these results were independently verified. In a more recent study, the same group forwarded a flexible plasmonic patch design that was able to detect cocaine, fentanyl, and heroin at 1.0 nM concentrations.[144] Collectively, these results provide a significant stride forward in advancing the use of Au nanoplates in real-world clinical settings.

The detection of environmentally persistent pollutants is of vital importance as their presence in air, food, soil, and water can lead to long- and medium-term health threats including carcinogenicity, mutagenicity, and chronic toxicity. With many of these pollutants existing only at trace levels within the environment but where their accumulation in the body over time is hazardous, there is a pressing need for high-sensitivity/selectivity detection if long-term exposures are to be mitigated. As such, a number of studies have been forwarded that use

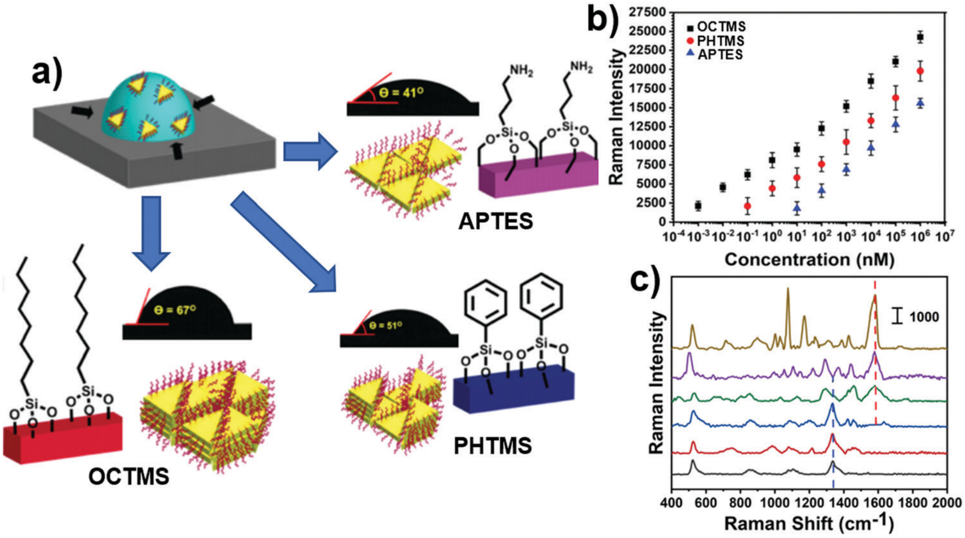

Fig. 16 (a) Schematic showing the Au nanotriangle evaporation assembly process for Si substrate surfaces modified by APTES, PHTMS, and OCTMS. (b) Plot of the SERS intensity for the 1334 $\text{cm}^{-1}$ fentanyl peak as a function of its concentration for nanotriangle assemblies formed on the various surface-modified substrates. (c) SERS spectra for samples derived from the human plasma of six patients in which drugs were detected. Adapted with permission from ref. 93. Copyright 2020 Royal Society of Chemistry.

nanoplates as active elements in the SERS detection of persistent organic pollutants and toxic inorganic elements.

Pesticides pose a health risk if they persist at unacceptable levels in the food and ground water supply. In a recent study, Wang *et al.*[16] devised a platform for SERS detection and demonstrated its effectiveness as a sensor for the fungicide thiram and the insecticide methyl parathion. The functionality of such pesticides is reliant on their adherence to a sprayed crop but where maximum allowable levels on fruits and vegetables can be subject to regulation.[46] The SERS substrate was unique in that Ag nanoplates were used to decorate graphene sheets that were then spin-coated on a Si substrate. By incorporating both Ag nanoplates and graphene, the authors combined two attractive SERS substrates into a single hybrid platform with the goal of obtaining increased sensitivity. The study demonstrated levels of detection of 40 nM for thiram and 600 nM for methyl parathion, a linear relationship between the SERS intensity and concentration over a wide range, and excellent reproducibility. Moreover, they showed that Ag nanoplates, when replaced with equivalent quantities of nanospheres, result in a limit of detection for thiram of 100 nM, a result that shows that the nanoplate geometry significantly enhances sensing performance. In a related study, D'Agostino *et al.*[46] also investigated thiram as a probe molecule for SERS sensing using Ag nanoplates formed on glass through a seed-mediated synthesis. An interesting aspect of their study was that they demonstrated sensor performance using samples prepared from green apple peels that were purposely contaminated with thiram. A similar demonstration was carried out by Jiang *et al.*[22] on apples contaminated with methyl parathion. Polychlorinated biphenyls (PCBs) represent another notable example of a persistent organic pollutant whose detection was investigated using nanoplate-based SERS substrates. Using Ag nanoplates formed on ITO through electrodeposition as SERS substrates, Zhu *et al.*[63] were able to achieve a lower detection limit of 100 nM. Another example is the study by Lin *et al.*[26] who investigated the SERS detection of pyrene, a polycyclic aromatic hydrocarbon formed during the incomplete combustion of organic compounds. Their SERS substrate, formed by the assembly of colloidal Au nanoplates on a Si substrate, showed a limit of detection toward pyrene of 0.5 nM as well as reusability if suitably cleaned before reuse. The SERS detection of Hg, an inorganic element whose toxicity is well-established, was demonstrated by Li *et al.*[143] using a SERS substrate composed of an organized assembly of Au nanoplates and nanorods separated by nanogaps with widths of 2 to 3 nm. In their study, they showed that the detection of $\text{Hg}^{2+}$ ions was possible at the parts-per-trillion level where it was possible to discriminate between them and other heavy metal ions.

**3.1.2 Biosensing using SERS.** The sensing of biological species using SERS is a subject of intense interest that encompasses the detection of a wide variety of analytes including proteins, DNA, RNA, viruses, bacteria, exosomes, and cells as well as the monitoring of biological events as they occur.[155–160] With the ability to sample liquid specimens and numerous disease biomarkers appearing in bodily fluids (*e.g.*, blood, saliva), SERS has the potential to provide a rapid noninvasive approach for the detection of biomarkers that can diagnose disease, evaluate its progression during treatment, or even predict its occurrence in a healthy individual before it happens. Given that survivability against diseases such as cancer is closely connected to its early detection and preemptive measures act to prevent heart disease, the SERS detection of low-level biomarkers has the potential to provide life-changing benefits. Moreover, advancements in benchtop and handheld SERS detection devices are making point-of-care detection viable. With the understanding that antigen–antibody interactions allow for high specificity detection, some of the earliest substrate-based nanoplate work focused on the attachment and detection of antibodies onto their surface.[57] Since then, nanoplate-based SERS sensors have been demonstrated in the detection of numerous biological species including microRNAs,[150] DNA,[20,61] cardiac troponin I protein,[145] C-reactive protein,[146] streptavidin/biotin,[21] biotin/avidin,[77] Jagged1 protein,[149] and I223R/H275Y viruses.[148] Of particular note is the work of Masterson *et al.*[150] who recently demonstrated the detection of highly specific microRNA biomarkers in the plasma taken from six metastatic bladder cancer patients. The sensing modality used was unique in that it combined SERS and plasmon-enhanced fluorescence (PEF) detection to create a dual-mode nanoplasmonic sensor that has a far greater likelihood of avoiding false-negative and false-positive diagnoses.

Using an entirely different modality by which nanoplates are utilized in SERS sensing applications, Hwang *et al.*[146] demonstrated high-performance sensors for the detection of an important biomarker linked to cardiovascular disease. By taking advantage of the vapor phase assembly techniques described in Section 2.4.1, they were able to first synthesize vertically aligned triangular Au nanoplates on a sapphire substrate with edge lengths between 20 to 30 μm. The so-formed nanoplates were then detached from the substrate and laid horizontally on a Si substrate. With bulk-scale dimensions, such structures are not valued for their plasmonic response but for their ultraflat, ultraclean, and single-crystalline (111) surfaces because these surfaces are ideal for immobilizing the bioreceptors needed to enact biosensing modalities with high specificity and sensitivity.[77] The atomically smooth surface is of particular importance because it allows for a densely packed, well-ordered arrangement of bioreceptors where each is optimally oriented for a binding event. Such configurations have been shown to provide up to an 8-fold increase in the binding capacity.[161]

Fig. 17a shows a scheme used in the detection of C-reactive protein (CRP), a prognostic biomarker for cardiovascular disease.[146] The bioreceptor is first assembled by attaching Cys3-protein G (red) to a triangular Au nanoplate that in turn binds to the antibody against CRP (green). Upon exposure to this bioreceptor, CRP (violet) binds to its surface with high specificity. Even though the target molecule is now captured, its detection with SERS is not yet possible because a plasmonic nanoparticle is not present. This is reconciled by exposing the CRP to another CRP antibody that has been functionalized with a spherical Au nanoparticle. A Raman dye (*i.e.*, rhodamine B isothiocyanate) applied to the Au nanoparticle then acts as a reporter molecule for SERS detection. Even though the nanoplate itself is not plasmonic, it still acts to strongly enhance the SERS signal due to the nanogap formed between its planar surface and the spherical Au nanoparticle. With the SERS signal being dependent on the number of such nanogaps formed over the entire nanoplate surface, the sensor provides a quantitative measure of the CRP concentration.

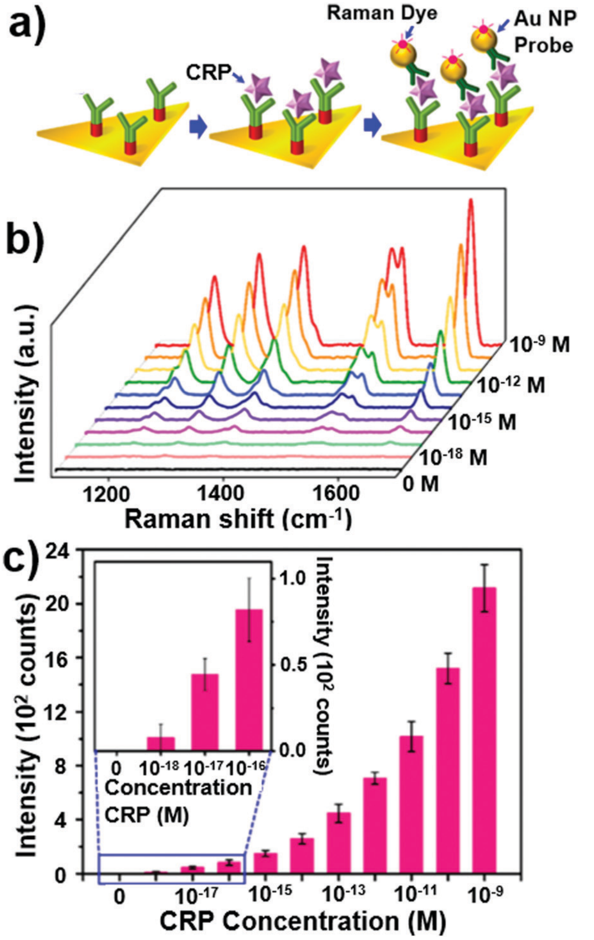

Fig. 17 (a) Schematic depiction of a SERS detection platform in which CRP bioreceptors are formed on a Au nanoplate after which they are exposed to CRP antibodies functionalized with spherical Au nanoparticles (NP). SERS detection then proceeds through the detection of a Raman dye that binds to the Au nanoparticle. (b) SERS spectra showing the response obtained from the Raman dye for CRP concentration ranging from 0 to $10^{-9}$ M. (c) Intensity of the 1643 $cm^{-1}$ peak as a function of CRP concentration. Fig. 17 adapted with permission from ref. 146. Copyright 2019 American Chemical Society.

Fig. 17b shows the SERS spectra for sensors exposed to CRP concentrations ranging from 0 to $1 \times 10^{-9}$ M. As anticipated, the SERS signal rises as the concentration is increased. Fig. 17c, which shows a plot of the SERS intensity for the 1643 $cm^{-1}$ peak as a function of CRP concentration, reveals that detection is possible at the remarkably low level of $10^{-17}$ M where the complete absence of CRP (*i.e.*, 0 M) leads to a negligible signal. Further validation of the sensing platform proceeded by comparing the performance of the sensor to an equivalent sensor fabricated from a thin film of Au. The thin film sensor underperformed the nanoplate sensor by a wide margin, sensing CRP at levels of only $10^{-9}$ M, and with far greater background signals due to the nonspecific binding of Au nanoparticles. The differences were attributed to the far greater surface roughness expressed by the Au film that led to the decreased mobilization and alignment of CRP antibodies and the unwanted binding of Au nanoparticles directly onto the rough Au surface. With an exceedingly high sensitivity, complete specificity, and the suppression of nonspecific binding, the Au nanoplate sensing platform has been demonstrated in the detection of (i) antiviral drug-resitant viruses,[148] (ii) the Jagged1 protein whose overexpression is linked to prostate and breast cancer,[149] and (iii) the cardiac troponin 1 (cTnIs) protein, a biomarker that can diagnose acute myocardial infarction (*i.e.*, a heart attack).[145]

### 3.2 LSPR-Based applications

Resonantly excited plasmonic nanostructures have large absorption and scattering cross sections, and as such, exhibit a prominent LSPR peak in the extinction spectrum. The position of this peak, which is readily tuned through changes to the size, shape, and composition of the nanostructure, is also strongly dependent on the dielectric environment in which the nanostructure is placed and whether it is in close proximity to other plasmonic nanostructures. Such phenomena act as the foundation for LSPR-based devices with spectroscopic readouts that are of high relevance to chemical and biological detection[162,163] and active plasmonics.[164,165] This section provides examples where substrate-based nanoplates have been used to advance these applications.

**3.2.1 LSPR sensors.** In its most basic design, an LSPR sensor operates by having a chemical or biological event occur on or near a plasmonic nanostructure that alters the local dielectric environment to an extent that it gives rise to a measurable spectral shift in the plasmon resonance.[162,163] The performance of a given nanostructure as a candidate material for an LSPR sensor is assessed using metrics referred to as the refractive index sensitivity and the figure of merit (FOM). The refractive index sensitivity provides a measure of the LSPR shift occurring when the index of refraction of the surrounding medium is increased by one refractive index unit (RIU). The FOM, which is the ratio of the refractive index sensitivity to the full width at half maximum (FWHM) of the LSPR resonance, takes into account the fact that a narrower LSPR peak leads to more sensitive detection. Nanostructure architectures that give rise to a high refractive index sensitivity and FOM are, therefore, highly valued for the purpose of LSPR sensing. Triangular nanoplates offer significant advantages over other nanostructure architectures in that their plasmon resonance is readily tuned throughout the visible and infrared spectral ranges and the localized electromagnetic field enhancements at their sharp tips and edges are known to promote high refractive index sensitivities. Additionally, their flat surfaces often prove ideal for the attachment of biological receptors used in sensing modalities offering high specificity. Although hexagonal nanoplates share some of these advantages, they are considered inferior in terms of the accessible refractive index sensitivities. Single-particle spectroscopy measurements have, however, shown that vertically aligned hexagonal nanoplates perform better than those lying flat on the substrate.[166]

Substrate-based LSPR sensors, while of obvious utility, require design considerations that take into account the influence and often confounding effects of the substrate. The mere act of placing a plasmonic nanostructure on a substrate places it in an asymmetric dielectric environment that leads to a red shift and broadening of the plasmonic resonance and can impact both the position and intensity of hot spots.[85,167] Further complicating factors can arise due to changes in the dielectric environment caused by chemical agents used to attach colloidal structures to substrate surfaces. When such influences are combined with the fact that the subtleties of triangular nanoplate geometries (*e.g.*, tip sharpness, side faceting) can also have pronounced consequences, the *a priori* deduction of plasmonic sensor properties can prove exceedingly challenging. In one prominent example, Joshi *et al.*[168] measured refractive index sensitivities for colloidal Au nanotriangles with edge lengths of 28, 35, and 42 nm as 370, 397, and 578 nm per RIU but then saw this upward sloping trend reversed to 647, 538, and 447 nm per RIU when the same structures were affixed to glass substrates with MPTES. Notwithstanding, triangular nanoplates act as excellent substrate-based LSPR sensors with reported refractive index sensitivities and FOM values as high as 647 nm per RIU and 5.1, respectively.[168] The use of triangular nanoplates as a substrate-based LSPR sensor was first demonstrated by Beeram and Zamborini[103] in the detection of human immunoglobulin G (IgG) and has since been used in the detection of streptavidin,[168,169] microRNAs,[18,170,171] hydrogen,[79] and boric acid.[172] In the remainder of this section, LSPR sensor work related to cancer detection is highlighted.

LSPR biosensing strategies, like SERS, have taken advantage of microRNA disease biomarkers to obtain specificity in detection by functionalizing plasmonic nanostructures with the complimentary microRNA sequence. In a recent study, Masterson *et al.*[170] not only used this approach in the detection of bladder cancer but also demonstrated a Au nanotriangle-based LSPR sensing platform offering multiplexing and high-throughput capabilities. Multiplexing, which is the concurrent detection of multiple biomarkers, significantly improves sensing modalities in that the detection of multiple biomarkers for the same disease decreases the likelihood of false positives and false negatives and provides the opportunity to screen for multiple diseases using a single liquid biopsy. Fig. 18 shows a schematic illustrating the LSPR sensing scheme that utilizes a multiwell plate that allows the contents of each well to be spectroscopically analyzed in an automated sequence by a microplate reader. Plasmonic nanotriangles affixed to glass substrates are glued to the bottom of each well after which receptors that target a specific biomarker are bonded to their surface. It is important to note that the receptors in one well can be chosen to be the same or different from that in a neighboring well. An LSPR spectrum is obtained for the contents of each well that acts as a point of reference. A patient's plasma is then applied to each well, followed by a dwell-and-rinse procedure. Each of the wells is then spectroscopically reassessed to determine if a shift in the LSPR has occurred.

Fig. 18b shows the results of a calibration run in which the concentration of six different microRNA types (D–H), all of which are associated with bladder cancer, were systematically varied followed by a spectroscopic measurement that recorded the shift in the LSPR resonance. Control samples testing for false positives and false negatives (B,C) as well as a blank well (A) were also analyzed. The data reveals all of the anticipated trends and shows the technique to be sensitive to $1 \times 10^{-7}$ nM concentrations. Important to note is that all of this data was obtained in a single instrument run. The authors then used these capabilities to analyze the plasma from 20 bladder cancer patients and ten healthy individuals. They demonstrated that

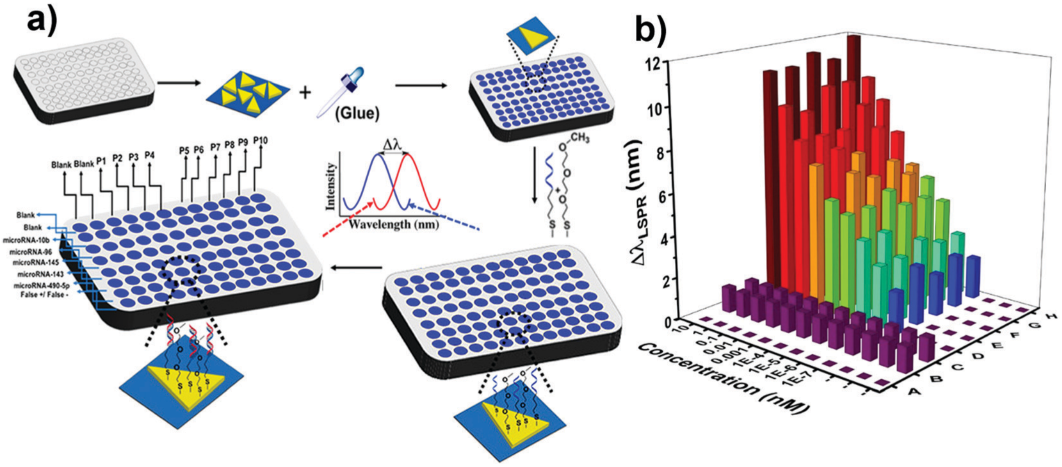

Fig. 18 (a) LSPR sensing scheme that allows for the sequential spectroscopic detection of multiple biomarkers. (b) Three-dimensional histogram showing the observed shift in the LSPR resonant wavelength ($\Delta\lambda_{LSPR}$) as a function of the microRNA concentration for six different micro-RNA types (D–H) as well as a blank (A) and controls that act as a false positive (B) and false negative (C). Fig. 18 adapted from ref. 170 with permission. Copyright 2020 American Chemical Society.

the multiplexing strategy was not only able to detect bladder cancer with high specificity but was also able to differentiate between the cancer patients who were metastatic and those who were not. The demonstration forwards the use of LSPR sensors as a point-of-care diagnostic tool.

**3.2.2 Active plasmonics.** The field of active plasmonics, as the name implies, aims to create plasmonic-based systems that are responsive to time-varying stimuli.[164,165] One modality for achieving active systems is to have an organized group of nanostructures whose relative orientation to one another is modified by the chemical environment in which they are placed. With the LSPR being highly sensitive to coupling phenomena, the reconfiguration results in changes to the optical response. It, therefore, becomes possible to actuate a specific optical response based on a chemical control.

Lin *et al.*[82] carried out such a demonstration using the Au nanoplate–nanocube–nanosphere configuration shown schematically in Fig. 19a that was formed using DNA-mediated assembly (see Section 2.5.2). Crucial to this proof-of-principle demonstration is the chemical response of the oligonucleotide when exposed to an ethanol–water mixture in that it extends or collapses depending on their relative concentrations. Fig. 19b shows SEM images of structures that were exposed to water and an 80% ethanol–water mixture where the configuration was "frozen" in place prior to removal from the liquid by encasing it in silica. It reveals that the degree of separation between the various structures depends on the chemical environment, an influence that translates into a significantly altered plasmonic response. Spectroscopic measurements taken as the ethanol concentration is varied from 0 to 80% show a shift in the LSPR that is consistent with simulations in which the distance between nanostructures is varied (Fig. 19c and d), a trend that also manifests itself in optical images as a continuously varying color change (Fig. 19e). Using a somewhat different modality Lu *et al.*[36] demonstrated the active switching of a plasmonic Fano resonance in aqueous media. The demonstration utilized a Au nanosphere–nanoplate dimer resting on a Si substrate (see Section 2.1.4) where the nanosphere was coated with PANI (*i.e.*, polyaniline), a polymer whose dielectric properties can be readily manipulated through alterations to its proton-doping level. With the dimer structure exhibiting a prominent Fano resonance that is highly sensitive to the local dielectric environment and the proton-doping level manipulated through variations

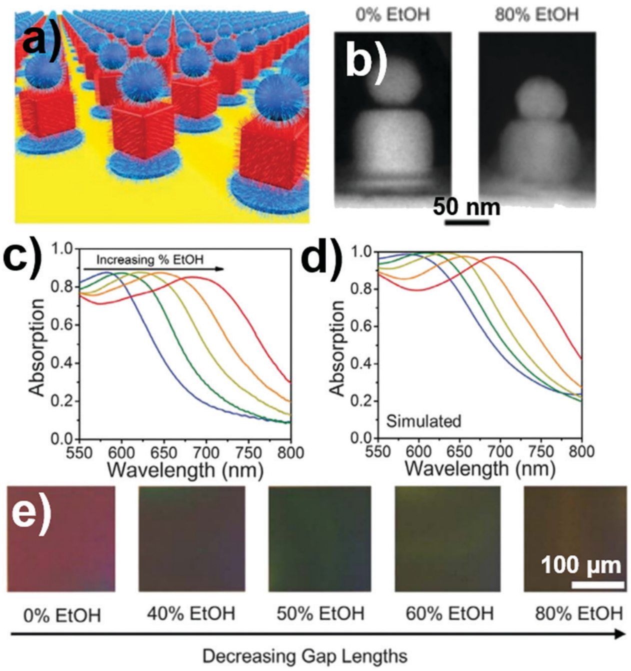

Fig. 19 (a) Schematic of a periodic array of the Au plate–cube–sphere configurations formed on a Au surface. (b) SEM images showing the shape-change these configurations undergo when exposed to ethanol (EtOH). (c) Measured and (d) simulated optical response as the structures undergo a chemically-induced reconfiguration. (e) Optical images showing the observed color change as the array is exposed to increasing ethanol concentrations. Adapted with permission from ref. 82. Copyright 2018 American Association for the Advancement of Science.

to the pH, the position of the resonance can be controllably altered with switching times of approximately 2 min. Given that the effect is reversible in both instances, these demonstrations provide important examples in the design of smart material systems actuated by changes to the chemical environment.

### 3.3 Other sensors

Skin-mountable strain sensors are ideal for tracking human body motion and activities that range from walking to pulse-rate monitoring.[173] In a proof-of-principle demonstration, Kim *et al.*[174] used Ag nanoplates to fabricate a stretchable resistive-type strain sensor. The design took advantage of a cyanuric-acid-based synthesis that sees nanotriangles form and then fuse into micrometer-scale structures expressing a zigzag pattern (Fig. 20a, inset). With a high electrical conductivity and a flat planar geometry, stacked assemblies of such structures were considered ideal for facilitating sliding motions while maintaining a percolative electrical pathway. Sensor fabrication proceeded by drop-casting the zigzag structures onto a patterned PDMS substrate followed by a low temperature thermal annealing procedure. Cu tape, applied to both ends of the strip, acted as electrical contacts. Sensor fabrication was completed by coating the exposed Ag structures with a protective PDMS layer.

Strain sensor performance was assessed for stretchability, gauge factor, response time, and cyclability. Fig. 20a shows the change in resistance ($\Delta R$) normalized to its initial value ($R_0$) for a sensor that is strained by 30%. The results reveal that the sensor shows a highly-desirable near-linear response for strains up to 27%. Also advantageous is that the gauge factor, which is equal to $\Delta R/\varepsilon R_0$ where $\varepsilon$ is the applied strain (*i.e.*, $\Delta L/L_0$ where $L$ is the sensor length), shows a near constant value of approximately 2000 for strains between 5 and 27%. The sensor also showed a response time constant near 0.1 s as well as the ability to maintain sensitivity over 200 cycles. As a comparison, identically produced sensors were fabricated using Ag nanowires and nanoplates instead of the zigzag structures, both of which underperformed by a wide margin. In a demonstration as skin-mountable sensors, devices were applied as patches to a person's index finger, larynx, and wrist and evaluated for their ability to monitor bending, repetitive speech, and pulse rate, respectively. Fig. 20b–d shows images of the attached sensors and the response recorded. All three demonstrations recorded the anticipated cyclic signal, and in doing so, further demonstrated sensor viability.

Nanoplates have also been incorporated into various sensing platforms that take advantage of their catalytic properties, plasmon-enhanced fluorescence, or ultraflat electrically conducting surfaces. Electrochemical sensors, whose most basic working principle is to generate current flows in an external circuit as a result of a reaction occurring on the working electrode, provide a straightforward mode of detection that is widely used in chemical and biological sensors.[175,176] The electrochemical reaction can show specificity toward a specific analyte if the working electrode is decorated with catalytic nanostructures designed to promote a specified reaction while showing little to no catalytic activity toward other interfering species that are likely to coexist with the analyte. Noble metal nanoplates, hence, provide sensing opportunities that take advantage of their unique catalytic response as well as the high specific surface area that can arise from a growth trajectory that is normal to the substrate surface. With the application requiring that the nanoplates be immobilized on a conducting substrate, their synthesis *via* electrochemical means (see Section 2.3) provides the most obvious avenue for fabricating the working electrodes. Sensor demonstrations for the detection of $H_2O_2$,[25,58,177] $N_2H_4$,[177] $NaNO_2$,[177] and nitrite ions[71] have been carried out using Au, Ag, and Pt nanoplates that show specificity and a signal that varies linearly with analyte concentration. Interestingly, Wang *et al.*[177] showed that Ag nanoplates formed on reduced graphene oxide (rGO), when incorporated into an electrochemical sensor, exhibit far greater chemical stability against $Cl^-$ ions and $H_2O_2$ than those where rGO was absent. Metal enhanced Fluorescence

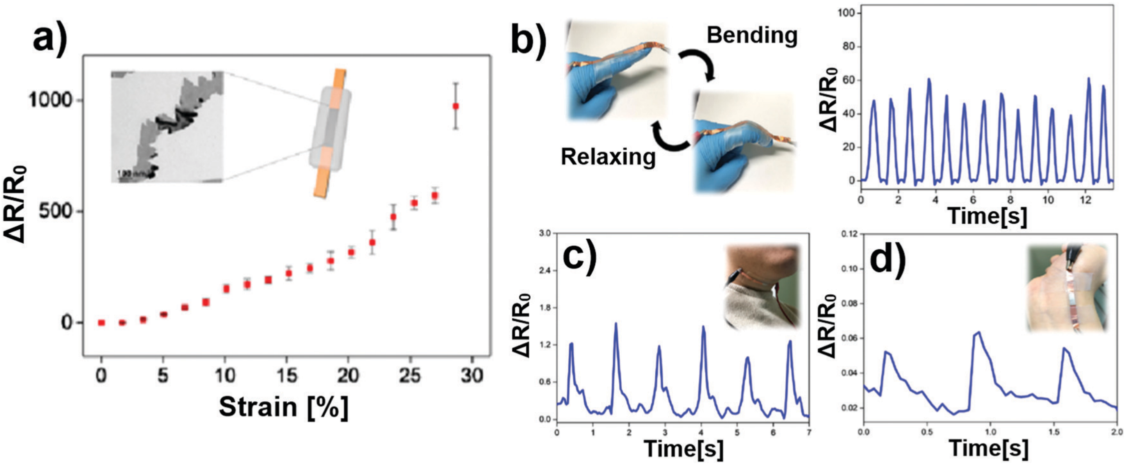

Fig. 20 (a) Relative resistance change as a function of strain for a resistance-type strain sensor using zigzag-shaped Ag nanoplates (inset) as an electrically conducting component. The cyclic responses obtained as sensors record the (b) bending and relaxing of an index finger, (c) larynx motions obtained when an individual repeatedly says "hello", and (d) pulse rate as measured by a person's throbbing wrist. Fig. 20 adapted with permission from ref. 174. Copyright 2018 American Chemical Society.

(MEF) represents another sensing modality that is based on the ability of a plasmonic nanoparticle to enhance the fluorescence of an adjacent fluorophore.[178,179] Substrate-based nanoplates have been used for this purpose to detect microRNA biomarkers for bladder cancer[150] and protein-immobilized indocyanine green (ICG).[48] Large-area nanoplates can also benefit sensing modalities related to conducting atomic force microscopy (CAFM)[180] in that they provide atomically flat conducting surfaces onto which self-assembled monolayers can be formed. The charge transport across the molecule can then be assessed by forming a circuit in which current from the conductive probe is passed through the molecule to the nanoplate. Jeong *et al.*[181] demonstrated this possibility using Au nanoplates derived from a vapor phase assembly synthesis to probe an alkanethiol monolayer. The understanding gained from such measurements can be of high value to the burgeoning field of molecular electronics.[182]

### 3.4 Catalysis

With highly desirable facets and an abundance of edge and corner sites, crystalline nanoplates present significant opportunities to the field of heterogeneous catalysis. Although such applications often employ nanostructure supports, the use of planar substrates can be disadvantageous since highly textured and liquid-dispersed platforms allow for a larger overall contact area between the catalytic nanostructures and reactants. Nevertheless, substrate-based nanoplates have unique characteristics that make them a viable option when firmly affixed to a substrate with their edges projecting out of the substrate surface so as to offer a large specific surface area with an open porosity. Under such circumstances, nanoplates can be synthesized that are ligand-free, robustly adhering, and physically connected to an underlying electrical contact. As such, they have been demonstrated as catalysts,[45,49] photocatalysts,[80] electrocatalysts,[49,68,72,75] and electrophotocatalysts[183] in a variety of reactions that include the methanol oxidation reaction (MOR),[75] oxygen evolution reaction (OER),[183] glucose[68] and formic acid oxidation,[72] and the reduction of carbon dioxide,[49] 4-nitrophenol,[45,49,80] and hydrogen peroxide.[49] In this section, examples are highlighted that capitalize on the unique aspects of substrate-bound nanoplates.

Muench *et al.*,[49] using Ag nanoplates derived from a seed-mediated synthesis, demonstrated their use as catalysts when

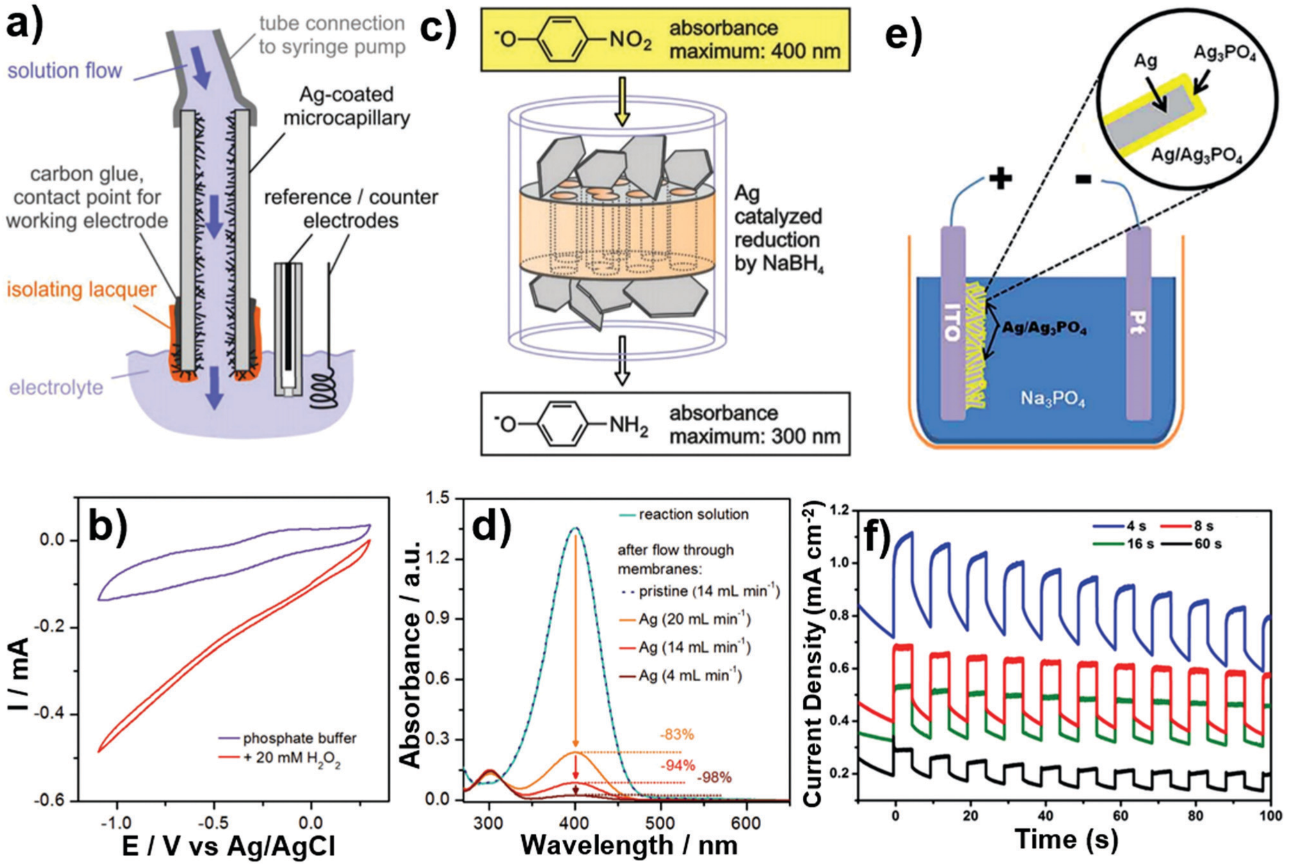

Fig. 21 (a) Schematic showing a continuous flow electrochemical cell and (b) the cyclic voltammograms obtained when it is used exclusively on the buffer solution and for $H_2O_2$ reduction. (c) Schematic of the continuous flow reactor used to catalytically reduce 4-nitrophenol and (d) absorbance spectra showing the 300 nm 4-nitrophenolate peak for the reactants and the reaction product obtained at three different flow rates. (e) Schematic showing the composite nanoplate photoanode configuration and (f) the time-dependent current density obtained in a photoelectrochemical cell for an oxygen evolution reaction occurring as photoanodes with four different $Ag_3PO_4$ layer thicknesses are illuminated with a pulsed light source. (a–f) Reproduced with permission from ref. 49 and 183, respectively. Copyright 2018 WILEY-VCH. Copyright 2015 Royal Society of Chemistry.

deployed in two different continuous flow microreactors. In the first demonstration, the interior walls of glass microcapillaries were coated with an electrically connected network of nanoplates formed by flowing reactants through the tube. The tube and the associated network were then incorporated into an electrochemical cell where it acts as the working electrode through which reactants are flowed (Fig. 21a). The performance of the cell was then demonstrated using $H_2O_2$ reduction as a model reaction. A comparison of the cyclic voltammograms obtained when flowing $H_2O_2$ at 1 mL $min^{-1}$ to the phosphate buffer (Fig. 21b) indicate a functioning microreactor. In the second demonstration, Ag nanoplate catalysts were formed on both the front and back surfaces of a porous polycarbonate membrane after which it was inserted into a syringe in the place of a syringe filter. This simple assembly (Fig. 21c) was then used as a flow microreactor for the model catalytic reaction that sees 4-nitrophenol reduced to 4-aminophenol by borohydride, and in doing so, takes advantage of the exceptionally high catalytic activity that Ag has toward this reaction.[184] The performance of the microreactor was then demonstrated by passing reactants through it at various flow rates followed by a spectroscopic analysis of the product. Fig. 21d shows the absorbance spectra for the initial reactants and for identical reactants after being passed through the reactor at three different flow rates. In all three instances, the 400 nm 4-nitrophenolate peak is diminished with the 4 ml $min^{-1}$ flow rate showing the highest conversion efficiency (*i.e.*, 98%).

Wu *et al.*[183] carried out a synthesis in which Ag nanoplates were electrodeposited on ITO. These structures were then exposed to a second electrochemical reaction in a phosphate solution that formed a semiconducting $Ag_3PO_4$ layer on each nanoplate (Fig. 21e) where the time of reaction was used to tune the layer thickness. The resulting structure was then tested as a composite nanoplate photoanode in a photoelectrochemical water splitting reaction. The role of the photoanode is to generate electron–hole excitations followed by efficient charge separation that sees the photoinduced electrons transported to the cathode. These electrons are then used in a hydrogen evolution reaction (HER) while the photoinduced holes participate in an oxygen evolution reaction (OER) at the anode. The role of the Ag nanoplates is, therefore, to indirectly enhance light absorption by providing a large specific surface area substrate for $Ag_3PO_4$ and, by creating an electrical pathway between $Ag_3PO_4$ and the ITO layer, facilitate rapid charge transport. The experimental configuration used to evaluate the photoelectrochemical catalytic activity saw the anode illuminated with a 100 mW $cm^{-2}$ chopped light source under a 0.5 V bias. Fig. 21f shows the time-dependent response of the current density for four photoelectrochemical cells that differ in that the semiconductor layer was progressively thickened by varying the $Ag_3PO_4$ deposition time between 4 and 60 s. The pulsed nature of the response clearly indicates that there is benefit derived from illumination, a result that was confirmed by monitoring the $O_2$ evolution at the anode. Another interesting aspect of this work is that the use of Ag nanoplates improved the durability of the $Ag_3PO_4$ semiconductor by providing a reservoir of Ag that is able to compensate for low-level losses experienced during the OER. In a broader sense, the work provides an excellent example showing that the catalytic activity of nanoplates toward a specific reaction can be enhanced by altering the chemical makeup of the nanoplate surface through the deposition of dissimilar materials onto its surface[49] or by the galvanic replacement of Ag.[45]

## 4. Summary and outlook

This review has documented the exciting and vibrant literature dedicated to the synthesis and application of substrate-immobilized noble metal nanoplates. At its core is a seemingly simple nanostructure architecture whose synthesis is complicated by the need for chemical controls that compel an isotropic metal to grow in a highly anisotropic manner. When achieved, it gives rise to highly coveted properties that act as enablers for truly remarkable application-based research. At the same time, there is no sense of satisfaction or contentment with the current state-of-the-art in nanoplate synthesis, assembly, and processing techniques. Instead, device performance, design, ease of manufacturing, and the ability to test new device concepts are challenged by a toolset in need of a significant upgrade. This section highlights some of the opportunities and challenges faced where emphasis is placed on the need for applications to act as the driving force for future innovation.

Despite the many different methods for populating substrate surfaces with noble metal nanoplates, all of them are easily put into one of two categories depending on whether the nanoplates are formed directly on a substrate or as colloid followed by their placement on a substrate. Neither of these methods have emerged as a best practice technique since both are faced with formidable challenges. The synthesis of nanoplates directly on substrate surfaces is the more conceptually appealing approach but where its implementation is fraught with difficulties, many of which can be traced back to the nanostructures that seed nanoplate growth. Although it is well-understood that seeds with stacking fault defects are conducive to nanoplate formation, methods for successfully forming such seeds are, for the most part, derived from empirical observations. These methods, hence, remain poorly understood and in need of breakthroughs that improve yield and dictate both the position and growth trajectory of the nanoplate. Additionally, nanoplate syntheses directly on substrate surfaces are underdeveloped in terms of establishing the practices needed to impose chemical and physical controls over the nanoplate growth mode. This deficiency is, however, the greatest strength of the colloidal method as it is bolstered by a diverse, well-developed, and impressive collection of synthetic protocols that are increasingly augmented by shape-purification methods that can, to a large extent, rid the product of undesirable geometries. Nevertheless, improvements in yield, size and shape uniformity, and reproducibly growing and maintaining sharp corners would all prove beneficial. The greater concern, instead, stems from deficiencies in nanoplate placement. The two-dimensional nature of the nanoplate is advantageous in that there is a natural tendency for them to lie flat on a surface but this property becomes disadvantageous when large specific surface areas requiring the on-edge configuration are required. Thin nanoplates are also more prone to stacking when assembled into close-packed configurations, a property that can prove beneficial or detrimental depending upon the application. Although self-assembly techniques for obtaining close-packed arrays of nano-triangles have seen significant progress, these methods are still in need of significant improvement since the assemblies are (i) highly defected and fragmented, (ii) limited by the homogeneity of the colloid, and (iii) require nanoplate capping agents that often diminish nanoplate performance in applications and which can prove undesirable in biosensing applications due to toxicity concerns (*e.g.*, CTAB). Moreover, current methods able to place nanoplates in periodic arrays are disadvantaged by (i) the need for electron beam lithography, (ii) defects caused by the imperfection of the colloid, and (iii) an inability to produce large-area arrays in a timely and cost-effective manner. Taken together, none of the fabrication methods described in this review is likely to emerge as a universal approach. Instead, it is more probable that application-specific trade-offs will act as a determining factor in deciding which method prevails.

Even though noble metal nanoplates are the obvious point of interest for this review, it is their immobilization on a substrate that links all of the work discussed. As such, one should not lose sight of the fact that the substrate does not have to act merely as a passive support. Instead, it should be thought of as a potential synthetic lever and as a means by which to enhance and enable device performance. As a synthetic lever, it has been shown to facilitate electrochemical and photochemical reactions, impose a heteroepitaxial relationship upon a seed or growing nanoplate, and dictate directed assembly processes through the patterning of its surface. In applications, substrates have enabled flexible electronics, enhanced SERS signals, and facilitated electrocatalytic and photoelectrochemical responses. These successes are, however, dwarfed by as of yet unexplored opportunities. Substrate materials, as well as thin films deposited on their surface, collectively exhibit nearly every known material property, and as a result, provide a near limitless toolbox for obtaining coupled and synergistic responses with plasmonic materials. Nanoplates connected to substrate materials with pristine interfaces that are unobstructed by capping or adhesion agents are ideal for this purpose but where such capabilities are still underdeveloped.

As nanoplate-based applications move beyond proof-of-principle demonstrations, increasing attention will have to be paid to nanomanufacturing issues such as device durability, shelf-life, ease of manufacturing, cost, yield, and throughput. The chemical stability and biocompatibility of Au is proving to be of such benefit that it is emerging as the material of choice for many sensor applications. Nevertheless, concerns still remain with regard to preserving sharp nanoplate corners, especially in liquid media where nanoplate reshaping is a greater concern.[53,185] It should, however, be recognized that bonds formed with the substrate act as a stabilizing influence that is absent in colloidal systems. The use of Ag is far more problematic from the standpoints of durability and shelf-life as it is known to tarnish in air,[186] leach in aqueous environments,[187,188] and undergo shape changes when heated.[189] If it were not for these environmental sensitivities, then Ag would be the material of choice for many applications in plasmonics. Recently, Preston *et al.*[190] demonstrated that an ultrathin and pinhole-free oxide layer, when deposited on substrate-based plasmonic structures using atomic layer deposition (ALD), protected it from oxidation, leaching, high temperature, and extreme pH environments. Such a solution could prove effective for nanoplate applications involving plasmonic enhanced fluorescence[191,192] and shell-isolated nanoparticle-enhanced Raman spectroscopy[193,194] (SHINERS) where a thin dielectric layer is employed as part of the detection scheme. Qin and co-workers[195–197] have also demonstrated that a thin Au layer, when deposited over Ag colloids, provides chemical stability while preserving or even enhancing the plasmonic properties of Ag. Such mitigation strategies, as well as others employed in colloidal chemistry,[198] could see Ag nanoplates assume a larger role in emerging sensor applications.

The integration of noble metal nanoplates into wafer-based technologies has delivered application-based discoveries that are founded on the great strides made in synthesis and processing. There, however, remain grand challenges that, if resolved, would propel the field to new heights, the foremost of which is the ability to define single-crystal nanoplates on any substrate surface with arbitrary size, shape, composition, and orientation at site-selective positions. Such a capability would allow plasmonic energy, including that confined to hot spots, to be placed at addressable positions, markedly improve the performance of sensors, forward metamaterial applications, create chiral geometries, and provide a platform for discovery in pursuit of new phenomena and devices. Although such capabilities may seem far off or even improbable, we truly believe that the path forward will be the most exciting part of the journey and look forward to discoveries that continue to demonstrate noble metal nanoplates as a unique and indispensable building block for substrate-based device applications.

## Conflicts of interest

The authors declare no competing financial interest.

## Acknowledgements

This work is supported by National Science Foundation Awards to S. N. (DMR-1803917, CMMI-1911991).

## Notes and references

1 Y. Chen, Z. Fan, Z. Zhang, W. Niu, C. Li, N. Yang, B. Chen and H. Zhang, Two-Dimensional Metal Nanomaterials:

Synthesis, Properties, and Applications, *Chem. Rev.*, 2018, **118**, 6409–6455.

2 J. E. Millstone, S. J. Hurst, G. S. Métraux, J. I. Cutler and C. A. Mirkin, Colloidal Gold and Silver Triangular Nanoprisms, *Small*, 2009, **5**, 646–664.

3 H. Hu, J. Zhou, Q. Kong and C. Li, Two-Dimensional Au Nanocrystals: Shape/Size Controlling Synthesis, Morphologies, and Applications, *Part. Part. Syst. Charact.*, 2015, **32**, 796–808.

4 X. Hong, C. Tan, J. Chen, Z. Xu and H. Zhang, Synthesis, Properties and Applications of One- and Two-Dimensional Gold Nanostructures, *Nano Res.*, 2015, **8**, 40–55.

5 B. An, M. Li, J. Wang and C. Li, Shape/Size Controlling Syntheses, Properties and Applications of Two-Dimensional Noble Metal Nanocrystals, *Chem. Sci. Eng.*, 2016, **10**, 360–382.

6 J. Turkevich, P. C. Stevenson and J. Hillier, A Study of the Nucleation and Growth Processes in the Synthesis of Colloidal Gold, *Faraday Discuss.*, 1951, **11**, 55–75.

7 S. Kasani, K. Curtin and N. Wu, A review of 2D and 3D Plasmonic Nanostructure Array Patterns: Fabrication, Light Management and Sensing Applications, *Nanophotonics*, 2019, **8**, 2065–2089.

8 W. Wang, M. Ramezani, A. I. Väkeväinen, P. Törmä, J. G. Rivas and T. W. Odom, The Rich Plasmonic World of Nanoparticle Arrays, *Mater. Today*, 2018, **21**, 303–314.

9 P. Zheng, S. K. Cushing, S. Suria and N. Wu, Tailoring Plasmonic Properties of Gold Nanohole Arrays for Surface-Enhanced Raman Scattering, *Phys. Chem. Chem. Phys.*, 2015, **17**, 21211–21219.

10 M. Li, S. K. Cushing, J. Zhang, S. Suri, R. Evans, W. Petros, L. F. Gibson, D. Ma, Y. Liu and N. Wu, Three-Dimensional Hierarchical Plasmonic Nano-Architecture Enhanced Surface-Enhanced Raman Scattering Immunosensor for Cancer Biomarker Detection in Blood Plasma, *ACS Nano*, 2013, **7**, 4967–4976.

11 T. Siegfried, Y. Ekinci, O. J. F. Martin and H. Sigg, Engineering Metal Adhesion Layers That Do Not Deteriorate Plasmon Resonances, *ACS Nano*, 2013, **7**, 2751–2757.

12 Y. Yang, C. Gu and J. Li, Sub-5 nm Metal Nanogaps: Physical Properties, Fabrication Methods, and Device Applications, *Small*, 2019, **15**, 1804177.

13 Y. Wang, X. Zou, W. Ren, W. Wang and E. Wang, Effect of Silver Nanoplates on Raman Spectra of P-Aminothiophenol Assembled on Smooth Macroscopic Gold and Silver Surface, *J. Phys. Chem. C*, 2007, **111**, 3259–3265.

14 C. Wang, B. Liu and X. Dou, Silver Nanotriangles-Loaded Filter Paper for Ultrasensitive SERS Detection Application Benefited by Interspacing of Sharp Edges, *Sens. Actuators, B*, 2016, **231**, 357–364.

15 X. Y. Zhang, A. Hu, T. Zhang, W. Lei, X. J. Xue, Y. Zhou and W. W. Duley, Self-Assembly of Large-Scale and Ultrathin Silver Nanoplate Films with Tunable Plasmon Resonance Properties, *ACS Nano*, 2011, **5**, 9082–9092.

16 X. Wang, C. Zhu, X. Hu, Q. Xu, H. Zhao, G. Meng and Y. Lei, Highly Sensitive Surface-Enhanced Raman Scattering Detection of Organic Pesticides Based on Ag-Nanoplate Decorated Graphene-Sheets, *Appl. Surf. Sci.*, 2019, **486**, 405–410.

17 G. K. Joshi, K. A. Smith, M. A. Johnson and R. Sardar, Temperature-Controlled Reversible Localized Surface Plasmon Resonance Response of Polymer-Functionalized Gold Nanoprisms in the Solid State, *J. Phys. Chem. C*, 2013, **117**, 26228–26237.

18 G. K. Joshi, S. Deitz-McElyea, T. Liyanage, K. Lawrence, S. Mali, R. Sardar and M. Korc, Label-Free Nanoplasmonic-Based Short Noncoding RNA Sensing at Attomolar Concentrations Allows for Quantitative and Highly Specific Assay of MicroRNA-10b in Biological Fluids and Circulating Exosomes, *ACS Nano*, 2015, **9**, 11075–11089.

19 T. Liyanage, A. Rael, S. Shaffer, S. Zaidi, J. V. Goodpaster and R. Sardar, Fabrication of a Self-Assembled and Flexible SERS Nanosensor for Explosive Detection at Parts-Per-Quadrillion Levels from Fingerprints, *Analyst*, 2018, **143**, 2012–2022.

20 L. Bi, Y. Rao, Q. Tao, J. Dong, T. Su, F. Liu and W. Qian, Fabrication of Large-Scale Gold Nanoplate Films as Highly Active SERS Substrates for Label-Free DNA Detection, *Biosens. Bioelectron.*, 2013, **43**, 193–199.

21 L. Bi, J. Dong, W. Xie, W. Lu, W. Tong, L. Tao and W. Qian, Bimetallic Gold–Silver Nanoplate Array as a Highly Active SERS Substrate for Detection of Streptavidin/Biotin Assemblies, *Anal. Chim. Acta*, 2013, **805**, 95–100.

22 T. Jiang, X. Wang, J. Tang and S. Tang, Seed-Mediated Synthesis of Floriated Ag Nanoplates as Surface Enhanced Raman Scattering Substrate for in Situ Molecular Detection, *Mater. Res. Bull.*, 2018, **97**, 201–206.

23 M. Sun, H. Qian, J. Liu, Y. Li, S. Pang, M. Xu and J. Zhang, A Flexible Conductive Film Prepared by the Oriented Stacking of Ag and Au/Ag Alloy Nanoplates and Its Chemically Roughened Surface for Explosive SERS Detection and Cell Adhesion, *RSC Adv.*, 2017, **7**, 7073–7078.

24 K. Li, K. Jiang, L. Zhang, Y. Wang, L. Mao, J. Zeng, Y. Lu and P. Wang, Raman Scattering Enhanced within the Plasmonic Gap Between an Isolated Ag Triangular Nanoplate and Ag Film, *Nanotechnology*, 2016, **27**, 165401.

25 R. Ning, W. Lu, Y. Zhang, X. Qin, Y. Luo, J. Hu, A. M. Asiri, A. O. Al-Youbi and X. Sun, A Novel Strategy to Synthesize Au Nanoplates and Their Application for Enzymeless $H_2O_2$ Detection, *Electrochim. Acta*, 2012, **60**, 13–16.

26 W. H. Lin, Y. H. Lu and Y. J. Hsu, Au Nanoplates as Robust, Recyclable SERS Substrates for Ultrasensitive Chemical Sensing, *J. Colloid Interface Sci.*, 2014, **418**, 87–94.

27 J. Kim, X. Song, F. Ji, B. Luo, N. F. Ice, Q. Liu, Q. Zhang and Q. Chen, Polymorphic Assembly from Beveled Gold Triangular Nanoprisms, *Nano Lett.*, 2017, **17**, 3270–3275.

28 S. Ye, S. D. Connell, J. R. McLaughlan, L. Roach, Z. Aslam, N. Chankhunthod, A. P. Brown, R. Brydson, R. J. Bushby, K. Critchley, P. L. Coletta, A. F. Markham and S. D. Evans, One-Step Preparation of Biocompatible Gold Nanoplates with Controlled Thickness and Adjustable Optical Properties for Plasmon-Based Applications, *Adv. Funct. Mater.*, 2020, **30**, 2003512.

29 Y. Huang, P. Kannan, L. Zhang, Y. Rong, L. Dai, R. Huang and T. Chen, Close-Packed Assemblies of Discrete Tiny Silver Nanoparticles on Triangular Gold Nanoplates as a High Performance SERS Probe, *RSC Adv.*, 2015, **5**, 94849–94854.

30 D. A. Walker, K. P. Browne, B. Kowalczyk and B. A. Grzybowski, Self-Assembly of Nanotriangle Superlattices Facilitated by Repulsive Electrostatic Interactions, *Angew. Chem.*, 2010, **122**, 6912–6915.

31 Q. Fu, G. Ran and W. Xu, Direct Self-Assembly of CTAB-Capped Au Nanotriangles, *Nano Res.*, 2016, **9**, 3247–3256.

32 L. Scarabelli, M. Coronado-Puchau, J. J. Giner-Casares, J. Langer and L. M. Liz-Marzán, Monodisperse Gold Nanotriangles: Size Control, Large-Scale Self-Assembly, and Performance in Surface-Enhanced Raman Scattering, *ACS Nano*, 2014, **8**, 5833–5842.

33 Y. H. Lee, C. K. Lee, B. Tan, J. M. Rui Tan, I. Y. Phang and X. Y. Ling, Using the Langmuir–Schaefer Technique to Fabricate Large-Area Dense SERS-Active Au Nanoprism Monolayer Films, *Nanoscale*, 2013, **5**, 6404–6412.

34 F. Liebig, R. M. Sarhan, M. Sander, W. Koopman, R. Schuetz, M. Bargheer and J. Koetz, Deposition of Gold Nanotriangles in Large Scale Close-Packed Monolayers for X-ray-Based Temperature Calibration and SERS Monitoring of Plasmon-Driven Catalytic Reactions, *ACS Appl. Mater. Interfaces*, 2017, **9**, 20247–20253.

35 X. Cui, Y. Lai, F. Qin, L. Shao, J. Wang and H. Q. Lin, Strengthening Fano Resonance on Gold nanoplates with Gold Nanospheres, *Nanoscale*, 2020, **12**, 1975–1984.

36 W. Lu, X. Cui, T. H. Chow, L. Shao, H. Wang, H. Chen and J. Wang, Switching Plasmonic Fano Resonance in Gold Nanosphere–Nanoplate Heterodimers, *Nanoscale*, 2019, **11**, 9641–9653.

37 F. Qin, Y. Lai, J. Yang, X. Cui, H. Ma, J. Wang and H. Q. Lin, Deep Fano Resonance with Strong Polarization Dependence in Gold Nanoplate-Nanosphere Heterodimers, *Nanoscale*, 2017, **9**, 13222–13234.

38 X. Cui, F. Qin, Q. Ruan, X. Zhuo and J. Wang, Circular Gold Nanodisks with Synthetically Tunable Diameters and Thicknesses, *Adv. Funct. Mater.*, 2018, **28**, 1705516.

39 Y. Lai, X. Cui, N. Li, L. Shao, W. Zhang, J. Wang and H. Q. Lin, Asymmetric Light Scattering on Heterodimers Made of Au Nanorods Vertically Standing on Au Nanodisks, *Adv. Opt. Mater.*, 2021, **9**, 2001595.

40 Y. Sun and G. P. Wiederrecht, Surfactantless Synthesis of Silver Nanoplates and Their Application in SERS, *Small*, 2007, **3**, 1964–1975.

41 Y. Sun, Direct Growth of Dense, Pristine Metal Nanoplates with Well-Controlled Dimensions on Semiconductor Substrates, *Chem. Mater.*, 2007, **19**, 5845–5847.

42 Y. Metal Sun, Nanoplates on Semiconductor Substrates, *Adv. Funct. Mater.*, 2010, **20**, 3646–3657.

43 Y. Sun, Synthesis of Ag Nanoplates on GaAs Wafers: Evidence for Growth Mechanism, *J. Phys. Chem. C*, 2010, **114**, 857–863.

44 D. Zhao, X. Lin, R. Jia, N. Gao and D. Liu, Plasticity Promoted Band Structure Engineering Achieved by Arrayed Indentation on GaAs Wafers, *Adv. Opt. Mater.*, 2016, **4**, 1601–1607.

45 Y. Sun and C. Lei, Synthesis of Out-of-Substrate Au–Ag Nanoplates with Enhanced Stability for Catalysis, *Angew. Chem., Int. Ed.*, 2009, **48**, 6824–6827.

46 A. D'Agostino, A. M. Giovannozzi, L. Mandrile, A. Sacco, A. M. Rossi and A. Taglietti, In Situ Seed-Growth Synthesis of Silver Nanoplates on Glass for the Detection of Food Contaminants by Surface Enhanced Raman Scattering, *Talanta*, 2020, **216**, 120936.

47 Y. K. Kim and D. H. Min, Surface Confined Successive Growth of Silver Nanoplates on a Solid Substrate with Tunable Surface Plasmon Resonance, *RSC Adv.*, 2014, **4**, 6950–6956.

48 K. Aslan, J. R. Lakowicz and C. D. Geddes, Rapid Deposition of Triangular Silver Nanoplates on Planar Surfaces: Application to Metal-Enhanced Fluorescence, *J. Phys. Chem. B*, 2005, **109**, 6247–6251.

49 F. Muench, R. Popovitz-Biro, T. Bendikov, Y. Feldman, B. Hecker, M. Oezaslan, I. Rubinstein and A. Vaskevich, Nucleation-Controlled Solution Deposition of Silver Nanoplate Architectures for Facile Derivatization and Catalytic Applications, *Adv. Mater.*, 2018, **30**, 1805179.

50 F. Muench, A. Vaskevich, R. Popovitz-Biro, T. Bendikov, Y. Feldman and I. Rubinstein, Expanding the Boundaries of Metal Deposition: High Aspect Ratio Silver Nanoplatelets Created by Merging Nanobelts, *Electrochim. Acta*, 2018, **264**, 233–243.

51 C. N. Grabilla, D. Freppona, M. Hettingera and S. M. Kuebler, Nanoscale Morphology of Electrolessly Deposited Silver Metal, *Appl. Surf. Sci.*, 2019, **466**, 230–243.

52 A. A. Umar, M. Oyama, M. M. Salleh and B. Y. Majlis, Formation of High-Yield Gold Nanoplates on the Surface: Effective Two-Dimensional Crystal Growth of Nanoseed in the Presence of Poly(vinylpyrrolidone) and Cetyltrimethylammonium Bromide, *Cryst. Growth Des.*, 2009, **9**, 2835–2840.

53 S. D. Golze, R. A. Hughes, S. Rouvimov, R. D. Neal, T. B. Demille and S. Neretina, Plasmon-Mediated Synthesis of Periodic Arrays of Gold Nanoplates using Substrate-Immobilized Seeds Lined with Planar Defects, *Nano Lett.*, 2019, **19**, 5653–5660.

54 T. B. Demille, R. D. Neal, A. S. Preston, Z. Liang, A. G. Oliver, R. A. Hughes and S. Neretina, Epitaxially Aligned Single-Crystal Gold Nanoplates Formed in Large-Area Arrays at High-Yield, *Nano Res.*, DOI: 10.1007/s12274-021-3473-1.

55 A. A. Umar and M. Oyama, Formation of Gold Nanoplates on Indium Tin Oxide Surface: Two-Dimensional Crystal Growth from Gold Nanoseed Particles in the Presence of Poly(vinylpyrrolidone), *Cryst. Growth Des.*, 2006, **6**, 818–821.

56 M. Morsin, M. M. Salleh, A. A. Umar and M. Z. Sahdan, Gold Nanoplates for a Localized Surface Plasmon Resonance-Based Boric Acid Sensor, *Sensors*, 2017, **17**, 1–10.

57 S. R. Beeram and F. P. Zamborini, Selective Attachment of Antibodies to the Edges of Gold Nanostructures for Enhanced Localized Surface Plasmon Resonance Biosensing, *J. Am. Chem. Soc.*, 2009, **131**, 11689–11691.

58 L. Zhong, S. Gan, X. Fu, F. Li, D. Han, L. Guo and L. Niu, Electrochemically Controlled Growth of Silver Nanocrystals on Graphene Thin Film and Applications for Efficient Nonenzymatic $H_2O_2$ Biosensor, *Electrochim. Acta*, 2013, **89**, 222–228.

59 S. H. Park, J. G. Son, T. G. Lee, H. M. Park and J. Y. Song, One-Step Large-Scale Synthesis of Micrometer-Sized Silver Nanosheets by a Template-Free Electrochemical Method, *Nanoscale Res. Lett.*, 2013, **8**, 1–6.

60 G. Liu, W. Cai and C. Liang, Trapeziform Ag Nanosheet Arrays Induced by Electrochemical Deposition on Au-Coated Substrate, *Cryst. Growth Des.*, 2008, **8**, 2748–2752.

61 S. Yang, D. Slotcavage, J. D. Mai, F. Guo, S. Li, Y. Zhao, Y. Lei, C. E. Cameron and T. J. Huang, Electrochemically Created Highly Surface Roughened Ag Nanoplate Arrays for SERS Biosensing Applications, *J. Mater. Chem. C*, 2014, **2**, 8350–8356.

62 G. Liu, W. Cai, L. Kong, G. Duan and F. Lü, Vertically Cross-Linking Silver Nanoplate Arrays with Controllable Density Based on Seed-Assisted Electrochemical Growth and Their Structurally Enhanced SERS Activity, *J. Mater. Chem.*, 2010, **20**, 767–772.

63 C. Zhu, G. Meng, Q. Huang and Z. Huang, Vertically Aligned Ag Nanoplate-Assembled Film as a Sensitive and Reproducible SERS Substrate for the Detection of PCB-77, *J. Hazard. Mater.*, 2012, **211–212**, 389–395.

64 G. Liu, G. Duan, L. Jia, J. Wang, H. Wang, W. Cai and Y. Li, Fabrication of Self-Standing Silver Nanoplate Arrays by Seed-Decorated Electrochemical Route and Their Structure-Induced Properties, *J. Nanomater.*, 2013, 365947.

65 Q. Wu, P. Diao, J. Sun, T. Jin, D. Xu and M. Xiang, Electrodeposition of Vertically Aligned Silver Nanoplate Arrays on Indium Tin Oxide Substrates, *J. Phys. Chem. C*, 2015, **119**, 20709–20720.

66 J. Wang and S. Pan, Electrodeposition of Vertically Standing Ag Nanoplates and Nanowires on Transparent Conductive Electrode Using Porous Anodic Aluminum Oxide Template, *Nanotechnology*, 2017, **28**, 425601.

67 M. Usman, L. Pan, A. Sohail, Z. Mahmood and R. Cui, Fabrication of 3D Vertically Aligned Silver Nanoplates on Nickel Foam-Graphene Substrate by a Novel Electrodeposition with Sonication for Efficient Supercapacitors, *Chem. Eng. J.*, 2017, **311**, 359–366.

68 B. Seo, S. Choi and J. Kim, Simple Electrochemical Deposition of Au Nanoplates from Au(I) Cyanide Complexes and Their Electrocatalytic Activities, *ACS Appl. Mater. Interfaces*, 2011, **3**, 441–446.

69 F. Jia, K. Wong and R. Du, Direct Growth of Highly Catalytic Palladium Nanoplates Array onto Gold Substrate by a Template-Free Electrochemical Route, *Electrochem. Commun.*, 2009, **11**, 519–521.

70 F. Jia, K. W. Wong and L. Zhang, Electrochemical Synthesis of Nanostructured Palladium of Different Morphology Directly on Gold Substrate through a Cyclic Deposition/Dissolution Route, *J. Phys. Chem. C*, 2009, **113**, 7200–7206.

71 S. Ahn, S. Manivannan, Y. Seo and K. Kim, Shape-Controlled Electrodeposition of Standing Pt Nanoplates on Gold Substrates as a Sensor Platform for Nitrite Ions, *Bull. Korean Chem. Soc.*, 2019, **40**, 522–528.

72 Y. Li, P. Diao, T. Jin, J. Sun and D. Xu, Shape-Controlled Electrodeposition of Standing Rh Nanoplates on Indium Tin Oxide Substrates and Their Electrocatalytic Activity toward Formic Acid Oxidation, *Electrochim. Acta*, 2012, **83**, 146–154.

73 Y. Yoo, S. I. Kim, S. Han, H. Lee, J. Kim, H. S. Kim, J. P. Ahn, T. Kang, J. Choo and B. Kim, Epitaxially Aligned Submillimeter-Scale Silver Nanoplates Grown by Simple Vapor Transport, *Nanoscale*, 2019, **11**, 17436–17443.

74 S. J. Cho, A. Suri, X. Mei and J. Ouyang, In Situ Deposition of Gold Nanostructures with Well-Defined Shapes on Unfunctionalized Reduced Graphene Oxide through Chemical Reduction of a Dry Gold Precursor with Ethylene Glycol Vapor, *RSC Adv.*, 2013, **3**, 1201.

75 S. Yang, K. Park, B. Kim and T. Kang, Low-Temperature Vapor-Phase Synthesis of Single-Crystalline Gold Nanostructures: Toward Exceptional Electrocatalytic Activity for Methanol Oxidation Reaction, *Nanomaterials*, 2019, **9**, 595.

76 M. B. E. Griffiths, S. E. Koponen, D. J. Mandia, J. F. McLeod, J. P. Coyle, J. J. Sims, J. B. Giorgi, E. R. Sirianni, G. P. A. Yap and S. T. Barry, Surfactant Directed Growth of Gold Metal Nanoplates by Chemical Vapor Deposition, *Chem. Mater.*, 2015, **27**, 6116–6124.

77 Y. Yoo, H. Lee, H. Lee, M. Lee, S. Yang, A. Hwang, S.-i. Kim, J. Y. Park, J. Choo, T. Kang and B. Kim, Surfactant-Free Vapor-Phase Synthesis of Single-Crystalline Gold Nanoplates for Optimally Bioactive Surfaces, *Chem. Mater.*, 2017, **29**, 8747–8756.

78 Y. Yoo, S.-i. Kim, J. Kim and B. Kim, Geometry-Tailored Freestanding Epitaxial Pd, AuPd, and Au Nanoplates Driven by Surface Interactions, *Nanoscale*, 2020, **12**, 6537–6544.

79 K. D. Gilroy, A. Sundar, M. Hajfathalian, A. Yaghoubzade, T. Tan, D. Sil, E. Borguet, R. A. Hughes and S. Neretina, Transformation of Truncated Gold Octahedrons into Triangular Nanoprisms through the Heterogeneous Nucleation of Silver, *Nanoscale*, 2015, **7**, 6827–6835.

80 M. Hajfathalian, K. D. Gilroy, A. Yaghoubzade, A. Sundar, T. Tan, R. A. Hughes and S. Neretina, Photocatalytic Enhancements to the Reduction of 4-Nitrophenol by Resonantly Excited Triangular Gold-Copper Nanostructures, *J. Phys. Chem. C*, 2015, **119**, 17308–17315.

81 S. D. Golze, S. Porcu, C. Zhu, E. Sutter, P. C. Ricci, E. C. Kinzel, R. A. Hughes and S. Neretina, Sequential Symmetry-Breaking Events as a Synthetic Pathway for Chiral Gold Nanostructures with Spiral Geometries, *Nano Lett.*, 2021, **21**, 2919–2925.

82 Q.-Y. Lin, J. A. Mason, Z. Li, W. Zhou, M. N. O'Brien, K. A. Brown, M. R. Jones, S. Butun, B. Lee, V. P. Dravid, K. Aydin and C. A. Mirkin, Building Superlattices from Individual Nanoparticles via Template-Confined DNA-Mediated Assembly, *Science*, 2018, **359**, 669–672.

83 Y. Zhou, X. Zhou, D. J. Park, K. Torabi, K. A. Brown, M. R. Jones, C. Zhang, G. C. Schatz and C. A. Mirkin, Shape-Selective Deposition and Assembly of Anisotropic Nanoparticles, *Nano Lett.*, 2014, **14**, 2157–2161.

84 C. Zhao, G. Wang, T. Takarada, X. Liang, M. Komiyama and M. Maeda, Shape-Selective Isolation of Au Nanoplates from Complex Colloidal Media by Depletion Flocculation, *Colloids Surf., A*, 2019, **568**, 216–223.

85 B. J. Wiley, S. H. Im, Z. Y. Li, J. McLellan, A. Siekkinen and Y. Xia, Maneuvering the Surface Plasmon Resonance of Silver Nanostructures through Shape-Controlled Synthesis, *J. Phys. Chem. B*, 2006, **110**, 15666–15675.

86 T. B. Demille, R. A. Hughes and S. Neretina, Periodic Arrays of Dewetted Silver Nanostructures on Sapphire and Quartz: Effect of Substrate Truncation on the Localized Surface Plasmon Resonance and Near-Field Enhancement, *J. Phys. Chem. C*, 2019, **123**, 19879–19886.

87 D. Zang, S. Tarafdar, Y. Y. Tarasevich, M. D. Choudhury and T. Dutta, Evaporation of a Droplet: From Physics to Applications, *Phys. Rep.*, 2019, **804**, 1–56.

88 A. Shaikeea, S. Basu, S. Hatte and L. Bansal, Insights into Vapor-Mediated Interactions in a Nanocolloidal Droplet System: Evaporation Dynamics and Affects on Self-Assembly Topologies on Macro- to Microscales, *Langmuir*, 2016, **32**, 10334–10343.

89 S. Ni, L. Isa and H. Wolf, Capillary Assembly as a Tool for the Heterogeneous Integration of Micro- and Nanoscale Objects, *Soft Matter*, 2018, **14**, 2978–2995.

90 R. D. Deegan, O. Bakajin, T. F. Dupont, G. Huber, S. R. Nagel and T. A. Witten, Capillary Flow as the Cause of Ring Stains from Dried Liquid Drops, *Nature*, 1997, **389**, 827–829.

91 W. Han and Z. Lin, Learning from ''Coffee Rings'': Ordered Structures Enabled by Controlled Evaporative Self-Assembly, *Angew. Chem., Int. Ed.*, 2012, **51**, 1534–1546.

92 C. Kuttner, M. Mayer, M. Dulle, A. Moscoso, J. M. López-Romero, S. Förster, A. Fery, J. Pérez-Juste and R. Contreras-Cáceres, Seeded Growth Synthesis of Gold Nanotriangles: Size Control, SAXS Analysis, and SERS Performance, *ACS Appl. Mater. Interfaces*, 2018, **10**, 11152–11163.

93 T. Liyanage, A. N. Masterson, S. Hati, G. Ren, N. E. Manicke, D. E. Rusyniak and R. Sardar, Optimization of Electromagnetic Hot Spots in Surface-Enhanced Raman Scattering Substrates for an Ultrasensitive Drug Assay of Emergency Department Patients' Plasma, *Analyst*, 2020, **145**, 7662–7672.

94 T. P. Bigioni, X.-M. Lin, T. T. Nguyen, E. I. Corwin, T. A. Witten and H. M. Jaeger, Kinetically Driven Self Assembly of Highly Ordered Nanoparticle Monolayers, *Nat. Mater.*, 2006, **5**, 265–270.

95 V. Santhanam, J. Liu, R. Agarwal and R. P. Andres, Self-Assembly of Uniform Monolayer Arrays of Nanoparticles, *Langmuir*, 2003, **19**, 7881–7887.

96 D. Liu, W. Cai, M. Marin, Y. Yin and Y. Li, Air-Liquid Interfacial Self-Assembly of Two-Dimensional Periodic Nanostructured Arrays, *ChemNanoMat*, 2019, **5**, 13381360.

97 F. Liebig, R. M. Sarhan, C. Prietzel, A. Reinecke and J. Koetz, ''Green'' Gold Nanotriangles: Synthesis, Purification by Polyelectrolyte/Micelle Depletion Flocculation and Performance in Surface-Enhanced Raman Scattering, *RSC Adv.*, 2016, **6**, 33561–33568.

98 F. Qin, T. Zhao, R. Jiang, N. Jiang, Q. Ruan, J. Wang, L.-D. Sun, C.-H. Yan and H. Q. Lin, Thickness Control Produces Gold Nanoplates with Their Plasmon in the Visible and Near-Infrared Regions, *Adv. Opt. Mater.*, 2016, **4**, 76–85.

99 S. Neretina, R. A. Hughes, K. D. Gilroy and M. Hajfathalian, Noble Metal Nanostructure Synthesis at the Liquid–Substrate Interface: New Structures, New Insights, and New Possibilities, *Acc. Chem. Res.*, 2016, **49**, 2243–2250.

100 V. Germain, J. Li, D. Ingert, Z. L. Wang and M. P. Pileni, Stacking Faults in Formation of Silver Nanodisks, *J. Phys. Chem. B*, 2003, **107**, 8717–8720.

101 T. Tan, S. Zhang, J. Wang, Y. Zheng, H. Lai, J. Liu, F. Qin and C. Wang, Resolving the Stacking Fault Structure of Silver Nanoplates, *Nanoscale*, 2021, **13**, 195–205.

102 Y. Xia, K. D. Gilroy, H. C. Peng and X. Xia, Seed-Mediated Growth of Colloidal Metal Nanocrystals, *Angew. Chem., Int. Ed.*, 2017, **56**, 60–95.

103 S. R. Beeram and F. P. Zamborini, Purification of Gold Nanoplates Grown Directly on Surfaces for Enhanced Localized Surface Plasmon Resonance Biosensing, *ACS Nano*, 2010, **4**, 3633–3646.

104 B.-B. Xu, Z. C. Ma, L. Wang, R. Zhang, L. G. Niu, Z. Yang, Y.-L. Zhang, W.-H. Zheng, B. Zhao, Y. Xu, Q.-D. Chen, H. Xia and H. B. Sun, Localized Flexible Integration of High-Efficiency Surface Enhanced Raman Scattering (SERS) Monitors into Microfluidic Channels, *Lab Chip*, 2011, **11**, 3347–3351.

105 C. Li, M. Iqbal, J. Lin, X. Luo, B. Jiang, V. Malgras, K. C.-W. Wu, J. Kim and Y. Yamauchi, Electrochemical Deposition: An Advanced Approach for Templated Synthesis of Nanoporous Metal Architectures, *Acc. Chem. Res.*, 2018, **51**, 1764–1773.

106 A. Serrà and E. Vallés, Advanced Electrochemical Synthesis of Multicomponent Metallic Nanorods and Nanowires: Fundamentals and Applications, *Appl. Mater. Today*, 2018, **12**, 207–234.

107 P. Swetha and S.-P. Feng, High-Index Facet Defined Shape-Controlled Electrochemical Synthesis of Nanocrystals: A Mini Review, *Electrochem. Commun.*, 2018, **94**, 64–69.

108 I. Saldan, O. Dobrovetska, L. Sus, O. Makota, O. Pereviznyk, O. Kuntyi and O. Reshetnyak, Electrochemical Synthesis and Properties of Gold Nanomaterials, *J. Solid State Electrochem.*, 2018, **22**, 637–656.

109 G.-R. Li, H. Xu, X.-F. Lu, J.-X. Feng, Y.-X. Tong and C.-Y. Su, Electrochemical Synthesis of Nanostructured Materials for Electrochemical Energy Conversion and Storage, *Nanoscale*, 2013, **5**, 4056–4069.

110 Q. Xu, G. Meng and F. Han, Porous AAO Template-Assisted Rational Synthesis of Large-Scale 1D Hybrid and Hierarchically Branched Nanoarchitectures, *Prog. Mater. Sci.*, 2018, **95**, 243–285.

111 J. Kibsgaard, Y. Gorlin, Z. Chen and T. F. Jaramillo, Meso-Structured Platinum Thin Films: Active and Stable Electrocatalysts for the Oxygen Reduction Reaction, *J. Am. Chem. Soc.*, 2012, **134**, 7758–7765.

112 T.-H. Yang, Y. Shi, A. Janssen and Y. Xia, Surface Capping Agents and Their Roles in Shape-Controlled Synthesis of Colloidal Metal Nanocrystals, *Angew. Chem., Int. Ed.*, 2020, **59**, 15378–15401.

113 S. H. Park, J. G. Son, T. G. Lee, H. M. Park and J. Y. Song, One-Step Large-Scale Synthesis of Micrometer-Sized Silver Nanosheets by a Template-Free Electrochemical Method, *Nanoscale Res. Lett.*, 2013, **8**, 248.

114 I. Dutta, C. B. Munns and G. Dutta, An X-ray Diffraction (XRD) Study of Vapor Deposited Gold Thin Films on Aluminum Nitride (A1N) Substrates, *Thin Solid Films*, 1997, **304**, 229–238.

115 M. Hajfathalian, K. D. Gilroy, R. A. Hughes and S. Neretina, Citrate-Induced Nanocubes: A Reexamination of the Role of Citrate as a Shape-Directing Capping Agent for Ag-Based Nanostructures, *Small*, 2016, **12**, 3444–3452.

116 X. Xia, Y. Wang, A. Ruditsky and Y. Xia, 25th Anniversary Article: Galvanic Replacement: A Simple and Versatile Route to Hollow Nanostructures with Tunable and Well-Controlled Properties, *Adv. Mater.*, 2013, **25**, 6313–6333.

117 C. R. Henry, Morphology of Supported Nanoparticles, *Prog. Surf. Sci.*, 2005, **3-4**, 92–116.

118 C. V. Thompson, Solid-State Dewetting of Thin Films, *Ann. Rev. Mater. Res.*, 2012, **42**, 399–434.

119 P. Farzinpour, A. Sundar, K. D. Gilroy, Z. E. Eskin, R. A. Hughes and S. Neretina, Altering the Dewetting Characteristics of Ultrathin Gold and Silver Films using a Sacrificial Antimony Layer, *Nanotechnology*, 2012, **23**, 495604.

120 A. Sundar, P. Farzinpour, K. D. Gilroy, T. Tan, R. A. Hughes and S. Neretina, Organized Surfaces of Highly Faceted Single-Crystal Palladium Structures Seeded by Sacrificial Templates, *Cryst. Growth Des.*, 2013, **13**, 3847–3851.

121 F. Baletto, C. Mottet and R. Ferrando, Molecular Dynamics Simulations of Surface Diffusion and Growth on Silver and Gold Cluster, *Surf. Sci.*, 2000, **446**, 31–45.

122 R. A. Hughes, E. Menumerov and S. Neretina, When Lithography Meets Self-Assembly: A Review of Recent Advances in the Directed Assembly of Complex Metal Nanostructures on Planar and Textured Surfaces, *Nanotechnology*, 2017, **28**, 282002.

123 E. Menumerov, S. D. Golze, R. A. Hughes and S. Neretina, Arrays of Highly Complex Noble Metal Nanostructures using Nanoimprint Lithography in Combination with Liquid-Phase Epitaxy, *Nanoscale*, 2018, **10**, 18186–18194.

124 A. S. Preston, R. A. Hughes and T. B. Demille, Rey Davila, V. M., Neretina, S. Dewetted Nanostructures of Gold, Silver, Copper, and Palladium with Enhanced Faceting, *Acta Mater.*, 2019, **165**, 15–25.

125 P. Farzinpour, A. Sundar, K. D. Gilroy, Z. E. Eskin, R. A. Hughes and S. Neretina, Dynamic Templating: A Large Area Processing Route for the Assembly of Periodic Arrays of Sub-Micrometer and Nanoscale Structures, *Nanoscale*, 2013, **5**, 1929–1938.

126 Y. Zhai, J. S. DuChene, Y.-C. Wang, J. Qiu, A. C. Johnston-Peck, B. You, W. Guo, B. DiCiaccio, K. Qian, E. W. Zhao, F. Ooi, D. Hu, D. Su, E. A. Stach, Z. Zhu and W. D. Wei, Polyvinylpyrrolidone-Induced Anisotropic Growth of Gold Nanoprisms in Plasmon-Driven Synthesis, *Nat. Mater.*, 2016, **15**, 889–893.

127 W. Zhou, Z. Liu, Z. Huang, H. Lin, D. Samanta, Q.-Y. Lin, K. Aydin and C. A. Mirkin, Device-Quality, Reconfigurable Metamaterials from Shape-Directed Nanocrystal Assembly, *Proc. Natl. Acad. Sci. U. S. A.*, 2020, **117**, 21052–21057.

128 Q.-Y. Lin, E. Palacios, W. Zhou, Z. Li, J. A. Mason, Z. Liu, H. Lin, P. C. Chen, V. P. Dravid, K. Aydin and C. A. Mirkin, DNA-Mediated Size-Selective Nanoparticle Assembly for Multiplexed Surface Encoding, *Nano Lett.*, 2018, **18**, 2645–2649.

129 W. Zhou, Q.-Y. Lin, J. A. Mason, V. P. Dravid and C. A. Mirkin, Design Rules for Template-Confined DNA-Mediated Nanoparticle Assembly, *Small*, 2018, **14**, 1802742.

130 M. R. Jones, R. J. Macfarlane, B. Lee, J. Zhang, K. L. Young, A. J. Senesi and C. A. Mirkin, DNA-Nanoparticle Superlattices Formed from Anisotropic Building Blocks, *Nat. Mater.*, 2010, **9**, 913–917.

131 M. N. O'Brien, M. R. Jones, K. L. Kohlstedt, G. C. Schatz and C. A. Mirkin, Uniform Circular Disks with Synthetically Tailorable Diameters: Two-Dimensional Nanoparticles for Plasmonics, *Nano Lett.*, 2015, **15**, 1012–1017.

132 J. A. Mason, C. R. Laramy, C.-T. Lai, M. N. O'Brien, Q.-Y. Lin, V. P. Dravid, G. C. Schatz and C. A. Mirkin, Contraction and Expansion of Stimuli-Responsive DNA Bonds in Flexible Colloidal Crystals, *J. Am. Chem. Soc.*, 2016, **138**, 8722–8725.

133 H. Zhang, C. Kinnear and P. Mulvaney, Fabrication of Single-Nanocrystal Arrays, *Adv. Mater.*, 2020, **32**, 1904551.

134 S. Ni, J. Leemann, H. Wolf and L. Isa, Insights into Mechanisms of Capillary Assembly, *Faraday Discuss.*, 2015, **181**, 225–242.

135 C. Kuemin, L. Nowack, L. Bozano, N. D. Spencer and H. Wolf, Oriented Assembly of Gold Nanorods on the Single-Particle Level, *Adv. Funct. Mater.*, 2012, **22**, 702–708.

136 V. Flauraud, M. Mastrangeli, G. D. Bernasconi, J. Butet, D. T. L. Alexander, E. Shahrabi, O. J. F. Martin and J. Brugger, Nanoscale Topographical Control of Capillary Assembly of Nanoparticles, *Nat. Nanotechnol.*, 2017, **12**, 73–80.

137 T. Kraus, L. Malaquin, H. Schmid, W. Riess, N. D. Spencer and H. Wolf, Nanoparticle Printing with Single-Particle Resolution, *Nat. Nanotechnol.*, 2007, **2**, 570–576.

138 J. E. Millstone, S. Park, K. L. Shuford, L. Qin, G. C. Schatz and C. A. Mirkin, Observation of a Quadrupole Plasmon Mode for a Colloidal Solution of Gold Nanoprisms, *J. Am. Chem. Soc.*, 2005, **127**, 5312–5313.

139 R. Pilot, R. Signorini, C. Durante, L. Orian, M. Bhamidipati and L. Fabris, A Review on Surface-Enhanced Raman Scattering, *Biosensors*, 2019, **9**, 57.

140 J. Langer, D. J. de Aberasturi, J. Aizpurua, R. A. Alvarez-Puebla, B. Auguié, J. J. Baumberg, G. C. Bazan, S. E. J. Bell, A. Boisen, A. G. Brolo, J. Choo, D. Cialla-May, V. Deckert, L. Fabris, K. Faulds, F. J. García de Abajo, R. Goodacre, D. Graham, A. J. Haes, C. L. Haynes, C. Huck, T. Itoh, M. Käll, J. Kneipp, J. Kneipp, N. A. Kotov, H. Kuang, E. C. Le Ru, H. K. Lee, J.-F. Li, X. Y. Ling, S. A. Maier, T. Mayerhöfer, M. Moskovits, K. Murakoshi, J.-M. Nam, S. Nie, Y. Ozaki, I. Pastoriza-Santos, J. Perez-Juste, J. Popp, A. Pucci, S. Reich, B. Ren, G. C. Schatz, T. Shegai, S. Schlücker, L.-L. Tay, K. G. Thomas, Z.-Q. Tian, R. P. Van Duyne, T. Vo-Dinh, Y. Wang, K. A. Willets, C. Xu, H. Xu, Y. Xu, Y. S. Yamamoto, B. Zhao and L. M. Liz-Marzán, Present and Future of Surface-Enhanced Raman Scattering, *ACS Nano*, 2020, **14**, 28–117.

141 B. Sharma, R. R. Frontiera, A.-I. Henry, E. Ringe and R. P. Van Duyne, SERS: Materials, Applications, and the Future, *Mater. Today*, 2012, **15**, 16–25.

142 J. Koetz, The Effect of Surface Modification of Gold Nanotriangles for Surface-Enhanced Raman Scattering Performance, *Nanomaterials*, 2020, **10**, 2187.

143 D. D. Li, J. Wang, G. C. Zheng, J. H. Liu and W. H. Xu, A Highly Active SERS Sensing Substrate: Core-Satellite Assembly of Gold Nanorods/Nanoplates, *Nanotechnology*, 2013, **24**, 235502.

144 A. N. Masterson, S. Hati, G. Ren, T. Liyanage, N. E. Manicke, J. V. Goodpaster and R. Sardar, Enhancing Nonfouling and Sensitivity of Surface-Enhanced Raman Scattering Substrates for Potent Drug Analysis in Blood Plasma via Fabrication of a Flexible Plasmonic Patch, *Anal. Chem.*, 2021, **93**, 2578–2588.

145 H. Lee, H. Youn, A. Hwang, H. Lee, J. Y. Park, W. Kim, Y. Yoo, C. Ban, T. Kang and B. Kim, Troponin Aptamer on an Atomically Flat Au Nanoplate Platform for Detection of Cardiac Troponin I, *Nanomaterials*, 2020, **10**, 1402.

146 A. Hwang, E. Kim, J. Moon, H. Lee, M. Lee, J. Jeong, E.-K. Lim, J. Jung, T. Kang and B. Kim, Atomically Flat Au Nanoplate Platforms Enable Ultraspecific Attomolar Detection of Protein Biomarkers, *ACS Appl. Mater. Interfaces*, 2019, **11**, 18960–18967.

147 T. Deckert-Gaudig and V. Deckert, Ultraflat Transparent Gold Nanoplates—Ideal Substrates for Tip-Enhanced Raman Scattering Experiments, *Small*, 2009, **5**, 432–436.

148 K. Guk, H. Kim, M. Lee, Y. A. Choi, S. G. Hwang, G. Han, H.-N. Kim, H. Kim, H. Park, D. Yong, T. Kang, E.-K. Lim and J. Jung, Development of A4 Antibody for Detection of Neuraminidase I223R/H275Y-Associated Antiviral Multidrug-Resistant Influenza Virus, *Nat. Commun.*, 2020, **11**, 3418.

149 M. Lee, H. Kim, E. Kim, S. Y. Yi, S. G. Hwang, S. Yang, E.-K. Lim, B. Kim, J. Jung and T. Kang, Multivalent Antibody−Nanoparticle Conjugates To Enhance the Sensitivity of Surface-Enhanced Raman Scattering-Based Immunoassays, *ACS Appl. Mater. Interfaces*, 2018, **10**, 37829–37834.

150 A. N. Masterson, T. Liyanage, C. Berman, H. Kaimakliotis, M. Johnson and R. Sardar, A Novel Liquid Biopsy-Based Approach for Highly Specific Cancer Diagnostics: Mitigating False Responses in Assaying Patient Plasma-Derived Circulating MicroRNAs through Combined SERS and Plasmon-Enhanced Fluorescence Analyses, *Analyst*, 2020, **145**, 4173–4180.

151 A. Hakonen, P. O. Andersson, M. S. Schmidt, T. Rindzevicius and M. Käll, Explosive and Chemical Threat Detection by Surface-Enhanced Raman Scattering: A Review, *Anal. Chim. Acta*, 2015, **893**, 1–13.

152 R. Gillibert, J. Q. Huang, Y. Zhang, W. L. Fu and M. L. de la Chapelle, Explosive detection by Surface Enhanced Raman Scattering, *Trends Anal. Chem.*, 2018, **105**, 166–172.

153 C. A. F. Penido, M. T. T. Pacheco, I. K. Lednev and L. Silveira Jr., Raman Spectroscopy in Forensic Analysis: Identification of Cocaine and Other Illegal Drugs of Abuse, *J. Raman Spectrosc.*, 2016, **47**, 28–38.

154 C. Chen, W. Liu, S. Tian and T. Hong, Novel Surface-Enhanced Raman Spectroscopy Techniques for DNA, Protein and Drug Detection, *Sensors*, 2019, **19**, 1712.

155 J. Smolsky, S. Kaur, C. Hayashi, S. K. Batra and A. V. Krasnoslobodtsev, Surface-Enhanced Raman Scattering-Based Immunoassay Technologies for Detection of Disease Biomarkers, *Biosensors*, 2017, **7**, 7.

156 M. Chisanga, H. Muhamadali, D. I. Ellis and R. Goodacre, Enhancing Disease Diagnosis: Biomedical Applications of Surface-Enhanced Raman Scattering, *Appl. Sci.*, 2019, **9**, 1163.

157 J. Perumal, Y. Wang, A. B. E. Attia, U. S. Dinish and M. Olivo, Towards a Point-of-Care SERS Sensor for Biomedical and Agri-Food Analysis Applications: A Review of Recent Advancements, *Nanoscale*, 2021, **13**, 553.

158 Z. Huang, A. Zhang, Q. Zhang and D. Cui, Nanomaterial-Based SERS Sensing Technology for Biomedical Application, *J. Mater. Chem. B*, 2019, **7**, 3755–3774.

159 M. Chen, D. Liu, X. Du, K. H. Lo, S. Wang, B. Zhou and H. Pan, 2D Materials: Excellent Substrates for Surface-Enhanced Raman Scattering (SERS) in Chemical Sensing and Biosensing, *Trends Anal. Chem.*, 2020, **130**, 115983.

160 C. Song, S. Guo, S. Jin, L. Chen and Y. M. Jung, Biomarkers Determination Based on Surface-Enhanced Raman Scattering, *Chemosensors*, 2020, **8**, 118.

161 J. M. Lee, H. K. Park, Y. Jung, J. K. Kim, S. O. Jung and B. H. Chung, Direct Immobilization of Protein G Variants with Various Numbers of Cysteine Residues on a Gold Surface, *Anal. Chem.*, 2007, **79**, 2680–2687.

162 M. Li, S. K. Cushing and N. Wu, Plasmon-Enhanced Optical Sensors: A Review, *Analyst*, 2015, **140**, 386–406.

163 K. M. Mayer and J. H. Hafner, Localized Surface Plasmon Resonance Sensors, *Chem. Rev.*, 2011, **111**, 3828–3857.

164 F. Neubrech, M. Hentschel and N. Liu, Reconfigurable Plasmonic Chirality: Fundamentals and Applications, *Adv. Mater.*, 2020, **32**, 1905640.

165 N. Jiang, X. Zhuo and J. Wang, Active Plasmonics: Principles, Structures, and Applications, *Chem. Rev.*, 2018, **118**, 3054–3099.

166 H. Yin, Y. Guo, X. Cui, W. Lu, Z. Yang, B. Yang and J. Wang, Plasmonic and Sensing Properties of Vertically Oriented

Hexagonal Gold Nanoplates, *Nanoscale*, 2018, **10**, 15058–15070.

167 T. B. Demille, R. A. Hughes, N. Dominique, J. E. Olson, S. Rouvimov, J. P. Camden and S. Neretina, Large-Area Periodic Arrays of Gold Nanostars Derived from HEPES-, DMF-, and Ascorbic-Acid-Driven Syntheses, *Nanoscale*, 2020, **12**, 16489–16500.

168 G. K. Joshi, P. J. McClory, B. B. Muhoberac, A. Kumbhar, K. A. Smith and R. Sardar, Designing Efficient Localized Surface Plasmon Resonance-Based Sensing Platforms: Optimization of Sensor Response by Controlling the Edge Length of Gold Nanoprisms, *J. Phys. Chem. C*, 2012, **116**, 20990–21000.

169 G. K. Joshi, P. J. McClory, S. Dolai and R. Sardar, Improved Localized Surface Plasmon Resonance Biosensing Sensitivity Based on Chemically-Synthesized Gold Nanoprisms as Plasmonic Transducers, *J. Mater. Chem.*, 2012, **22**, 923–931.

170 A. N. Masterson, T. Liyanage, H. Kaimakliotis, H. G. Derami, F. Deiss and R. Sardar, Bottom-Up Fabrication of Plasmonic Nanoantenna-Based High-throughput Multiplexing Biosensors for Ultrasensitive Detection of microRNAs Directly from Cancer Patients' Plasma, *Anal. Chem.*, 2020, **92**, 9295–9304.

171 T. Liyanage, A. N. Masterson, H. H. Oyem, H. Kaimakliotis, H. Nguyen and R. Sardar, Plasmoelectronic-Based Ultrasensitive Assay of Tumor Suppressor microRNAs Directly in Patient Plasma: Design of Highly Specific Early Cancer Diagnostic Technology, *Anal. Chem.*, 2019, **91**, 1894–1903.

172 M. Morsin, M. M. Salleh, A. A. Umar and M. Z. Sahdan, Gold Nanoplates for a Localized Surface Plasmon Resonance-Based Boric Acid Sensor, *Sensors*, 2017, **17**, 947.

173 M. Amjadi, K.-U. Kyung, I. Park and M. Sitti, Stretchable, Skin-Mountable, and Wearable Strain Sensors and Their Potential Applications: A Review, *Adv. Funct. Mater.*, 2016, **26**, 1678–1698.

174 J. Kim, S. W. Lee, M. H. Kim and O. O. Park, Zigzag-Shaped Silver Nanoplates: Synthesis via Ostwald Ripening and Their Application in Highly Sensitive Strain Sensors, *ACS Appl. Mater. Interfaces*, 2018, **10**, 39134–39143.

175 C. Zhu, G. Yang, H. Li, D. Du and Y. Lin, Electrochemical Sensors and Biosensors Based on Nanomaterials and Nanostructures, *Anal. Chem.*, 2015, **87**, 230–249.

176 A. Chen and S. Chatterjee, Nanomaterials Based Electrochemical Sensors for Biomedical Applications, *Chem. Soc. Rev.*, 2013, **42**, 5425–5438.

177 J. Wang, G. Zhang, W. Sun, J. Sun, L. Luo, Z. Chang and X. Sun, Synthesis of Ultrastable Ag Nanoplates/Polyethylenimine-Reduced Graphene Oxide and Its Application as a Versatile Electrochemical Sensor, *Chem. – Eur. J.*, 2016, **22**, 10923–10929.

178 M. A. Badshah, N. Y. Koh, A. W. Zia, N. Abbas, Z. Zahra and M. W. Saleem, Recent Developments in Plasmonic Nanostructures for Metal Enhanced Fluorescence-Based Biosensing, *Nanomaterials*, 2020, **10**, 1749.

179 K. Aslan, I. Gryczynski, J. Malicka, E. Matveeva, J. R. Lakowicz and C. D. Geddes, Metal-Enhanced Fluorescence: An Emerging Tool in Biotechnology, *Curr. Opin. Biotechnol*, 2005, **16**, 55–62.

180 F. Hui and M. Lanza, Scanning Probe Microscopy for Advanced Nanoelectronics, *Nat. Electron.*, 2019, **2**, 221–229.

181 W. Jeong, M. Lee, H. Lee, H. Lee, B. Kim and J. Y. Park, Ultraflat Au Nanoplates as a New Building Block for Molecular Electronics, *Nanotechnology*, 2016, **27**, 215601.

182 N. Xin, J. Guan, C. Zhou, X. Chen, C. Gu, Y. Li, M. A. Ratner, A. Nitzan, J. F. Stoddart and X. Guo, Concepts in the Design and Engineering of Single-Molecule Electronic Devices, *Nat. Rev.*, 2019, **1**, 211–230.

183 Q. Wu, P. Diao, J. Sun, D. Xu, T. Jin and M. Xiang, Draining the Photoinduced Electrons Away From an Anode: The Preparation of Ag/$Ag_3PO_4$ Composite Nanoplate Photoanodes for Highly Efficient Water Splitting, *J. Mater. Chem. A*, 2015, **3**, 18991–18999.

184 E. Menumerov, R. A. Hughes and S. Neretina, One-Step Catalytic Reduction of 4-Nitrophenol through the Direct Injection of Metal Salts into Oxygen-Depleted Reactants, *Cat. Sci. Technol.*, 2017, **7**, 1460–1464.

185 F. Qin, T. Zhao, R. Jiang, N. Jiang, Q. Ruan, J. Wang, L.-D. Sun, C.-H. Yan and H.-Q. Lin, Thickness Control Produces Gold Nanoplates with Their Plasmon in the Visible and Near-Infrared Regions, *Adv. Opt. Mater.*, 2016, **4**, 76–85.

186 X. Wang, C. Santschi and O. J. F. Martin, Strong Improvement of Long-Term Chemical and Thermal Stability of Plasmonic Silver Nanoantennas and Films, *Small*, 2017, **13**, 700044.

187 E. Menumerov, R. A. Hughes, S. D. Golze, R. D. Neal, T. B. Demille, J. C. Campanaro, K. C. Kotesky, S. Rouvimov and S. Neretina, Identifying the True Catalyst in the Reduction of 4-Nitrophenol: A Case Study Showing the Effect of Leaching and Oxidative Etching using Ag Catalysts, *ACS Catal.*, 2018, **8**, 8879–8888.

188 K. A. Johnston, L. M. Stabryla, A. M. Smith, X. Y. Gan, L. M. Gilbertson and J. E. Millstone, Impacts of Broth Chemistry on Silver Ion Release, Surface Chemistry Composition, and Bacterial Cytotoxicity of Silver Nanoparticles, *Environ. Sci.: Nano*, 2018, **5**, 304–312.

189 G. Albrecht, M. Ubl, S. Kaiser, H. Giessen and M. Hentschel, Comprehensive Study of Plasmonic Materials in the Visible and Near-Infrared: Linear, Refractory, and Nonlinear Optical Properties, *ACS Photonics*, 2018, **5**, 1058–1067.

190 A. S. Preston, R. A. Hughes, T. B. Demille and S. Neretina, Plasmonics Under Attack: Protecting Copper Nanostructures from Harsh Environments, *Chem. Mater.*, 2020, **32**, 6788–6799.

191 J.-F. Li, C.-Y. Li and R. F. Aroca, Plasmon-Enhanced Fluorescence Spectroscopy, *Chem. Soc. Rev.*, 2017, **46**, 3962–3979.

192 J. Dong, Z. Zhang, H. Zheng and M. Sun, Recent Progress on Plasmon-Enhanced Fluorescence, *Nanophotonics*, 2015, **4**, 472–490.

193 S.-Y. Ding, J. Yi, J.-F. Li, B. Ren, D.-Y. Wu, R. Panneerselvam and Z.-Q. Tian, Nanostructure-Based

Plasmon-Enhanced Raman Spectroscopy for Surface Analysis of Materials, *Nat. Rev. Mater.*, 2016, **1**, 1–16.

194 J. Krajczewski and A. Kudelski, Shell-Isolated Nanoparticle-Enhanced Raman Spectroscopy, *Front. Chem.*, 2019, **7**, 410.

195 Y. Yang, J. Liu, Z. W. Fu and D. Qin, Galvanic Replacement-Free Deposition of Au on Ag for Core-Shell Nanocubes with Enhanced Chemical Stability and SERS Activity, *J. Am. Chem. Soc.*, 2014, **136**, 8153–8156.

196 J. Zhang, S. A. Winget, Y. Wu, D. Su, X. Sun, Z.-X. Xie and D. Qin, Ag@Au Concave Cuboctahedra: A Unique Probe for Monitoring Au-Catalyzed Reduction and Oxidation Reactions by Surface-Enhanced Raman Spectroscopy, *ACS Nano*, 2016, **10**, 2607–2616.

197 K. D. Gilroy, X. Yang, S. Xie, M. Zhao, D. Qin and Y. Xia, Shape-Controlled Synthesis of Colloidal Metal Nanocrystals by Replicating the Surface Atomic Structure on the Seed, *Adv. Mater.*, 2018, **30**, 1706312.

198 H. Kang, J. T. Buchman, R. S. Rodriguez, H. L. Ring, J. He, K. C. Bantz and C. L. Haynes, Stabilization of Silver and Gold Nanoparticles: Preservation and Improvement of Plasmonic Functionalities, *Chem. Rev.*, 2019, **119**, 664–699.